

# **Pseudobacterial nanocarriers for intracellular delivery of anti- infectives**

Dissertation  
zur Erlangung des Grades  
des Doktors der Naturwissenschaften  
der Naturwissenschaftlich-Technischen Fakultät  
der Universität des Saarlandes

von  
Arianna Castoldi

Saarbrücken

2019

Tag des Kolloquiums: 17/05/2019

Dekan: Prof. Dr. Guido Kickelbick

Vorsitzender: Prof. Dr. Guido Kickelbick

Berichterstatter: Prof. Dr. Claus-Michael Lehr

Prof. Dr. Rolf Hartmann

Akademischer Mitarbeiter: Dr. Stefan Boettcher

Die vorliegende Arbeit entstand auf Anregung und unter  
Anleitung von  
Herrn Prof. Dr. Claus-Michael Lehr  
am Institut für Pharmazeutische Technologie der  
Universität des Saarlandes und am Helmholtz-Institut für  
Pharmazeutische Forschung Saarland

"I believe in evidence. I believe in observation, measurement, and reasoning, confirmed by independent observers. I'll believe anything, no matter how wild and ridiculous, if there is evidence for it. The wilder and more ridiculous something is, however, the firmer and more solid the evidence will have to be."

Isaac Asimov

## Summary

Short Summary .....	9
Kurzzusammenfassung .....	10
1. General introduction.....	11
1.1 Bacterial infection: a never ending problem .....	12
1.1.1 Resistance mechanism of bacteria.....	13
Modification of antibiotic molecules .....	13
Decreased of antibiotic penetration and efflux pumps .....	14
Bacteria sheltering into the host cells.....	15
1.2 Enteropathogenic bacteria .....	18
1.2.1 Treatment for intracellular bacteria.....	22
1.3 Aspherical nanoparticles .....	25
1.3.1 Preparation methods .....	26
1.3.1.1 Bottom-up approach .....	27
1.3.1.2 Top-down approaches .....	28
Template-assisted method .....	28
Lithography method and PRINT®.....	30
Microfluidics .....	33
Stretching method.....	34
1.3.2 Influence of particle shape on biological processes.....	35
Influence of particles shape on blood circulation and <i>in vivo</i> biodistribution.....	35
Influence of particles shape on cellular uptake into phagocytic cells.....	37
Influence of particles shape on cellular uptake into non- phagocytic cells .....	39
Other influences of the particle shape .....	40

1.3.3	Aspherical functionalised particles .....	40
1.4	Aim .....	42
2.	Aspherical nanoparticles: preparation and characterisation .....	44
2.1	Introduction.....	45
2.2	Materials and methods.....	47
2.2.1	Materials .....	47
2.2.2	Preparation of spherical nanoparticles .....	47
2.2.3	Preparation of aspherical nanoparticles .....	48
2.2.4	Imaging of nanoparticles .....	50
2.2.5	Analysis of SEM pictures.....	51
2.2.6	Dynamic light scattering .....	52
2.2.7	Asymmetric flow field flow fractionation.....	52
2.2.8	Statistical analysis .....	53
2.3	Results and discussions .....	53
2.4	Conclusion .....	61
3.	Preparation and characterisation of bacteriomimetic nanoparticles .....	63
3.1	Introduction.....	64
3.2	Materials and methods.....	66
3.2.1	Materials .....	66
3.2.2	Preparation of fluorescently labelled nanoparticles .....	67
3.2.3	Nanoparticle surface functionalisation.....	67
3.2.4	Protein quantification .....	70
3.2.5	Imaging of nanoparticles .....	70
3.2.6	Nanosight analysis.....	70
3.2.7	FT-IR spectroscopy .....	71
3.2.8	DLS.....	71

3.2.9	Calculation of surface occupancy .....	71
3.2.10	Generation of 3D model of InvA497-fuctionalised nanoparticles.....	71
3.2.11	Statistical analysis.....	72
3.3	Results and discussions .....	72
3.4	Conclusion .....	82
4.	Uptake of invasin-functionalised bacteriomimetic nanoparticles into HEP-2 cells .....	83
4.1	Introduction.....	84
4.2	Materials and methods.....	86
4.2.1	Materials .....	86
4.2.2	Preparation of nanoparticles and functionalisation .....	86
4.2.3	Cell cultivation .....	87
4.2.4	Cytotoxicity studies .....	87
4.2.5	Uptake studies.....	87
4.2.6	Confocal imaging .....	88
4.2.7	FACS analysis .....	88
4.2.8	Statistical analysis .....	89
4.3	Results and discussion .....	89
4.4	Conclusion .....	94
5.	Efficacy studies of bacteriomimetic nanoparticles .....	95
5.1	Introduction.....	96
5.2	Materials and methods.....	97
5.2.1	Materials .....	97
5.2.2	AOT-gentamicin preparation .....	98
5.2.3	FT-IR spectroscopy .....	98
5.2.4	Preparation of drug-loaded nanoparticles .....	98

5.2.5	Zeta potential .....	100
5.2.6	Release test of AOT-gentamicin .....	100
5.2.7	Cell cultivation .....	100
5.2.8	Cytotoxicity of AOT-gentamicin loaded nanoparticles and AOT-gentamicin alone .....	101
5.2.9	Bacteria culture.....	101
5.2.10	Invasion assay optimisation.....	102
5.2.11	Cytotoxicity of infected HEp-2 after nanoparticles treatment.....	102
5.2.12	Efficacy study .....	103
5.2.13	Statistical analysis.....	104
5.3	Results and discussions .....	104
5.4	Conclusion .....	117
6.	Overall conclusion and outlook .....	119
7.	Appendix .....	123
7.1	Calculation of surface occupancy.....	123
7.2	Script for PovRay 3.7 .....	123
	References.....	126
	Abbreviations.....	145
	List of figures.....	148
	List of publications .....	151
	Curriculum Vitae .....	153
	Acknowledgement/ Ringraziamenti .....	155



## SHORT SUMMARY

Difficulties in the access and effective treatment of sheltered intracellular bacterial infections may potentially be overcome by encapsulating drugs into delivery systems functionalised with bacteria-derived invasive proteins. Although the potential of these proteins is clear, the promising application and indeed characteristics of invasive particles remains to be fully explored. The objectives of this study were therefore to determine the influence of shape on bacteriomimetic system characteristics, using invasive spherical and aspherical polymeric nanocarriers. Aspherical nanoparticles were prepared by an optimised combination of chemical functionalisation and thermomechanical stretching. InvA497, a C-terminal fragment of the Yersinia-derived protein invasin, was covalently coupled onto the surface of both spherical and aspherical nanoparticles. *In vitro* studies using drug-free nanoparticles indicated shape-dependent differences on receptor-mediated uptake by epithelial cells, being slightly faster for spherical nanoparticles. Both types of nanoparticles were then loaded with a preparation of antibiotic gentamicin, and tested for their ability to kill intracellular *Shigella flexneri* in human epithelial cells. Aspherical systems led to a higher killing of intracellular bacteria, potentially due to a more favorable drug release profile. This study provides a proof of concept that InvA497-functionalised aspherical bacteriomimetic nanocarriers may efficiently deliver otherwise non-permeable antibiotics across host cell membranes, enabling effective treatment of intracellular infections.

# KURZZUSAMMENFASSUNG

Eine wirksame Behandlung von intrazellulär lokalisierten und auf diese Weise geschützten bakteriellen Infektionen kann mit Hilfe von spezieller nanopartikulären Systemen, die mit invasiven, von Bakterien abgeleiteten Proteinen funktionalisiert sind, erreicht werden. Obwohl das Potenzial dieser Proteinen bereits bekannt ist, sind vielversprechende Anwendungen und Eigenschaften dieser bakteriomimetischen Transportsysteme noch gründlich zu erforschen.

Ziel dieser Arbeit war es, den Einfluss von zwei unterschiedlichen Partikelformen (sphärisch und asphärisch) auf die Wirksamkeit dieser bakteriomimetischen Systeme zu untersuchen. Asphärische Nanopartikel wurden durch eine optimale Kombination von chemischer Funktionalisierung und thermomechanischer Dehnung vorbereitet. InvA497, ein C-Endfragment des invasiven, von *Yersinia* abgeleiteten Proteins «Invasin», wurde kovalent an die Nanopartikeloberfläche gekoppelt. In vitro Untersuchungen mit wirkstofffreien Nanopartikeln zeigten formabhängige Unterschiede in der Rezeptor-vermittelten Aufnahme bei Epithelzellen Hep-2. Bei sphärischen Nanopartikeln war die Aufnahme etwas schneller. Beide Nanopartikelsysteme wurden daraufhin mit dem Antibiotikum Gentamicin geladen und auf deren Fähigkeit geprüft, intrazelluläre *Shigella flexneri* Erreger in menschlichen Epithelzellen zu töten. Asphärische Systeme zeigten eine höhere Fähigkeit zur Abtötung der intrazellulären Bakterien, möglicherweise bedingt durch ein vorteilhaftes Wirkstofffreisetzungsprofil.

Mit dieser Untersuchung konnte nachgewiesen werden, dass InvA497-funktionalisierte, asphärische, bakteriomimetische Nanoträger nicht permeable Antibiotika durch die Wirtszellmembran effizient transportieren können, um intrazelluläre Infektionen behandeln zu können.

# 1. GENERAL INTRODUCTION

## *1.1 BACTERIAL INFECTION: A NEVER ENDING PROBLEM*

Microorganisms, like bacteria, are one of the oldest forms of life on earth and have been reigned on our planet, evolving or outlasting many obstacles they have encountered, for more than 2 billion years [1]. While commonly classified phylogenetically [2], bacteria may also be categorised and described by means of their shape. Bacterial shape can vary from spheres (cocci) to rods (bacilli) of differing length and width, as well as more complex shapes, such as stars.

The incredible adapting mechanisms of bacteria have allowed them to survive still in the 21<sup>st</sup> century. Although with the introduction of antibiotics and vaccines the reign of bacteria was under treat, these old microorganisms have progressively neutralised the effectiveness of antibiotics by developing resistance. Nowadays, antibiotics resistance has reach a critical level and becomes a serious public health treat, invalidating major antimicrobial drugs that are currently used in the clinic [3].

The bacterial resistance emergency has been widely documented and has a huge economic impact on national health system [1]. According to the World Health Organisation (WHO) definition, a bacterial strain is considered resistant when it no longer responds to standard treatments and therefore the infection is difficult to treat [4]. In 2014, the WHO stated that the bacterial resistance crisis is becoming dire [5]. The increase of bacteria resistant strain will mean an increasing use of older and less effective techniques, including debridement, disinfection, amputation, and isolation, for controlling the infections. European Centre for Disease Prevention and Control (ECDC) reported that, every year, 25000 people die from infections caused by multi-resistant bacteria [6]. Moreover those resistant microorganisms cost about 1.5 billion euros in extra healthcare services and productivity losses per year to Europe [7].

A number of common multidrug resistance bacteria have been registered by the Centre for Disease Control and Prevention (CDC) [8]. Bacteria like staphylococci, enterococci, *Enterobacter* spp, *Klebsiella pneumoniae* and *Pseudomonas* spp, are commonly present in healthcare institutions [9-12] and the increased mortality rates in patients with bloodstream infections have been associated with the increased resistance of these bacteria to common antibiotics. Other examples of bacteria responsible for common healthcare-associated

infections and multidrug-resistant bacteria are *Mycobacterium tuberculosis*, *Escherichia coli*, *Staphylococcus aureus*, *Enterococci* spp., nontyphoidal *Salmonella*, *Shigella* spp. and *Neisseria gonorrhoeae*. Seven factors are now used by CDC to assess the antibiotic-resistant bacterial infections [13]: clinical impact, economic impact, incidence, 10-year projection of incidence, transmissibility, availability of effective antibiotics and barriers to prevention.

Three main causes have been recognised as enhancer of the drug resistance bacteria crisis [5]: the evolutionary response to the widespread use of antibiotics [14]; the increase of connection between human populations which enhances the spreading of the pathogens; the improper and prolonged use of antibiotic therapies.

### **1.1.1 RESISTANCE MECHANISM OF BACTERIA**

There are five major mechanisms used by antibiotic against bacteria [15]: interference with cell wall synthesis (like  $\beta$ -lactams), inhibition of protein synthesis (like macrolides and aminoglycosides), interference with nucleic acid synthesis (like fluoroquinolones), inhibition of metabolic pathway (like sulphonamides) and disruption of bacterial membrane structure (like polymyxins). Adapting mechanisms, like activation of enzymes responsible for drug degradation, modifications in membrane permeability, development of multidrug efflux pumps or sheltering of the microorganism inside the host cells, are the sophisticated mechanisms of drug resistance used by bacteria in order to avoid the action mechanism of antibiotics [16].

## **MODIFICATION OF ANTIBIOTIC MOLECULES**

Chemical alteration of the antibiotic molecules is one of the resistant mechanisms used by both Gram-negative and Gram-positive bacteria. In order to reduce or eliminate the activity of the antibiotic, particular enzymes are produced by the bacteria itself, which are capable of introducing chemical changes to the antimicrobial molecule. Most of the antibiotics neutralised by these methods explicate their action inferring with protein synthesis [12, 17]. The most frequent biochemical reactions catalysed by these bacterial enzymes include acetylation,

phosphorylation and adenylation. Penicillin-resistant *S. aureus* is an example of bacteria who use an enzyme,  $\beta$ -lactamases, in order to destruct molecules of a specific class of antibiotic, the  $\beta$ -lactam [12]. Molecules of this class of antibiotic are inactivated through the destruction of the amide bond of the  $\beta$ -lactam ring, which inactivates the effect of the antibiotic. In order to overcome this resistant, new  $\beta$ -lactam molecules with a wider spectrum of activity and less susceptibility to the enzyme were manufactured, however discover of these new compounds have been followed by the rapid appearance of new bacterial enzymes capable of neutralising these molecules.

## **DECREASED OF ANTIBIOTIC PENETRATION AND EFFLUX PUMPS**

Another resistant mechanism developed by bacteria, in particular Gram-negative bacteria, is to prevent the antibiotic's access to its intracellular or periplasmic target [11]. In this resistance mechanism the bacterial membrane, the porins and the efflux pumps act either as a barrier against the permeation of the antimicrobial drug or as a decreasing mechanism for the intra-bacterial antibiotic concentration, which cannot therefore exert its antimicrobial effect.

Many common antibiotics like  $\beta$ -lactams, tetracyclines and some fluoroquinolones, are highly hydrophilic molecules which are particularly affected by changes in permeability of the outer membrane. These molecules use porins, water-filled diffusion channels present inside the bacterial membrane in order to cross the bacterial barrier [18]. Alterations of the porins, achieved for example by a shift in the type of porins expression on the surface of the bacteria, can change the permeability of antibiotic molecules, although this mechanism results in low-level resistance [19]. Different types of porin-mediated antibiotic resistance have been described and characterised in different Gram-negative bacteria, for example *E. coli* is able to express three major proteins (known as OmpF, OmpC and PhoE) which increase the resistance mechanism to cephamycins and other  $\beta$ -lactams [11].

Efflux pumps are other structures present inside the bacterial membrane which are able to limit the uptake of antibiotic inside bacteria [20]. They can affect the intracellular bacterial concentration of antibiotics like protein synthesis inhibitors, fluoroquinolones,  $\beta$ -lactams, carbapenems and polymyxins. Many

classes of efflux pumps have been discovered in both gram-negative and gram-positive bacteria, which can be substrate-specific for a particular antibiotic or with broad substrate specificity.

## **BACTERIA SHELTERING INTO THE HOST CELLS**

Invasion of the bacteria inside the host cells is a mechanism used by the so called intracellular bacteria in order to protect themselves from the antibiotic action [21-23]. Intracellular bacteria have the ability of inducing their own phagocytosis into cells that are normally nonphagocytic, like M-cells [24]. These types of bacteria are able not only to hide in the cytosol of the host cells, but also in endosome, nucleus, Golgi apparatus or in the endoplasmic reticulum of the infected cells. As most common anti-infective agents have a poor membrane permeability, they will not be able to reach the infection when the bacteria are sheltered inside the cells. Moreover, the antibiotics, which are able to permeate the host cells, once inside the cell, are rapidly degraded or have a concentration below the therapeutic levels [25]. In table 1.1, a list of the most common intracellular bacteria is shown. This mechanism of resistance is used by bacteria localised in different cells, like macrophages or epithelial cells.

Table 1.1 Main intracellular bacteria with the associated diseases and their localisation. The table was modified from Abed et al.[26]

Bacterial pathogens	Associated disease(s)	Target cells
<b><i>Mycobacterium tuberculosis</i> [27]</b>	Tuberculosis	Macrophages, hepatocytes
<b><i>Salmonella</i> spp. [28, 29]</b>	Typhoid fever	Macrophages, enterocytes
<b><i>Brucella</i> spp. [30]</b>	Malta fever or undulant fever	Macrophages
<b><i>Listeria monocytogenes</i> [31]</b>	Listeriosis, meningitis in newborn babies	Macrophages, hepatocytes, enterocytes
<b><i>Yersinia pestis</i>[32]</b>	Plague	Macrophages
<b><i>E. coli</i>[33]</b>	Diarrhoeal illness, urinary tract infections, meningitis in neonates	Epithelial cells, macrophages
<b><i>P. aeruginosa</i> [34]</b>	Pneumonia, endocarditis, meningitis, nosocomial infection	Macrophages, epithelial cells
<b><i>Legionella pneumophila</i> [35]</b>	Pneumonia	Macrophages
<b><i>S. aureus</i> [36]</b>	Pneumonia, mastitis, phlebitis, endocarditis, nosocomial infections, urinary tract infections, osteomyelitis	Macrophages, polymorphonuclear neutrophils

For intracellular bacteria, the success of the infection depends on the interaction between the bacteria and the host cells and the messages sent from the bacteria to the infected cells and the other way around [37]. During the internalisation process the bacteria play therefore an active role in the bacteria-cell communication. Afterwards the microorganisms can either remain in a vacuole in which they replicate (like *Mycobacteria* spp. [38] and *L. pneumophila* [39]), or escape and replicate in the cytosol (like *Shigella* spp. [40] and *Listeria* spp. [41]).



Two major types of induced uptake are mainly used by invasive bacteria for colonisation of mammalian cells [37]: a “zipper” mechanism that involves a direct contact between a surface bacterial protein and its surface receptor on the cell host membrane, that create a vacuole which engulfs the bacterium; a “trigger” mechanism in which a signal is sent from the bacteria to the mammalian cell, inducing cytoskeletal rearrangements and resulting in macropinocytosis. The first strategy is used by *Yersinia* and *Listeria* [41], instead the second one by *Salmonella* and *Shigella* [40].

Almost for all intracellular bacteria, membrane-bound vacuole is part of their invasion process, however the intracellular life of the bacteria may vary. Bacteria can either remain in a vacuole, in which they replicate (like *Mycobacteria* [38], *S. aureus* [42] and *L. pneumophila* [39]), or escape and replicate in the cytosol (like *Shigella* spp. [40] and *Listeria* spp. [41]).

For surviving inside the vacuole the bacteria have to develop strategies for surviving in a hostile and changing environment, characterised by poor nutrient content, progressive decrease of the pH and delivery of antibacterial peptides and lysosomal enzymes [43]. For example some bacteria are able to develop a mechanism to prevent fusion of the bacteria-containing vacuole with lysosomes [37], which protects the niche of the pathogen inside the host cell [38]. Two major survival strategies are developed by bacteria, although some species, like *Salmonella* [44], may use a combination of both: bacteria develop a state of metabolic adaptation to the stress imposed by hostile conditions; microorganisms create for themselves a less hostile niche through alteration of the biogenesis and dynamics of their vacuole compartment, which allows their survival and growth.

Once the intracellular infection is established and the invasive bacteria are able to replicate, the pathogen will damage the host cells till death causing the clinical symptoms of disease. For example bacteria like *Pseudomonas*, *S. aureus*, tetanus, diphtheria, botulism, and cholera secrete toxins which are able to kill the infected cells [37, 45]. Other bacteria instead are able to damage the host cells though the activation of the apoptosis pathway [37].

## 1.2 ENTEROPATHOGENIC BACTERIA

Many common enteropathogenic bacteria, such as *Shigella flexneri* and *Yersinia pseudotuberculosis*, are capable of sheltering inside enterocytes, where, due to the common poor membrane permeability of anti-infective agents, they are difficult to reach [21-23]. These diarrhea-causing pathogens are able to resist non-specific host defences and disrupt the intestinal epithelium [46]. Depending on their virulent properties [24, 47], these enteropathogenic bacteria can invade either the local mucosa (*Shigella* spp. [48]) or the local intestinal region (*Yersinia* spp. [49]) and progress to a systemic infection (*Salmonella* spp. [50]).

The specific invasion strategy of a bacterium is affected by virulence factors, acting on the host cell membrane or from the intracellular side of mammalian cells. Each enteropathogenic bacterial species has a different invasion mechanism, which involves specific host cell-bacteria interactions; however the two steps common to each mechanism are the adhesion of the bacteria on the host membrane and the later invasion inside the cells.

For example, the adhesion and invasion strategy for *S. flexneri* (Figure 1.1) starts with the exhibition to bile salt of a specific protein (IpaB) on the type III secretion apparatus (T3SA), which is then activated [51, 52].

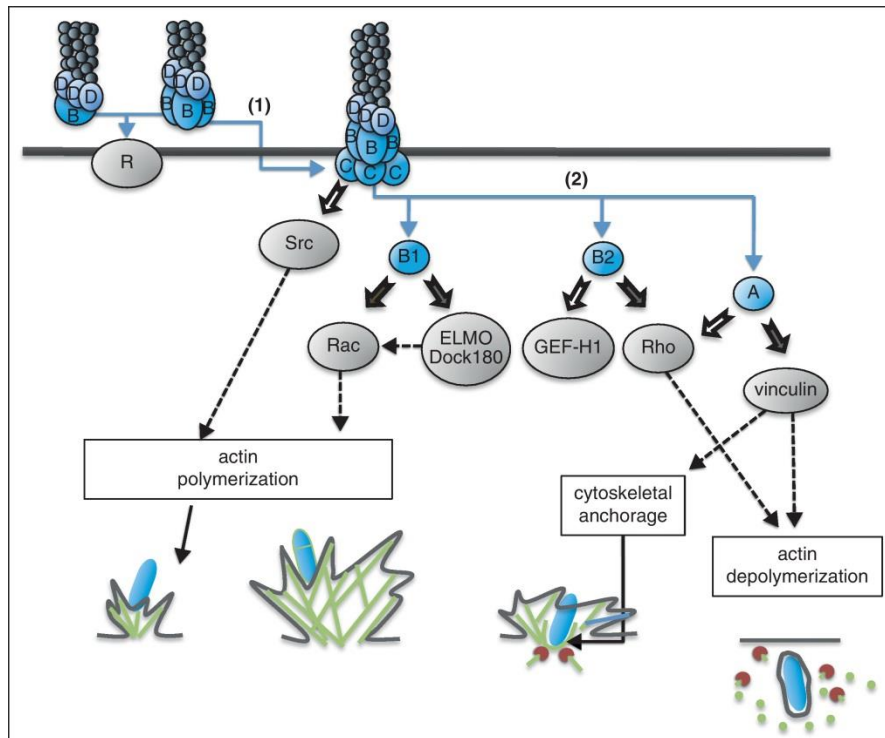


Figure 1.1 *Shigella* invasion of epithelial cells[51].

After exposition of the protein IpaB, the interaction between the cell surface receptor and the bacteria tip complex enhances the insertion of bacterial proteins, like IpaB, IpgB1, IpaA and IpaC, into the mammalian cell (1). A cascade of signals is then activated, causing reorganisation of the cytoskeleton, actin polymerisation and bacterial anchorage to the invasion site. C-terminal domain of IpaC will activate the Src tyrosine kinase and actin polymerisation (2). Reorganisation of the actin cytoskeleton (green) is also caused by injection from the bacteria of type III effectors, like IpgB1. This protein will activate Rac, which further amplifies actin polymerisation at invasion sites. Another bacterial protein, IpaA will promote the bacterial anchorage to the cytoskeleton at invasion sites and contribute to actin depolymerisation during the completion of the bacterial invasion process.

Adhesion to the host cells is then likely caused by interaction between filopodial extensions, surface sensory organelles on the surface of M cells, and the head of T3SA. Afterwards activated T3SA allows the injection of effector proteins, like IpaA, IpaB, IpgB1, IpgB2 and IpaC, into the host cell. IpaB/C complex is able to form a pore structure in the host cell membrane, which is then linked to the T3AS in order to further inject other effector proteins [53]. The injected effector proteins are important not only for the pore formation but for the invasion step as well. Reorganisation of the actin cytoskeleton - caused by Src tyrosine kinase activation mediated by IpaC and by activation of Ras-related C3 botulinum toxin (Rac) through IpgB1 - and depolymerisation of the actin filaments - mediated by IpaA - allow for the invasion of the bacteria inside the host. *S. flexneri* is normally

internalised inside the host cells via micropinocytosis and, when the invasion is completed, the bacteria are able to disrupt the vacuole structure [51, 54, 55].

Intracellular *S. flexneri* is then able to form an actin tail, which is used by the bacteria to move inside the cells and invade neighbouring epithelial cells. The intracellular bacteria will start to multiply into the cytosol and the infection will spread from cell to cell [56]. Once the bacteria invade and pass the M cells, they are able to release mediators which induce apoptosis of macrophages, B cells, and T cells [37]. Due to the hidden localisation, *S. flexneri* infections are difficult to treat with common antibiotics. A severe disruption of the integrity of the intestinal mucosa, associated with ulcers and mucosal abscesses, and a severe inflammation are the clinical symptoms of shigellosis [57, 58].

Another interesting invasion mechanism is done by *Yersinia* spp. These bacteria have an outer membrane protein called invasin. This is a well-characterised outer membrane invasion protein expressed on the surface of *Y. pseudotuberculosis* and *Yersinia enterocolitica*, which mediates an efficient entry of the bacteria into eukaryotic cells through interaction with  $\beta_1$  integrin receptors [59-61].

This protein is encoded by the invasin gene of *Y. pseudotuberculosis* and consists of 986 amino acids [62]. Invasin protein has an *N*-terminal  $\beta$ -barrel structure, which is located within the bacterial membrane of the bacterium, and a *C*-terminal part, orientated through the outside [63, 64] (Figure 1.2).

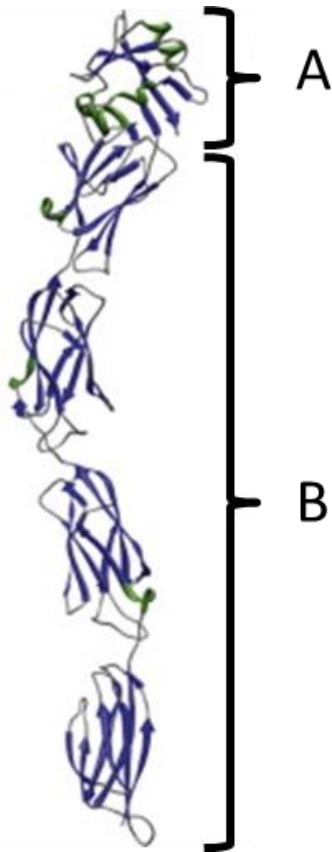


Figure 1.2 Structure of the extracellular binding domain of invasin [63].

The structure of the C-terminal part of invasin is shown in the figure. One cellular binding domain (A) and four immunoglobulin-like domain (B) form extracellular part of this bacterial protein.

The last 192 amino acids of the C-terminal region of invasin have been found to be particularly important for receptor binding and intracellular uptake [60]. The extracellular terminal region is composed of 4 immunoglobulin-like domains and one cell-binding domain, forming an elongated, rod-like structure [65]. Dersch *et al.* were able to produce and purify such a C-terminal, cell-invasive fragment of invasin, referred to as InvA497, which demonstrated a conserved binding capacity [60].

In order to initiate a bacterial infection, invasin is able to bind with  $\beta_1$  integrins on the apical surface of M cells located within the intestinal mucosa [66]. In order to invade the cells, the *Yersinia* bacteria need the intervention of another invasive protein located on its surface, YadA. Both YadA and invasin activate PI3 kinase upon binding to  $\beta_1$ -integrins [67, 68]. This triggers the production of short-lived host PIs, like Akt kinase, PLC-g1 and PKC isoforms PKCa and PKCb, which control the recruitment and activation of different phagocytosis cellular effectors

[68]. These two bacterial proteins on the surface of *Yersinia* bacteria are therefore able to initiate several intracellular signals which end with the internalisation of the bacteria through vacuoles. After translocation through intestinal M-cells, *Yersinia* bacteria are able to move into the subepithelial dome of the Peyer's patches. In this dome, the immune response will be activated via dendritic cells, macrophages and lymphocytes, resulting in an increased intracellular and paracellular permeability[56].

After invasion of the M cells, and in order to avoid uptake into the phagocytic cells and death, the *Yersinia* is able to inject a bacterial protein which interferes with phagocytosis, like Yops [37]. The bacteria therefore remain extracellular, allowing their survival and multiplication in lymphoid tissues.

### **1.2.1 TREATMENT FOR INTRACELLULAR BACTERIA**

For decades, intracellular enteropathogenic infections have been treated with anti-infective drugs. Due to the intracellular localisation of these bacteria, however, the number of antibiotics used and their action is limited. The antibiotic molecules must first overcome the intestinal barrier and then be internalised by the bacteria. One of the critical challenges for these types of infections is the concentration of the drugs that is able to reach the pathogens within their intracellular compartments.

Generally therapies against intracellular bacteria involve a combination of drugs administered for a long time [69]. Due to their short half-life, these antibiotics need to be frequently administered with a high dose in order to obtain the therapeutic effect. Therefore these therapies may develop side effects due to the drug's inherent toxicity and lead to high cost.

The preferred antibiotic therapy against enteropathogenic bacteria was fluoroquinolone, like ciprofloxacin. However, due to recent increased antibiotic resistance, macrolide, like azithromycin, are now preferentially used [70].

An ideal antibiotic treatment to eradicate intracellular bacteria need to have the following characteristics: the molecule need to be able to penetrate inside the host cells and gets into the infection site; the antibiotic needs to have a high efficacy, broad antibiotic spectrum and low toxicity.

In order to treat intracellular infections caused by enteropathogenic bacteria, incorporation of drug candidates into nanoparticles could be a solution. The first advantage of these systems is the increased stability and shelf life of the antibiotic molecules encapsulated into the nanoparticle [3, 71]. Moreover with the administration of nanoparticles, there is a controllable and relatively uniform distribution into the target tissue, which leads to a reduction of the side and toxic effect and a reduction of the administered dose [72-74].

It is demonstrated that encapsulation of antibiotics into liposomal or polymeric nanoparticles formulations increases the maximal tolerated dose and the therapeutic effect of the molecule compared with the free drug [75, 76]. Fattal *et al.* for example found an increase by 120-fold of the efficacy of ampicillin against *Salmonella typhimurium* when the antibiotic is encapsulated inside poly(isobutylcyanoacrylate) nanoparticles [77]. Ampicillin loaded nanoparticles were tested in a mice model with acute *Salmonella* infection. It was found that 100% of the infected mice treated with a single dose of the nanoparticles survived, whereas all the untreated animals died. Polymeric nanoparticles were able to reach the intracellular location of the *Salmonella* bacteria and the released antibiotic was able to kill the microorganisms. Ampicillin loaded liposomes were also tested on the same model, however the treatment was less efficient and only 60 % of the mice survived [78].

Nanoparticulate systems can also be used for the administration of both lipophilic antibiotic molecules, which are difficult to administrate due to solubility problem in water, or for hydrophilic antibiotic, which normally cannot penetrate the mammalian cell membrane, against intracellular bacteria [3, 74, 79, 80]. The difficult localisation of these bacteria can be overcome by the administration of antibiotic loaded nanoparticles, which are able to be internalised inside the cells and release the drug where the bacteria are localised. Targeting of the infection site can either be passive, where the distribution and uptake of the nanoparticles is casual, or active, where distribution and uptake can be driven by active vectoring [4].

For active target, the ligand is usually attached on the surface of the nanoparticles and, in accordance with the ligand-receptor binding theory [81], such structure is able to enhance the interactions with the cell membrane and the uptake of the system [4, 25, 82]. The ligand needs to be chosen depending on the

stability and selectivity for the target cells. For examples, different studies show that saccharides are the best ligand for macrophages or phagocytic cells targeting, due to the presence of a lectin receptors on the surface of phagocytic cells [4, 83-86].

Compared with non-functionalised nanoparticles, targeted delivery of antimicrobial drug may increase the success rate of therapy for chronic and persistent infections [87]. Specific target molecules on the particles surface have been shown to be able to recognise the unique surface properties of the targeted cells [81]. Bacterial molecules or and even bacterial invasion systems have been explored in the recent year as new strategies for active targeting. In this respect, the use of bacterial proteins which naturally mediate the invasion of bacteria into mammalian cells has been reported as a promising means of enhancing the permeation of carrier systems and potentially increasing the intracellular efficacy of their drug loads. These functionalised systems are called as bacteriomimetic particles.

For example, Salaman *et al.* were able to produce *Salmonella*-like nanoparticles, obtained by coupling *Salmonella* enteritidis flagellin or monnosamine, or *Brucella ovis* lipopolysaccharide loaded particle [88]. Adhesion of these systems on gastrointestinal mucosa of Wistar rats was tested as well as the immune response. It was found that only *Salmonella*-like nanoparticles were able to display a strong mucosa affinity and, after penetrating into the tissue, to induce a release of immunoglobulins [88].

Another type of bacteriomimetic system was produced by Gabor *et al.* using K99-fibriae from *E.coli* [89]. This system consists of mucoadhesive polyacrylic acid and K99-fimbriae covalently bound to this matrix system. The receptor specific adhesion of this bacteriomimetic system was confirmed on different types of epithelial cell lines, like Caco-2, SW620, SW480 and human colonocytes.

Although the use of bacteria protein or bacterial invasion systems could be a solution for specific tissue targeting, a few aspects must be considered. First the bacterial protein must be extract and purified from the bacteria using a reproducible method. These bacterial factors must also be stable during the coupling process on the particle system and their affinity for the receptor should not be altered. The possible immunogenic effect caused by the presence of



bacterial proteins or systems on the surface of the particle must also be considered.

In recent years, invasin and its uptake enhancer properties have been studied in the field of drug delivery. In particular gentamicin-loaded liposomes, surface functionalised with InvA497, were prepared and it was further demonstrated their ability to reach and kill intracellular bacteria located in various epithelial sub-cellular compartments [90, 91]. Similar results were found by Dawson *et al.*, who prepared poly (lactic-co-glycolic acid) (PLGA) nanoparticles functionalised with invasin and tested their uptake in HEP-2 cells [92]. It was shown that this polymeric system was able to penetrate the cells with an uptake mechanism dependent from the invasin density on the surface. Other study with latex nanoparticles with surface-coupled invasin shows an epithelial absorption and systemic distribution of these bacteriomimetic particles in rats [93].

In all these studies invasin was chosen for its strong affinity for the receptor  $\beta_1$ -receptor, located on different types of epithelial cells (HEp-2, Calu3), as well as for the possibilities of using an easy and quick coupling procedure for the covalently linkage with the particle.

### *1.3 ASPHERICAL NANOPARTICLES*

Typically, nano- and microparticles have been produced with spherical shape. However, a large number of examples of non-spherical shapes can be found in natural systems, such as bacteria, virus, fungi and erythrocytes, where the importance of the non-spherical shape is demonstrated [94-96].

Recent studies have shown the possible application of aspherical particles in order to modify biodistribution and circulation in the blood stream or cellular internalisation and trafficking. Moreover application of particles with an aspherical shape has been studied for some field of the nanomedicine, like therapy for cancer or pulmonary application.

In the following subsection, the most common preparation for aspherical particles as well as the influence of shape on biological process will be discussed.

### 1.3.1 PREPARATION METHODS

New methods for the production of aspherical particles have been discovered or optimised, in order to study the influence of aspherical drug delivery systems on biological systems and processes, such as uptake, distribution and clearance. These preparation methods can be divided in two categories [97-99]: methods where the aspherical systems are produced or synthesised *de-novo*, also called bottom-up approaches; and methods that utilise already formed spherical particles as precursors, also known as top-down methods.

These different methods were designed in order to produce micro- or nanoparticles with a specific shape and size, using either inorganic or organic materials. Although some progress has been made in the production of aspherical systems, these methods are not all suitable for large scale production, like industry, but are rather designed for laboratory scale-production and testing.

Comparing the two different categories, bottom-up approaches could be readily scalable to larger production and different material can be used, however the particle size and uniformity is not always reproducible and only some shapes can be produced [97]. In contrast, top-down approaches require specific machinery or templates in order to create the aspherical systems. Examples of aspherical particles with complex shape produced with different approaches are shown in Figure 1.3

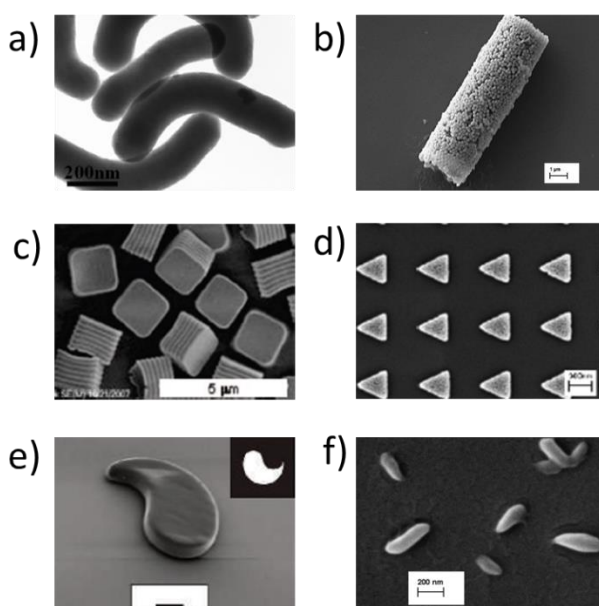


*Figure 1.3 Examples of aspherical systems produced by different preparation methods.*

*a) silica 'worms', scale bar 200 nm [100]; b) rod shape microparticles prepared using the template-assisted method, scale bar 1  $\mu\text{m}$  [101]; c) Trojan horse PRINT® (Particle Replication in Non-wetting Templates) particles loaded with doxorubicin, scale bar 5  $\mu\text{m}$  [102]; d) triangular particles produced using a lithography approach, scale bar 300 nm [103]; e) particles prepared with microfluidics, scale bar 10  $\mu\text{m}$  [104]; f) aspherical polymeric nanoparticles produced by a stretching method, scale bar 200 nm.*

### **1.3.1.1 BOTTOM-UP APPROACH**

A classical bottom-up approach is the synthesis of aspherical particles from organic or inorganic materials, using specific preparation conditions which enhance the formation of the non-spherical shape. For example, crystals of different metals can be grown into cubes or rods [105], or even more complex structures like dots [106]. For the production of particles with bottom-up approaches different inorganic material can be used, like gold [107, 108], silver and silica [100, 109], however the encapsulation of drug or surface modification is difficult or, in some cases, even not possible.

For the synthesis of organic aspherical systems, different polymers or self-assembly block copolymers (like self-assembly polymer made by blocks of poly(ethylene oxide), poly(ethyl ethylene) and poly(perfluoropropylene oxide)) can be used [110]. In this case, the ratio and orientation of hydrophobic and hydrophilic domains as well as the particle synthesis conditions (such as temperature, solvent, polymer concentration) have a big influence on the shape and dimension of the aspherical systems [111]. It was found that for squalene-based nanoparticles for example, where an anticancer drug was conjugate with the lipid chain, the position of the squalene moiety relative to the drug determined the shape of the self-assembly system [112].

Due to the limitation of the bottom-up techniques, such as the difficulties in the preparation of uniform batches of particle or in the encapsulation of drug or in the surface modification of the systems, these approaches are not commonly used.

### **1.3.1.2 TOP-DOWN APPROACHES**

Much progress has been made in recent years with respect to top-down approaches, and new techniques, like the template-assisted method [113-115], PRINT® technique (Particle Replication in Non-wetting Templates) [97, 116], lithography techniques [103, 117, 118], microfluidics [119-121] and stretching of spherical polymeric nanoparticles [122-124], have been optimised. In the next paragraphs, the characteristics of these preparation techniques will be explored.

#### **TEMPLATE-ASSISTED METHOD**

The template-assisted method is used to prepare rod-like or cylindrical particles, forcing a raw material or spherical particulate systems into a template, usually made with anodised aluminum oxide (AAO) and track-etched polymer membranes [115, 117]. The employed raw material or spherical particle systems are deposited inside the membrane pores using different techniques, depending on the filling material itself, such as electrochemical deposition, electrophoretic deposition or direct filling with a solution [113]. Spherical nanoparticles are usually directly filled inside the pores of the membrane (Figure 1.4 a) and through cross-linking agents [125] or the use of heat [126], the spheres are bonded together in order to form a new system with an aspherical shape (Figure 1.4 b). Alumina membranes and polycarbonate track-etched membranes are the two most common used mold. The dimension of the nanoparticles depends on the pore size of the mold and by the thickness of the membrane. The newly formed aspherical system is then removed from the membrane pores using different methods. Due to the nature of the membrane, the most common used method for the dissolving the mold are organic solvent, like tetrahydrofuran or ethyl acetate [127]. These solvents, however, limited the material that can be used for the preparation of the aspherical nanoparticles, as these organic solvents can compromise the stability of the encapsulated drug and dissolve polymeric nanoparticles used for the preparation. Other methods, like acid solution (like phosphoric acid solution [128]) sonication and pressure, have been recently tested, with better results.

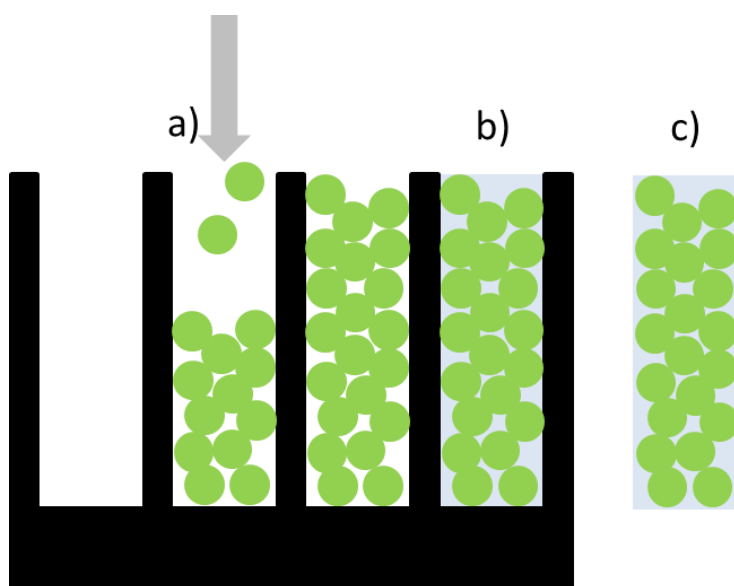


Figure 1.4 Schematic representation of the template-assisted method.

a) The pores of the alumina or polycarbonate track-etched membranes are used as template and filled with spherical nanoparticles. b) A cross-linking agent or heat are used in order to connect the nanoparticles. c) The newly formed aspherical nanoparticles are then removed from the membrane stamp and collected.

Kohler *et al.* were able to create rod-like microparticles by filling a polycarbonate membrane with spherical silica nanoparticles, and crosslinking these nanoparticles with a polyelectrolyte layer-by-layer coating. The interconnection of the spherical nanoparticulates resulted in a new system with an elongated shape [125]. Further studies have also demonstrated the possibility of using these aspherical microparticles for gene delivery and macrophage targeting [101, 129]. A different approach was used by Yin *et al.*, where polystyrene beads were used to fill the membrane and interconnection between the nanoparticles is formed using via thermal treatment at a temperature slightly higher than the glass transition temperature [126].

Protein nanotubes, made with glucose oxidase protein, have also been prepared using AAO membranes as templates, and glutaraldehyde as a cross-linking agent to hold the protein layers together [128]. Layers of protein were infiltrated through the pores of the AAO membrane and a phosphoric acid solution was used in order to dissolve the mold. It was demonstrated that not only the activity of glucose oxidase was preserved after the treatment with the acid solution, but also increased with the number of layers of glucose oxidase.

While the template-assisted method appears to result in a reproducible particle shape, a considerable limitation of this method is that only rod-like or microtubes particles can be produced. Moreover, the ability of the spherical precursor systems and eventually also any encapsulated drug to resist the harsh conditions required to dissolve the membrane and liberate the produced particles is a problem of this technique. Drug can either be encapsulated into the spherical nanoparticle or mixed with the linking agent that interconnects the spherical systems. In both cases, if the drug is able to keep its activity after dissolving the membrane, the kinetic released would be probably slow and depends on the layers of linking agent used during the preparation process.

## **LITHOGRAPHY METHOD AND PRINT®**

In the late 90's Whitesides *et al.* developed a new high-resolution and low-cost method for the fabrication of differently-shaped nanoparticles, the nanoimprinting lithography method [130]. Using an elastomeric mold produced using an elastomeric or fluorocarbon-based silane rigid template, micrometer and nanometer sized particles of various shape morphologies, like worm shape nanoparticles or nanorods, were able to be stamped. In order to produce these particles, a polymeric solution (like a polymer-coated silica or quartz substrate or polyethylene glycol (PEG) derivatives of different molecular weight) is forced into the mold, and through heat or ultraviolet (UV) stimulation, particles are formed with the exact shape and dimensions of the mold. Following this finding by Whitesides *et al.*, lithography was optimised in order to produce nanoparticles with different shape [103, 131, 132].

Lithography allows not only for the preparation of empty nanoparticles, but also for drug loading and particle surface functionalisation [103]. Roy *et al.* have used the lithography technique, to prepare cubes, triangular and pentagonal cylinders particles loaded with protein, antibodies or nucleic acids [103]. They were able for example to encapsulate streptavidin-CY5 within nanoimprinted PEG diacrylates particles by mixing the protein with the polymeric solution before the formation of the particles.

Two of the major problems regarding this technique are the excess of material during the formation of the particles and the need to detach the formed

systems from the mold. To solve the latter problem, many groups cover the surface of the mold with an extra layer of a polymer which, unlike the particle polymer component, is then dissolved with acetone [132] or with water [133].

A considerable improvement in the preparation of aspherical nanoparticles was achieved with the introduction of the previously mentioned PRINT® technique. The non-wetting properties of a perfluoropolyether (PFPE) mould are used in this technique in order to form particle systems with the shape of the template cavity. With this technique the physical properties of produced particles (such as size, shape, homogeneity) can be controlled, and surface functionalisation and drug encapsulation may also be achieved [116]. Another advantage of this technique is the possibility for encapsulation of DNA, protein or small molecules inside nanoparticles [134, 135].

Like in the above mentioned lithography methods, in the PRINT® process a liquid precursor of the nanoparticles, like monomers, is forced into the mold and through a solidification process, using techniques such as lyophilisation, solvent evaporation, thermal curing/annealing or photo-chemical cross-linking [135], the polymer chains and the particles are formed (Figure 1.5). Comparing with lithography however, the non-wetting and non-swelling properties of the mold allow for the production of single and not-interconnected particles, also on the nanoscale, without residual of the layer.

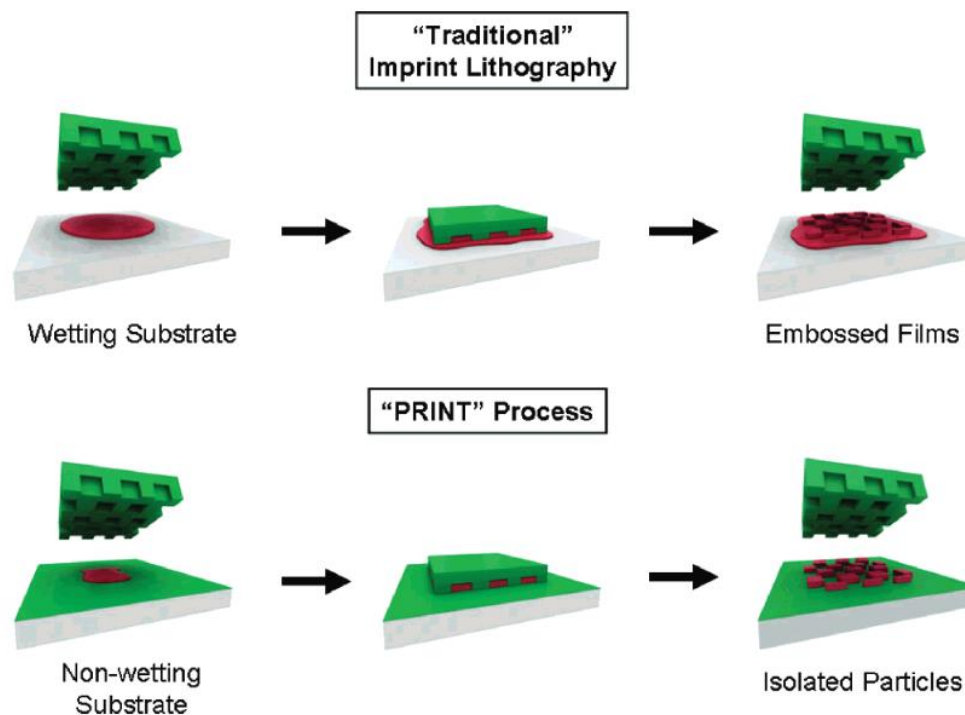


Figure 1.5 Differences between traditional imprint lithography and PRINT® technology.

With the PRINT® approach, the liquid, raw substance is forced into the cavity of a non-wetting PFPE mold, resulting in the formation of isolated particles. Figure reproduced with permission from ref.[116].

The shape of PRINT®-formed particles depends on the morphology of the mold cavity. Gratton *et al.* were able to form poly(ethylene glycol) hydrogel particles with different shapes (cubic and cylindrical) and of different sizes (micro- and nanoparticles) by changing the mold cavity [136]. Petros *et al.* were able to produce PRINT® particles also with a cubic shape, and with encapsulated doxorubicin [102]. This system was tested on cancer cells (HeLa cells) where it was demonstrated that drug release was triggered by the reducing environment of the tumor. This innovative technique can also be used to combine common and biodegradable polymers like PLGA with antigens from the influenza virus (HA antigen) in order to produce a vaccine delivery system with an aspherical shape [137]. In comparison with PLGA-based nanoparticles produced with other techniques, such as solvent evaporation method[138], the extent of HA on the particle surface was greater with the PRINT® produced formulation compared with other spherical formulation. Due to the high concentration on the surface of the



PRINT® prepared nanoparticles, PLGA-HA functionalised system was able to generate responses to influenza hemagglutinin in murine models.

For both PRINT® and lithography methods, a big problem is the purification step, used to remove the fragment of particles after the mold is removed. Moreover the material and degradation of the drug during the preparation process can limit the use these techniques. These disadvantages are however mitigated for PRINT® by the high reproducibility and flexibility, and by the continuous progress in the mold manufacturing resulting in progressively decreasing costs [135].

## **MICROFLUIDICS**

Another technique that allows the preparation of particles with a non-spherical shape is that of microfluidics. A commonly microfluidics device setup is equipped with digital micromirror devices and two perpendicular microchannels, forming a T-junction structure [139]. Inside of these two channels a solution of the polymer precursors is passing through. The position of the two channels and the minute amounts of liquid that flow through them allow the creation of monodisperse emulsion droplets, with a shape dependent on the channel geometry [140]. Through the UV light projected by the micromirror devices on the microchannel, polymerisation process is initiated and particles with a precise shape and dimension are generated. Different types of microfluidics devices have been optimised for the formation of aspherical particles, employing microchannel of different architecture [119, 141], flow focusing channels [142], or incorporating co-flow based systems [143]. Moreover, other techniques as alternative to the UV polymerisation can be used depending on the material in order to create the nanoparticles, like solvent evaporation, thermal polymerisation or chemical polymerisation reactions [97].

In general, for microfluidics approaches, the shape and size of the particles produced depends on the channel geometry. Mainly rods, ellipsoids, discs or cylinders [144-146] have been produced to date, however as a result of the optimisation of channel design, particles with more complex shapes [147] (such as flat polygonal or curved structures [104], core-shell particle [148] or bullet shapes [149]) have also been reported.

Although optimisation of microfluidics devices has allowed the creation of complex systems, constraints in terms of microchannel dimension, and therefore of produced particle systems, there are some limitations to this technique. Particles produced using microfluidics approaches generally have a size between 10 and 100  $\mu\text{m}$  [120, 121, 150]. Difficulties in scale up and the high volume of liquid required are other two disadvantages of the microfluidics approach.

## **STRETCHING METHOD**

A simple and flexible lab-scale method for the production of aspherical micro- and nanoparticles has recently been developed and optimised – the film stretching method. This approach was firstly developed by Ho *et al.* [151] and optimised by Mitragotri *et al.* [123]. The film stretching method allows for the preparation of polymeric aspherical micro- and nanocarriers of different shapes using a custom-made stretching machine [151]. In this setup, spherical polymeric particle precursors are dispersed within a polyvinyl alcohol (PVA) and glycerol film, which is then mounted onto the stretching apparatus. The entire setup is then immersed in an oil bath at high temperature or in an organic solvent [123], and the film is stretched by the application of a tensile force. Stretching of the film results in a change in shape of the contained particles. The particle systems are then fixed into their new shape by extracting the solvent or reducing the temperature as appropriate. Depending on the extent to which the film is stretched and in which dimensions, different particle shapes can be obtained, including rod-shaped or elliptical nanoparticles (major dimension between 0.35 and 2.5  $\mu\text{m}$  in length and a minor dimension between 0.2 and 2  $\mu\text{m}$ ) as well as disk systems [152].

For the film stretching method, spherical particles made by different material, like polystyrene nanoparticles or spherical systems made with shape-memory polymers, were used and stretched in order to obtain aspherical systems [98, 123, 153-157]. Examples of the application of this technique was done by Mitragotri *et al.*, who were able to produce polystyrene cylindrical nanoparticles coated with an antibody in order to target the vascular endothelium [158] and also trastuzumab coated polystyrene nanorods and nanodisks to check shape influence on growth inhibition of HER2+ breast cancer cells [159].

Although with the film stretching methods, micro- and nanoparticles with a complex shape can be easily prepared, the preparation condition (heat or organic solvent) to which the drug or protein should be exposed, it's a limitation.

### **1.3.2 INFLUENCE OF PARTICLE SHAPE ON BIOLOGICAL PROCESSES**

The importance of the shape of particles in biological interactions is clearly important, starting with the shape variation of bacteria themselves [94-96]. In the recent years the scientist community started to study this correlation and recent publications reported the influence of particle shape and design on circulation time and biodistribution and on the later interaction with cells [99, 160]. Correlation between particle shape and the efficacy of the treatment have also been studied for different types of disease like cancer.

#### **INFLUENCE OF PARTICLES SHAPE ON BLOOD CIRCULATION AND *IN VIVO* BIODISTRIBUTION**

The geometry of the particle systems plays an important role in the blood circulation and *in vivo* biodistribution.

Decuzzi *et al.* have demonstrated the difference between the trajectories in the flow channel, which simulate the blood vessel, of discoidal and spherical particles, due to the difference in particle shape [161, 162]. The forces governing the trajectory and movement of particles in the blood stream (such as van der Waals interactions, electrical double layers, steric interactions, and solvation), contribute to a different extent depending on the particle geometry. Other groups have tried to compare blood levels of aspherical systems with their spherical counterparts, concluding that the circulation time was increased by the asphericity of the particles [163-166].

Additionally, the group of Discher observed a longer circulation time of self-assembled filomicelles as compared to a spherical control [167, 168]. Surprisingly, the length of these long circulating filomicelles (approximately 8  $\mu\text{m}$ ) is equivalent

to the diameter of red blood cells. The increased circulation time for this elongated system was also seen to correlate to an improvement of efficacy, when the filomicelles were loaded with paclitaxel and tested in mice against tumor. When administered to tumor-bearing mice, accumulation of the particles inside the tumor was registered and as a consequence a reduction of the tumor size was observed.

A different approach was used by Chambers *et al.*, where the *in vivo* circulation lifetime of polystyrene disks coated with antibodies was prolonged by attaching the systems at the surface of red blood cells [169]. This new method was called “cellular-hitchhiking” [170].

Another group, Arnida *et al.*, reported for gold nanorods a longer circulation time in blood, associated with a less distribution into the liver and higher accumulation in mice with orthotopic ovarian tumors, compared with their spherical counterparts [164]. However, after 2 hours the uptake in liver of nanorods with the lower aspect ratio significantly increased comparing with more elongated rod. This indicates an influence of both geometry and size on the rate of organ dependent uptake [171].

Studies have been also conducted on the influence of the morphology of the particulate systems on the distribution and targeting of specific organs.

A biodistribution study in tumor-bearing mice has shown preferential accumulation of discoidal silica particles in the lungs, heart and spleen tissue compared to spherical, quasi-hemispherical and cylindrical particles of similar volumes [161].

The possibility of using aspherical systems for targeting of specific organs has been explored in recent years. Muro *et al.* demonstrated that elliptical disks coated with an intercellular adhesion molecule (ICAM-1) not only displayed a longer circulation time *in vivo*, but also an accumulation in the endothelial cells of lungs [172].

Interesting results were found by Gratton *et al.* regarding the different biodistribution of cuboid and rod-like nanoparticles. Biodistribution study shows that cylindrical systems were distributed mainly to the liver and the spleen when injected in healthy mice [173].

Overall, these promising results create the possibility to use the geometry of drug loaded particles for prolonging the circulation time and targeting specific organs or tissues.

## **INFLUENCE OF PARTICLES SHAPE ON CELLULAR UPTAKE INTO PHAGOCYtic CELLS**

In terms of cellular uptake, the effect of particle shape on cellular internalisation processes has also been a subject of recent research focus.

A first in-depth study into the mechanism of uptake of particles with different geometries was conducted by Herd *et al.* [100]. Silica nanoparticles with different shapes (worm-like, cylindrical and spherical) were produced and particle internalisation was studied on non-phagocytic cells (primary and immortalised epithelial cells). In order to study the specific uptake mechanism, chemical inhibitors of endocytosis were also used. Spherical particles were observed to be mostly internalised through clathrin-mediated endocytosis by phagocytic cells, whereas for elongated particles (worm and cylindrical), macropinocytosis or phagocytic mechanisms were the preferential route of uptake. Interestingly, Herd *et al.* also concluded that the phenotype of the cells plays an important role on the transport mechanism, as a variation of the uptake of both elongated and spherical particles was registered between cells of the same type but with a different phenotype.

Other studies conducted by Agarwal *et al.* hypothesised that three factors play an important role in the uptake mechanism of aspherical particles: adhesion forces between the particle surface and cell membranes; the energy required for cell membrane deformation to occur around the particle; and the extent of sedimentation of particles on the surface of cells [174].

Many studies have been conducted on the cellular internalisation of aspherical systems in phagocytic cells like macrophages [98, 153, 175, 176]. Uptake of aspherical nanoparticles (oblate ellipsoids, prolate ellipsoids, elliptical disks, rectangular disks and so-called 'UFOs') into such cells has been observed to be significantly inhibited in comparison with the spherical control, to an extent

dependent on the specific shape itself [176]. Champion *et al.* were able to demonstrate that the particle shape and its orientation relative to a macrophage cell surface are the major factors influencing the internalisation process [152, 176], and that elongated nanoparticles with a high aspect ratio (such as worm or rod-shaped particles) were internalised to a lesser extent by alveolar rat macrophages compared with the spherical control [177]. The possible orientation of the spherical and elongated systems hypothesised by Champion *et al.* is shown in figure 1.6.

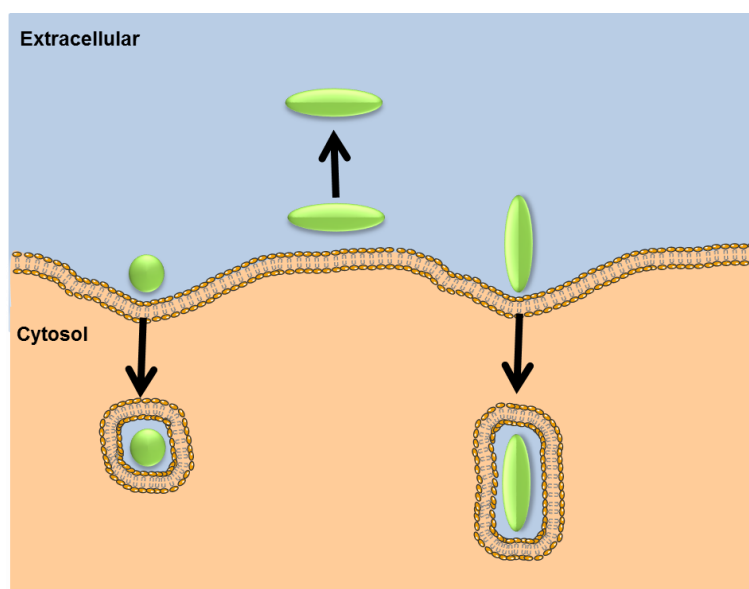


*Figure 1.6 Uptake of particles into macrophages depending on the shape and orientation.*

*The possible orientation of both spherical and elongated particles into macrophages is shown. Due to their shape and the possibilities to have only one orientation, spherical systems can always be internalised. However for the elongated formulation, only the particles with the right orientation on the cell surface can be internalised.*

A further inhibition for the uptake into macrophages was seen for elongated PEGylated polymeric or gold nanoparticles [153, 164], indicating that a combination of shape with other nanoparticle characteristics, like the material of the particle, can modulate the uptake.

Uptake of particulate systems into macrophages was seen also to be influenced not only by the geometry, but also by the size. Arnida *et al.* reported an increase after 2 hours of the uptake into liver of nanorods with the lower aspect ratio compared with uptake of more elongated rod [171].

## **INFLUENCE OF PARTICLES SHAPE ON CELLULAR UPTAKE INTO NON-PHAGOCYtic CELLS**

The influence of the shape on uptake by non-phagocytic cells has also been studied.

Qiu *et al.* were able to demonstrate a reduction of uptake of gold nanorods in a human breast adenocarcinoma cell line [178]. The influence of cell penetrating peptides on the uptake of cylindrical nanoparticles has also been studied. The effect of cell penetrating peptide was not registered for cylindrical nanostructures, however a slower escape from the cells, in order to target intracellular site, was also measured comparing with the spherical control [179].

Interesting results were found by Gratton *et al.* regarding the different uptake of aspherical particle by epithelial cells [136, 180]. Cuboid and rod-like nanoparticles, produced with the PRINT® approach, were observed to be internalised differently by HeLa cells. In particular, rod-like particles were internalised faster into HeLa cells than the cuboid, probably due to the larger surface area of these particles, which allows for more interaction between the particles and the cell membrane. The kinetics of particle uptake into HeLa cells were also registered as being dependent on particle shape, volume, aspect ratio and size.

Hinde *et al.* have also studied the advantages of nanoparticles with high aspect ratios, such as worms and rods, for delivery of doxorubicin into the nuclei of epithelial breast cancer cells, demonstrating the impact of various nanocarrier shapes on anticancer formulations [181].

A recent study from Dong *et al.* showed the influence of particle geometry on gastrointestinal transit and absorption, demonstrating that nanorods have a longer retention time in the gastrointestinal track and penetrate better into space of villi than the spherical system [182].

## **OTHER INFLUENCES OF THE PARTICLE SHAPE**

The shape of particulate delivery systems not only impacts on the mechanism and degree of cellular uptake, but also may have differential effects on other cellular aspects such as cell viability, early apoptosis, adhesion, migration and cytoskeleton formation [183]. Huang *et al.* discovered that mesoporous silica nanoparticles with a high degree of asphericity can affect cellular functions more than particles with a smaller aspect ratio [183].

A recent study from Cooley *et al.* have done a systematic studies that integrate various particle of different shape (spherical, oblate, prolate, rod) and size (micro and nano scale) to explore their wall-localization behaviour in the blood flow [184]. It was found that the amount of red blood cells in the flow have a great influence on the particle localisation in the blood vessels and that aspherical nanoparticle might be more favourable for *in vivo* vascular delivery compared to the spherical control.

### **1.3.3 ASPHERICAL FUNCTIONALISED PARTICLES**

Although uptake or biodistribution studies on nanoparticles with complex shape have been conducted, a particular interest was given to the uptake of systems with a high aspect ratio (like cylinder, worm-like shape and ellipsoid). The previously described results show the advantage of elongated particles over their spherical counterparts in terms of blood circulation, biodistribution to specific site and passive cellular uptake thanks to the particular geometry. This positive effect however needs to be further studied and as well the possibility of target moieties to increase the uptake specificity needs to be explored. The large surface area of aspherical systems could be used as scaffold for targeting moieties, increasing the available area between the carrier systems and the target and also the number of target moieties. In figure 1.7 a schematic representation of the possible interaction between spherical and aspherical nanoparticles functionalised on the surface with target moieties and the cells is given.



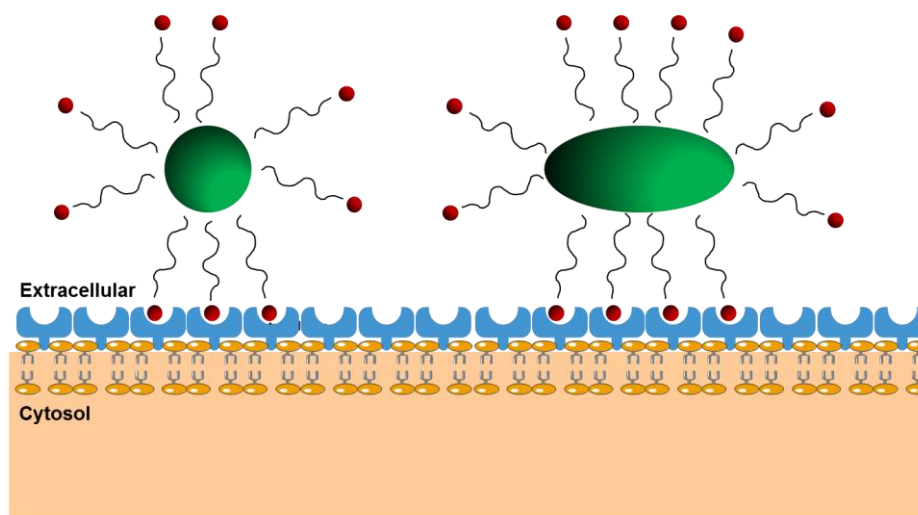


Figure 1.7 Interaction of particles with different shape and with target moieties with the cells.

Spherical and aspherical particles with targeting moieties on the surface are represented. Due to the larger surface area of the aspherical systems, the available area between the carrier systems and the target is higher compared with the spherical particle. This can make the interaction between the aspherical formulation and the cells more favourable.

Park *et al.* conducted a systematic study regarding the influence of shape and surface properties on targeting of mouse xenograft tumors, using iron oxide nanoparticles as a model system [185]. In this study, two different types of tumor-homing peptides were coated on the surface of nanoworms and nanosphere. It was found that the elongated particles have a more efficient targeting capacity comparing with the nanosphere due to the multivalent interactions between the specific moieties on the particle surface and the target cells. Other studies show that biotinylated worm micelles, produced with poly(ethylene glycol)-based diblock copolymer, can bind to biotin-receptors of smooth muscle cells [186]. Using another approach, rod-like nanomicelles with a bioactive peptide on the surface and loaded with doxorubicin were synthesised and a specific tumor binding as well as target therapeutic effect was observed *in vivo* [187].

The large surface of worm-like structure seems therefore to have a positive effect on the targeting properties of the system. That, combined with the enhanced circulation that was mentioned before, could have a great influence on the efficacy of drug-loaded worm particle.

Rod shape or cylindrical particles were also used for exploring the potential of shape combined with specific target moieties.

Using the previously described “cellular-hitchhiking”, Anselmo *et al.* were able to combine the advantages of rod shape on pulmonary delivery with the increased circulation time. This was accomplished by antibodies mediated attachment of nanoparticles to the surface of red blood cells [170]. Surface of the rod nanoparticles was therefore coated with antibodies anti-ICAM-1 and a reduction of liver and spleen uptake was observed in favour of an increased accumulation in lung endothelium.

Initial studies looking at the influence of surface functionalised cylindrical particles on uptake by non-phagocytic epithelial cells have shown that aspherical nanoparticles surface-functionalised with biotin had an enhanced uptake in human enterocytes [188] and that trastuzumab-coated nanorods had a higher uptake in breast cancer cell lines than spherical or disk-shaped nanoparticles [159]. Another study has shown the benefits of elongated particles with surface-adsorbed antibody or protein in targeting the endothelium [158], further highlighting the possibility of studying aspherical systems for delivery of chemotherapeutics.

It seems therefore clear the potential as drug delivery system of aspherical system with specific target moieties on the surface. Future studies should be oriented on exploring particles with specific target systems on the surface, like bacterial protein or viruses, and their possible application as drug delivery system. Moreover, the binding of the functionalised particles with their target should be optimised in function of the optimal number of ligand and considering the force necessary to internalise the targeted nanoparticles inside the cell [171].

## *1.4 AIM*

The importance of bacterial invasion factors for bacteria itself is well studied and known. Proteins like invasins are used by bacteria to elegantly penetrate inside host cells, where they can hide from antibiotics and natural body defences. Moreover recent studies have shown the possibility of employing bacterial proteins to enhance the cellular uptake of particles. Although the importance of bacterial proteins for the invasion bacterial process is known, other characteristics of the bacteria might influence the internalisation process, including the shape of the microorganism. As discussed so far, the value of the shape is recognised in nature, as demonstrated in structures ranging from intracellular organelles to

bacteria, although the real implication behind each shape still remains to be fully elucidated. It was largely demonstrated that shape is an important parameter also for a particulate system [98, 117]. The potential as drug delivery system of bacteriomimetic particles, with both bacterial-like shape and bacterial protein on the surface, against different type of disease, like intracellular infection, still remains to be fully explored.

The objectives of this study are related with this last question: what is the potential in drug delivery of a bacteriomimetic system with an aspherical shape and InvA497 protein conjugated on the surface? The following work was therefore focused on investigating the influence of shape on the physico-chemical characteristics of bacteriomimetic systems, using InvA497-functionalised polymeric nanoparticles with spherical and aspherical morphology, and on evaluating the potential of both spherical and aspherical drug-loaded systems for accessing and killing intracellular bacteria.

In order to address this question the objectives of thesis were:

- preparation of aspherical nanoparticles made with PLGA and the characterisation of the system;
- conjugation of InvA497 on the surface of both aspherical and spherical nanoparticles and characterisation of the systems;
- evaluation of the cytotoxicity and uptake of aspherical and spherical nanoparticles on HEP-2 cells in order to investigate the influence of shape on internalisation of bacteriomimetic system;
- incorporation of an antibiotic inside the bacteriomimetic nanoparticles and evaluation of the efficacy of the resulting system against intracellular *S. flexneri*.

## 2. ASPHERICAL NANOPARTICLES: PREPARATION AND CHARACTERISATION

The stretching machine was designed and build by Rudolf Richter from the Physics Department of Saarland University. A.C. would also like to acknowledge Dr. Chiara de Rossi for her contribution, help and support during all the experiments.

## 2.1 INTRODUCTION

Numerous types of nanoparticle formulations have been studied to date for pharmaceutical and medical applications, and have been extensively employed more specifically as drug delivery systems. The importance of the material used for nanoparticle preparation (e.g. polymeric, lipidic, organic/inorganic) is widely recognised, as this influences particle characteristics such as size, surface chemistry and mechanical properties [117, 122, 189]. However, due to the fact that typically the shape of nanoparticulate delivery systems is spherical, the true impact of another important parameter has largely been underestimated to date: the shape of nanoparticles [160, 190-192].

We can find numerous examples of the importance of non-spherical colloidal structures in biological systems, from blood cells to viruses and bacteria [94, 95]. Recent studies have shown the possibility of using non-spherical particle for altering biodistribution and circulation in the blood stream [161, 184] or influencing the interaction of the carrier with its target [152, 175-177].

Recognition of the importance and applications of non-spherical drug delivery systems has increased in recent years; as a result, significant progress has been made in the development of new methods for preparing non-spherical particulate carriers, all of which focus on simple but efficient and reproducible preparation method. As described in detail in the previous chapter, these include chemical synthesis approaches [97], template-assisted methods [125, 193, 194], PRINT® technology [97, 116], lithography techniques [103, 117], stretching of spherical polymeric particles [122-124] and other approaches involving the fabrication of carbon nanotubes and aspherical structures composed of silica derivatives [122, 195].

In the present work, the film stretching method, developed by Ho *et al.* [151] and Mitragotri *et al.* [123], was employed. This method allows for the preparation of polymeric carrier systems of different shapes using a custom-made stretching machine [151]. In this setup, spherical particles are first dispersed in a PVA and glycerol film, which is then mounted onto the stretching apparatus (see below). The entire apparatus is then immersed in an oil bath at high temperature, or in an organic solvent [123], and the film, together with its contained particles, is stretched by the application of a tensile force. Depending on the extent to which

the film is stretched and in which dimensions, different shapes of particles can be obtained - this includes rod-shaped or elliptical particles with a major axis length of 0.35-2.5  $\mu\text{m}$ , and a minor axis of 0.2-2  $\mu\text{m}$  [152]. This method has been used previously to prepare aspherical nanoparticles made of PLGA [153] or polystyrene [158, 175, 177] as well as particles consisting of more complex polymers [154].

Before being selected for use in the current work, the advantages and disadvantages of the film stretching method as compared with other methods described in literature were first evaluated, with particular respect to the size of the aspherical nanoparticles produced. Although this method exposes particles and any loaded drug to harsh conditions during the stretching process, the flexibility in size, in the nano range, and shape of produced particles, the low production costs and the possibility of using different polymers, represent the advantages of this technique.

Although the film stretching method is quite well described in literature, the characterisation of the stretched aspherical nanoparticles remains to be fully explored. Mathaes *et al.* [124] showed that techniques like flow cytometry and Vi-Cell XR Coulter Counter could be used for the characterisation of aspherical microparticles, however for aspherical nanoparticles only two techniques (asymmetric flow field flow fractionation (AF4) and dynamic light scattering (DLS)) are mentioned without a deep discussion.

The following work focuses on the development and optimisation of the preparation procedure for producing aspherical PLGA nanoparticles from spherical precursors. In particular parameters like the influence of the thickness of the film, in which the spherical nanoparticles were immobilised for stretching, on the size and shape of the final produced aspherical nanoparticles was examined. Size and morphological analysis of the aspherical nanoparticles were conducted using techniques including scanning electron microscopy (SEM), DLS and AF4, in order to determine the most suitable method for the analysis of aspherical nanoparticles and for the comparison with the spherical precursor.

## **2.2 MATERIALS AND METHODS**

### **2.2.1 MATERIALS**

For the nanoparticle preparation, PLGA (Resomer RG 503 H, lactic/glycolic acid 50/50 wt/wt; MW 40 300 Da; inherent viscosity 0.41 dl/g; from Evonik Industries AG, Darmstadt, Germany), PVA (Mowiol<sup>®</sup> 4–88, Kuraray Specialties Europe GmbH, Frankfurt, Germany), glycerol and mineral oil (Sigma-Aldrich, Steinheim, Germany) were used. Trehalose, employed as a cryoprotectant for freeze drying, was sourced from Sigma-Aldrich (Sigma-Aldrich, Steinheim, Germany). For the size analysis sodium dodecyl sulfate (SDS, Sigma-Aldrich, Steinheim, Germany) was used. All the other solvents and chemicals used were of at least analytical grade, and distilled de-ionised water with conductivity of less than 18.2 MΩ/cm at 25 °C was employed.

### **2.2.2 PREPARATION OF SPHERICAL NANOPARTICLES**

Spherical PLGA nanoparticles were prepared using the double emulsion method [196, 197]. Briefly, PLGA was first dissolved in 2 ml ethyl acetate (EtAch) to give a 20 mg/ml solution. A 400 µl quantity of water was then added drop-wise to the PLGA/EtAch solution, with simultaneous sonication at 12 W for 30 s (Digital sonifier 450, Branson Ultrasonic Corporation, Danbury, USA), in order to create the first water-in-oil (w/o) emulsion. The w/o emulsion was then poured into 4 ml of 2% (w/v) PVA solution, and the two phases were sonicated again (12 W for 30 seconds) to create a w/o/w double emulsion. After adding 15 ml of water, the formed double emulsion was left to stir overnight to allow for solvent evaporation. Following overnight stirring, the PVA excess was purified from the nanoparticle dispersion by centrifugation (10 000 g for 12 minutes at 12 °C). Nanoparticle suspensions were stored at 4 °C for maximum 1 week before further use, or were freeze dried (Alpha 2-4 LSC, Christ, Osterode am Harz, Germany) with 0.31 mg/ml of trehalose as cryoprotectant and stored at room temperature.

### 2.2.3 PREPARATION OF ASPHERICAL NANOPARTICLES

Aspherical nanoparticles were prepared in accordance with the film stretching method previously described by Ho *et al.* [151] and Champion *et al.* [123]. Briefly, 0.1% (w/v) of spherical nanoparticles prepared as described above was mixed with a solution of 10% PVA and 2% glycerol (v/v), and the resulting dispersion was dried overnight in a mould in order to create a flat, dry film. The film was then cut into rectangular sections (2x3 cm), each of which in turn were immobilised in an in-house fabricated stretching machine, and stretched after immersion in oil and heating (Figure 2.1). The film thickness was measured with a surface testing instrument MiniTest 3100 (ElektroPhysik Dr Steingroever GmbH & Co. KG, Cologne, Germany). The metal structure of the machine is composed of two main parts (Figure 2.1a): the upper part, consisting of a rotating screw and a metal cable, and the lower part, consisting of a moveable clamp together with a base-mounted fixed clamp. Film sections are immobilised between the moveable and fixed clamps, as shown in Figure 2.1b. The operator then applies a mechanical force by turning the rotating screw. Transfer of this force down the metal cable results in upward movement of the moveable clamp, and stretching of the immobilised film together with its component nanoparticles



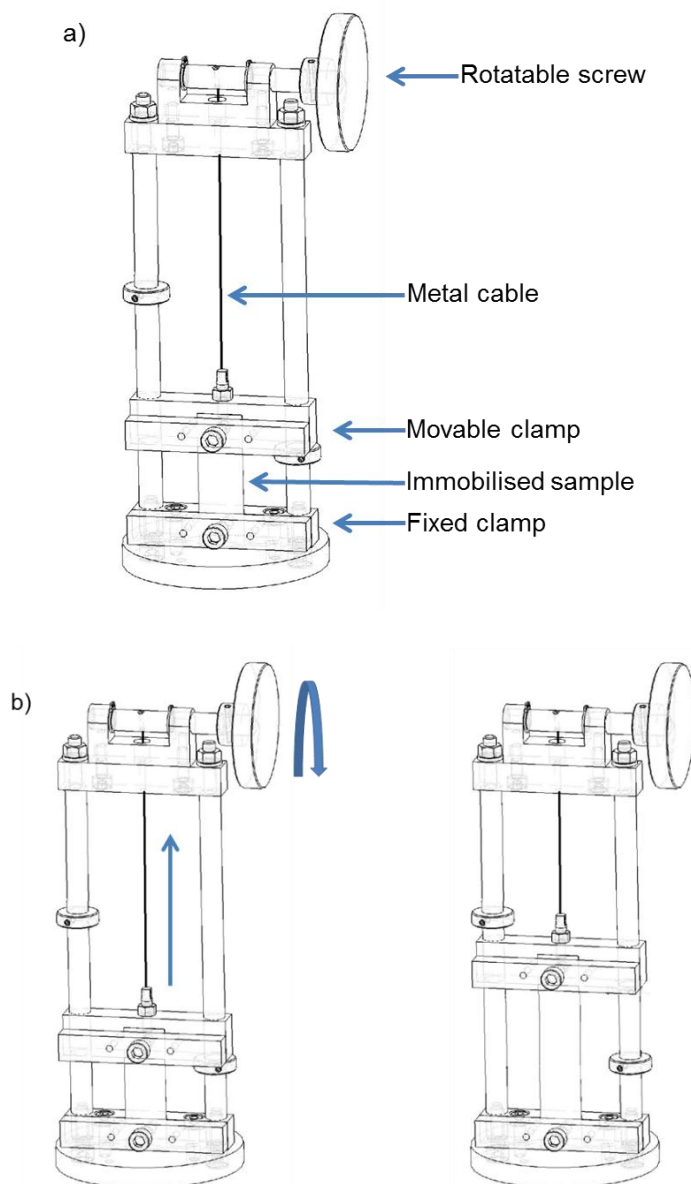


*Figure 2.1 Schematic picture of the stretching machine.*

*a) important parts (fixed and movable clamp for the particle containing film, rotatable screw and the metal cable) of the machine are shown; b) through the rotation of the screw and the movement of the upper clamp, the film is stretched.*

In the current work, following mounting of a film section, the stretching machine was immersed in mineral oil at 54 °C and allowed to equilibrate for 30 s. The rotating screw was then turned at a constant rate over a period of 90 s until the film was elongated to twice its original length. Two small stops on the machine sides allowed the operator to stop at the stretching endpoint. Through the applied thermomechanical stress, the shape of spherical nanoparticles is transformed into

an ellipsoid (Figure 2.2). The elongation entity was adjusted so that the major side of the rectangular section of the film was elongated to twice its original length. This procedure was repeated in order to stretch all film sections.

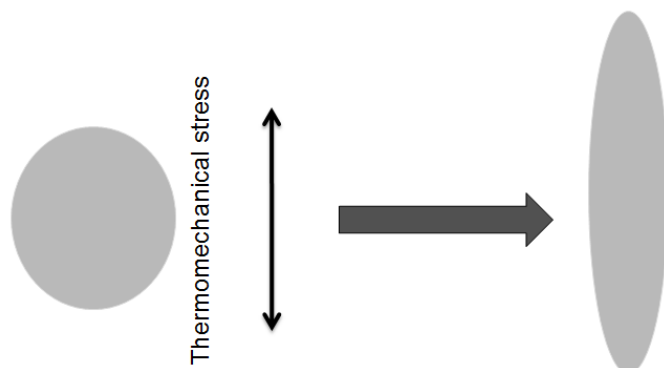


*Figure 2.2 Schematic representation of the aspherical nanoparticle preparation procedure. A thermomechanical stress is applied to the spherical PLGA nanoparticles immobilised in the PVA film, in order to recover nanoparticles with an aspherical shape.*

Following stretching, film sections were collected, allowed to cool, and washed with isopropanol to remove excess oil. Films were then dissolved in water to release the stretched nanoparticles, which were purified using multiple cycles of high speed centrifugation (20 min, 16 000 g, 12 °C) followed by 5-6 cycles of centrifugation (10 min, 1 179 g, 4 °C) with Centrisart tubes with a 300 kDa molecular weight cut off (MWCO) membrane (Sartorius, Göttingen, Germany). Aliquots of purified aspherical nanoparticles (1 ml volume) were stored at 4 °C until further characterisation.

#### **2.2.4 IMAGING OF NANOPARTICLES**

The morphology of both spherical and aspherical nanoparticles was characterised using SEM (Zeiss EVO HD 15, Carl Zeiss AG, Oberkochen, Germany) at an accelerating voltage of 5 kV. Samples were diluted and after drying overnight sputter coated (Quorum Q150R ES, Quorum Technologies Ltd, Laughton, United Kingdom) with gold, prior to analysis.

## 2.2.5 ANALYSIS OF SEM PICTURES

For aspherical nanoparticles, SEM images were then used to calculate common shape descriptors, such as major and minor axis length, aspect ratio (AR), Feret's diameter and minor Feret's diameter (Figure 2.3) using ImageJ software (Fiji).

Following fitting of aspherical nanoparticles as ellipsoid or spheroid structure, the major and minor particle axes were measured as the distances a-b and c-d respectively (Figure 2.3a). The AR of aspherical nanoparticles was calculated as the ratio between the major and the minor axis length. In addition, the Feret's diameter and minor Feret's diameter were calculated for aspherical nanoparticles. The Feret's diameter is defined as the distance between two parallel tangents of the particle at an arbitrary angle, also known as the maximum caliper (Figure 2.3b). The minimum caliper is defined as the minor Feret's diameter.

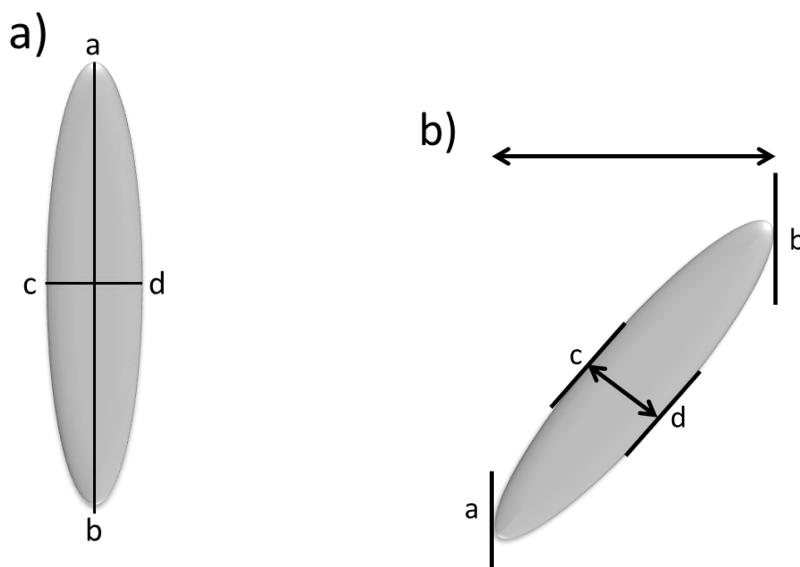


*Figure 2.3 Schematic representations of the shape descriptors used to characterise aspherical nanoparticles .*

*a) when the shape of nanoparticle was fitted as ellipsoid, major (a-b line) and minor (c-d line) axis was measured; b) Feret's diameter (a-b line) and minor Feret's diameter (c-d line) were also measured..*

Using ImageJ software the major and minor axis distribution were found and the D10, D50 and D90 were extrapolated from the cumulative intensity. The cumulative intensity of the major or minor axis was calculated expressing the size intensity as percentage. D10, D50 and D90 parameters are defined as the

diameter value below which 10% (for D10), 50% (for D50) or 90% (for D90) of the particle population lies.

## **2.2.6 DYNAMIC LIGHT SCATTERING**

Size and polydispersity index (PDI) of spherical and aspherical nanoparticle dispersions was performed by DLS using a Zetasizer Nano (Malvern Instruments Ltd, Worcestershire, United Kingdom).

## **2.2.7 ASYMMETRIC FLOW FIELD FLOW FRACTIONATION**

A Wyatt Eclipse AF4 system (Wyatt Technology, Dernbach Germany), combined with an UltiMate<sup>®</sup> 3000 system (Thermo Fisher Scientific Inc., Waltham, Massachusetts, USA) equipped with UV detection, a Wyatt Down Eos multi-angle laser light scattering (MALLS) detector (Wyatt Technology, Dernbach Germany) and a Wyatt Quasi-Elastic-Light-Scattering (QELS) detector (Wyatt Technology, Dernbach Germany), was used. For the analysis of aspherical nanoparticles, the large separation channel was equipped with a 30 kDa cut-off regenerated cellulose membrane. A 500  $\mu$ l volume of aspherical PLGA nanoparticles was injected. The focusing period was 7 min with an applied focus flow of 1 ml/min. The detector flow was set to 0.2 ml/min in order to have a laminar flow of the mobile phase (0.5% SDS in water with pH adjusted to 9.5). This flow creates a parabolic flow profile of the injected nanoparticles, with a faster stream in the middle of the channel as compared with near the channel walls. A cross flow was kept constant at 0.11 ml/min in order to drive the sample toward the channel bottom. For smaller particles, diffusion serves as a stronger counteracting motion than it does for larger particles - as a consequence, larger particles accumulate closer to the channel bottom and elute later. Samples are therefore separated according to their hydrodynamic size with smaller nanoparticles eluting before larger ones.

All samples were measured in triplicate. Particle diameters were calculated using the Astra software (version 5, Wyatt Technology).

## 2.2.8 STATISTICAL ANALYSIS

Where appropriate, data are expressed as mean  $\pm$  standard deviation (SD). The data was analysed using SigmaPlot Version 11 (Systat Software Inc., San Jose, CA, USA). Comparisons between groups were performed using Student's *t* test (two-sided) or ANOVA with post-hoc Bonferroni adjustment for experiments with more than two subgroups. Results were considered statistically significant at *p* values  $<0.05$ .

## 2.3 RESULTS AND DISCUSSIONS

Spherical nanoparticles prepared by a double emulsion method were embedded in a PVA film and stretched as described above in order to prepare aspherical nanoparticles. PLGA was selected as a particle material for its relatively low glass transition temperature ( $T_g$ ) of approximately 45 °C [198], important for the film stretching method due to the more deformability of the polymeric material above that temperature. In the present work, the preparation of aspherical nanoparticles was optimised and the produced system was characterised. Aspherical nanoparticles were imaged using SEM and the obtained pictures were analysed using ImageJ software, in order to compare imaging analysis and data obtained from characterisation with light-based technique, like DLS and AF4. The chief objective of this work was to explore the characterisation of PLGA aspherical nanoparticles, looking in-depth at the effect of preparation parameters on size distribution and evaluating the most common analytical techniques used for the characterisation of spherical nanoparticles. Although similar work has been conducted by Mathaes *et al.*, only the characterisation of stretched commercially available polystyrene microparticles was conducted and discussed, with a marginal interest on the stretched 40 nm nanoparticles.

After preparing spherical PLGA nanoparticles, aspherical systems were prepared using the film stretching method. As described in literature, a mechanical stimulus was applied to force a change of the nanoparticle shape from spherical to aspherical, taking advantage of plastic state of the PLGA and its deformability when heated above the  $T_g$ . Spherical PLGA nanoparticles were therefore immobilised in a PVA film and the cut sections were immersed into a mineral oil

bath warmed to 54 °C, after fixation on the previously described stretching device. This temperature was selected to be higher than the  $T_g$  of PLGA [198] but lower than the  $T_g$  of PVA (around 85 °C). The PVA was removed by centrifugation and the collected nanoparticles were first imaged using SEM (Figure 2.4). Spherical nanoparticle precursors were also imaged, for comparison.

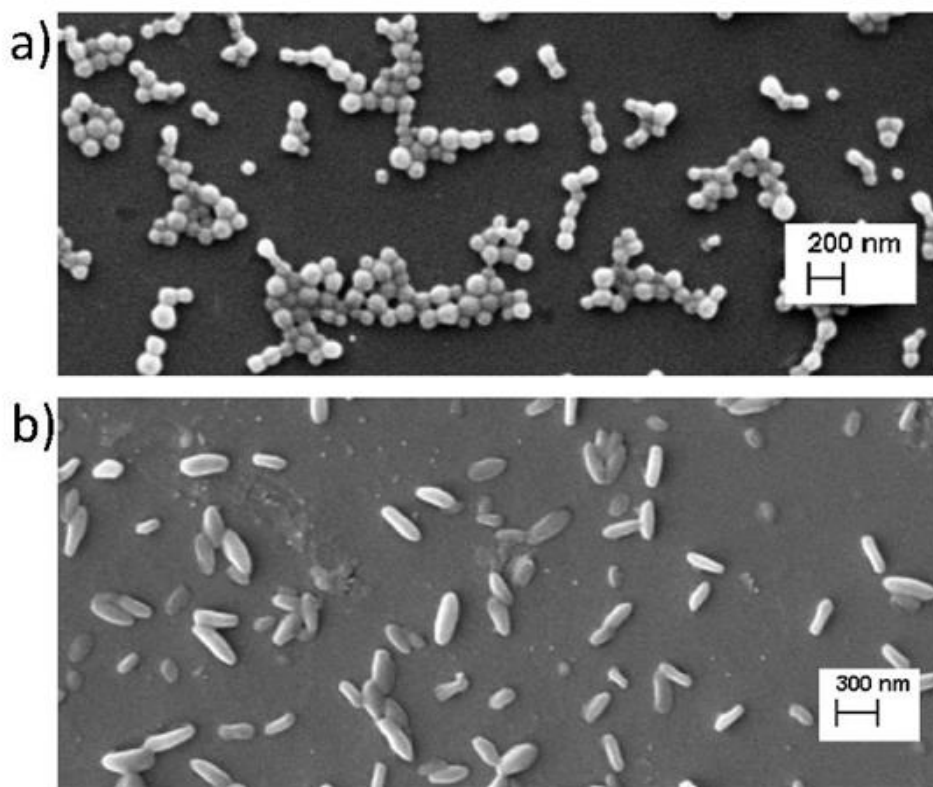


*Figure 2.4 Comparative morphology of spherical and aspherical nanoparticles. SEM image of spherical nanoparticles (a), and aspherical nanoparticles produced from spherical precursors using the film stretching method (b).*

As shown in figure 2.4, the spherical and aspherical shape of the two formulations was confirmed. The asphericity of the nanoparticles in figure 2.4b is clearly seen from the SEM picture. Only small residual of PVA was found in the aspherical nanoparticle solution.

Using DLS, the hydrodynamic diameter of both spherical and aspherical nanoparticle dispersions was analysed based on the light intensity fluctuations of scattered light (Figure 2.5). Although a significant difference between the mean diameters of precursor spherical nanoparticles and aspherical nanoparticles was found using DLS, the 240 nm hydrodynamic

diameter measured from the aspherical system with DLS does not correspond with the major length observed with SEM pictures. Instead, a measure of 300 nm was rather found. This discrepancy in results is likely due to the DLS technique limitations, which assumes that the detected particles have a spherical shape [100]. Also the observed increase in the measured PDI and in its variability for aspherical nanoparticles compared with the same parameter measured for the spherical formulation is likely related with the technique limitations. These limitations make DLS not suitable for measuring the size of aspherical nanoparticles. Mathaes *et al.* [124] used the hydrodynamic radius, obtained with DLS, to characterise the size parameter of 40 nm stretched polystyrene nanoparticles. Although the current work does not exclude that a diameter obtained with DLS could be used to distinguish between spherical and aspherical nanoparticles, more accurate shape descriptors or techniques are needed for the characterisation of aspherical nanoparticles.

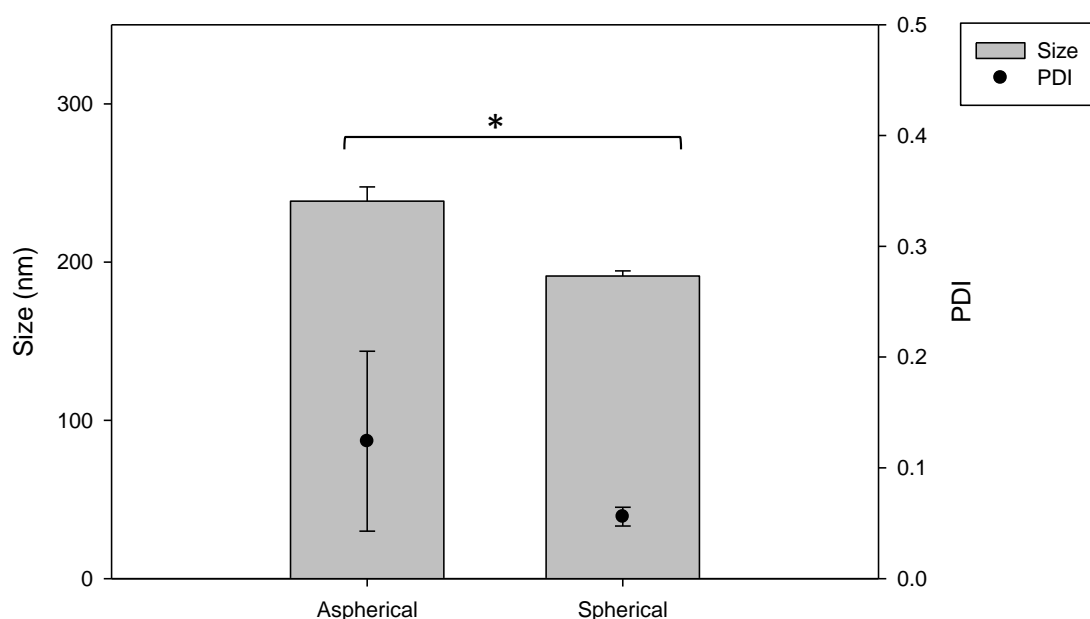


Figure 2.5 Size and PDI of aspherical and spherical PLGA nanoparticles.

Size, represented by grey bars, and PDI, represent by black data points, of aspherical and spherical nanoparticles. ( $n=3$ ).  $*=p<0.05$

Following these initial investigations, in which SEM image analysis was determined to give more accurate and in-depth sizing information with respect to produced aspherical nanoparticles, the stretching procedure used to prepare the

aspherical systems was optimised (with respect to the parameters of stretching rate, oil bath temperature and concentration of film-embedded nanoparticles). In particular the influence of the film thickness on the size distribution of resulting aspherical nanoparticles was investigated via SEM image analysis.

The film thickness, according to Champion *et al.* [123], is a key parameter influencing the shape and size of produced aspherical particles. To have a more in-depth look on this, after producing the film, the thickness of the cut sections was measured using MiniTest 3100. The thickness of film sections was found to fall into two broad categories; sections were therefore divided into two groups (between 50  $\mu\text{m}$  and 90  $\mu\text{m}$  and between 90  $\mu\text{m}$  and 120  $\mu\text{m}$ ) prior to stretching. After separately stretching film sections from each group, and recovering and purifying the stretched nanoparticles, the shape descriptors as outlined in Figure 2.3 were calculated (Table 2.1). As mentioned, two types of shape descriptors given by the ImageJ software were selected to describe the aspherical nature of the nanoparticles. Feret's diameter and minor Feret's diameter were measured as the longest and the shortest distance between two parallel tangents of the particle at an arbitrary angle, respectively; in addition, due the similarity between the observed shape of aspherical nanoparticles and an ellipsoid, the major and minor axis and AR were also considered as appropriate shape descriptors. The objective of employing these various measures was to compare shape descriptors (Feret's diameters), where the nanoparticles are directly measured, with shape descriptors (major and minor axis), where the nanoparticles are fitted to a known shape, and therefore an interpolation error can be made. This latter method has the advantages of giving additional information such as the AR and the volume of the nanoparticles (see chapter 3). In cases where the shape of aspherical nanoparticles perfectly fits with the dimensions of an ellipsoid, the Feret's diameters and the major and minor axis measures show a high degree of similarity; in contrast, a less accurate fit to an ellipsoidal shape will result in high degree of difference between Feret's diameters and major and minor axis measures. In this work, the longest axis of the nanoparticles (as measured by both major axis and Feret's diameter) and the shortest axis (measured by both minor axis and minor Feret's diameter) were measured as being approximately 300 nm and 130 nm respectively, indicating that the two shape descriptors are equivalent. Surprisingly, no significant differences in shape parameter were found for



aspherical particles produced by stretching of film sections of 50-90  $\mu\text{m}$  thickness as compared to 90-120  $\mu\text{m}$  thick sections. This indicates a lack of influence of the film thickness on the stretching procedure, and demonstrates that the nanoparticles have an ellipsoidal shape. Using the major and minor axis values also the asphericity of the nanoparticles was calculated, with an AR of around 2.5 found for both groups (Table 2.1).

As no difference was found between the major axis and the Feret's diameter or between the minor axis and the minor Feret's diameter and due to the ellipsoidal shape evidenced by SEM images, for future characterisation of the aspherical nanoparticles the major and minor axis were chosen as representative shape descriptors.

*Table 2.1 Shape descriptors of aspherical nanoparticles.*

*Shape descriptors were measured with ImageJ software, as a function of the thickness of the film in which nanoparticles were embedded for stretching. Data represents mean  $\pm$  SD (n=2 batches, each consisting of approximately 200 nanoparticles).*

Film thickness	50-90 $\mu\text{m}$	90-120 $\mu\text{m}$
Minor Feret's diameter (nm)	145.38 $\pm$ 12.09	126.29 $\pm$ 9.27
Feret's diameter (nm)	320.29 $\pm$ 21.54	299.65 $\pm$ 24.65
AR	2.43 $\pm$ 0.03	2.62 $\pm$ 0.4
Minor axis (nm)	128.44 $\pm$ 5.90	113.35 $\pm$ 8.6
Major axis (nm)	312.24 $\pm$ 17.68	294.19 $\pm$ 26.84

With this in mind, the distribution of aspherical nanoparticle major and minor axis measurements was further investigated (Figure 2.6). To define the distribution width, D10, D50 and D90 values were extrapolated from the cumulative intensity. The D50 is defined as the diameter value below which half of the particle population lies. Similarly, 90% of the particle population lies below the D90, and 10% of the population lies below the D10.

Distributions of aspherical nanoparticles show that only 10% of the population has a major axis below 180 nm and a minor axis below 80 nm. Instead the 90% of the produced nanoparticles has a major axis below 480 nm and a minor axis below 157 nm. The D50 extrapolated from both major and minor axis distributions was found around 310 nm for the major axis and 118 nm for the minor axis.

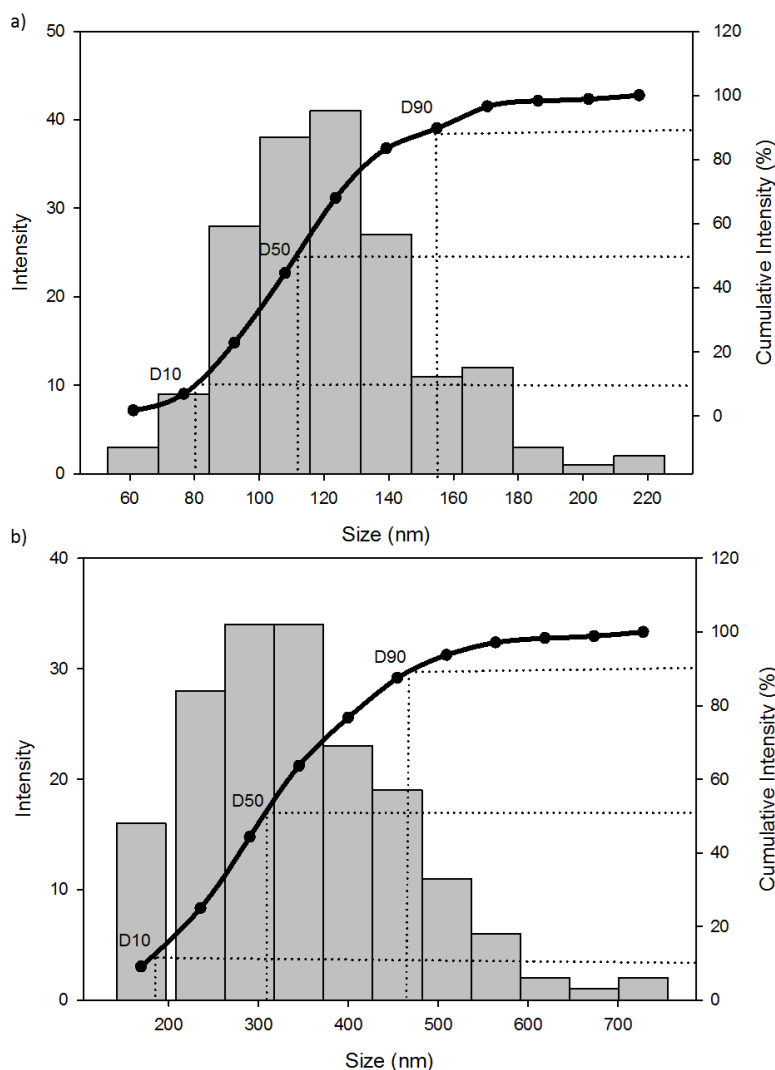


Figure 2.6 Distribution of shape descriptors.

Major (a) and minor (b) axis distributions of the aspherical nanoparticles are shown, as well as D10, D50 and D90 values for each descriptor. Analysis was done from data acquired from SEM images using ImageJ software (two batches,  $n=5$  images, each image containing 40 nanoparticles).

An alternative method to characterise aspherical nanoparticles, as described by Mathaes *et al.* [124] and also by other authors [199, 200], is via an AF4 system coupled with MALLS and QELS detectors. This technique allows a high-resolution separation depending on the size of the nanoparticles, within a very

thin flow stream against which a perpendicular force field is applied [201]. After the flow separation, the size of the nanoparticles is detected by two different detectors, MALLS and QELS, and a chromatogram illustrating the size parameters of nanoparticles as a function of their elution time is obtained. Moreover using the AF4 software approximation, the shape of the nanoparticles can be approximated to a rod and the rod length with its distribution can be extrapolated. This technique was therefore also employed in the current work for analysis of aspherical nanoparticles. Spherical nanoparticles were additionally analysed, for comparison purposes.

Although Mathaes *et al.* [124] were able to show a difference in the peak of the chromatograms and elution time of commercially available, 40 nm spherical and 3 times stretched aspherical nanoparticles, this was not found to be the case in the present work for spherical and aspherical PLGA nanoparticles. These contrasting findings are thought to be a result of the difference in nanoparticles material (polystyrene vs PLGA), fabrication and elongation (two or three times elongated) during the stretching procedure, and the important impact on the detection of the AF4 (Figure 2.7a). In the current work, the Astra software was used for data analysis and a rod model was selected in order to determine the length and size distribution of aspherical nanoparticles (Figure 2.7b). No difference in the curve for size distribution was found for three different batches of analysed aspherical particles, demonstrating the reproducibility of the film stretching method. Moreover the rod length was compared with the major axis measure extrapolated from SEM images, as discussed above (Figure 2.7c). No significant difference was found between the two parameters. Although it was not possible to differentiate from the chromatogram the shape of the nanoparticles, AF4 could be used to determine the size of PLGA aspherical nanoparticles.

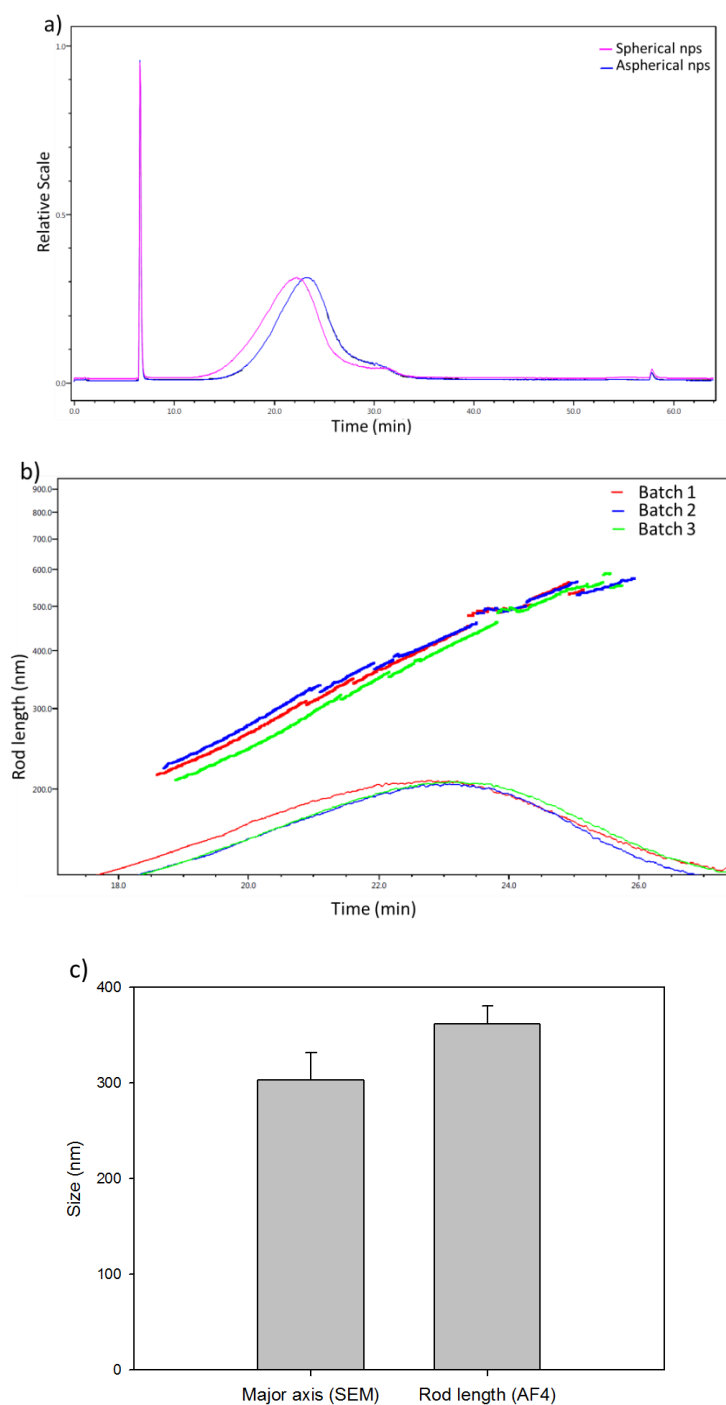


Figure 2.7 AF4 chromatograms of spherical and aspherical nanoparticles, and comparison of shape descriptors measured with AF4 and SEM image analysis.

Chromatograms (a) of aspherical and spherical nanoparticles (NPs), with (b) the rod length distribution of three independent batches of aspherical nanoparticles extrapolated using the ASTRA software shown; (c) comparison between the major axis measurement of aspherical nanoparticles as extrapolated from SEM images, and the rod length parameter of aspherical nanoparticles as determined with AF4. Results represent the mean  $\pm$  SE ( $n=3$ ).

To summarise, three different techniques (DLS, SEM and AF4) were used to characterise the produced aspherical nanoparticles, in order to identify a method which would provide a quick and easy means to differentiate between spherical and aspherical nanocarriers, while also providing an accurate and robust measure of aspherical particle shape parameters.

In considering the advantages and disadvantages of each technique, the expensive instrumentation and time required for the SEM image analysis approach are compensated for by the ability to actually visualise the size and shape of the particle sample, which is one of the fundamental requirements for the confirmation and characterisation of an aspherical system. Use of a readily available and rapid technique like DLS would reduce the cost and the analysis time, however due to the aspherical nature of the system this technique cannot be considered to give a reliable size result. The automatic approximation to a sphere is a limitation for the analysis of aspherical nanoparticles. Unless this problem is overcome, DLS technique could potentially be used only to distinguish between spherical precursors and stretched aspherical nanoparticles. The true extent of the shape change however cannot be explored in detail with sufficient accuracy. This problem could be avoided in the AF4 method using the appropriate software approximation; however, as it is evident from the similarity in the obtained chromatograms of eluted spherical and aspherical nanoparticles, AF4 analysis would in itself need to be supported by another technique, such as SEM.

## *2.4 CONCLUSION*

In this chapter, a method to produce aspherical nanoparticles from spherical precursors was employed and optimised. Various methods were then investigated for the characterisation of aspherical nanoparticles and an analytical method capable of differentiating between the shape of aspherical and spherical nanocarriers was identified.

For particle preparation, the film stretching method was selected and a stretching apparatus was subsequently fabricated. A procedure for obtaining aspherical nanoparticles by stretching of spherical precursors was then optimised, in order to obtain aspherical particles in the nano-size range. Physical characterisation of the produced aspherical nanoparticles was conducted via

microscopic analysis (SEM and ImageJ) as well as light-based techniques (DLS and AF4), in order to select the best analysis method. The possibility to produce a suitable shape descriptor (such as major axis or rod length) and the possibility to distinguish between the stretched aspherical and precursor spherical nanoparticles were the two main criteria for choosing the analysis methods. DLS was determined to be inappropriate for characterisation of the produced aspherical systems due to its limitation on the shape recognition capability; AF4 could potentially be used for determination of the major axis length of the aspherical nanoparticles, but its use was limited by the small amount of data that can be extrapolated and the impossibilities of distinguish between spherical and aspherical particles; the use of SEM imaging in conjunction with ImageJ analysis is considered the most accurate and descriptive technique for visualising and measuring shape parameters of the aspherical nanoparticles.

### 3. PREPARATION AND CHARACTERISATION OF BACTERIOMIMETIC NANOPARTICLES

The script code for 3D model and calculation of the surface occupancy were conducted by Dr Martin Empting from the Drug Design and Optimisation department of HIPS.

Parts of this chapter have been published in *Pharmaceutical Research*, with the title "Aspherical and Spherical InvA497-functionalized Nanocarriers for Intracellular Delivery of Anti-infective Agents"

### 3.1 INTRODUCTION

While delivery of anti-infective drugs via the oral route is an attractive and logical option for the treatment of gastrointestinal infections, the intracellular localisation of some pathogens, including particular species of bacteria, may act to limit the efficacy of orally-administered therapeutic agents. In the case of intracellular infections where the bacteria are hidden inside the host epithelial cells, encapsulation of drug candidates into nanoparticles functionalised with specific biomolecules (a strategy also referred to as active or ligand targeting) is a potential way to increase the treatment efficacy. In particular, by using biomolecules which have bioadhesive or invasive properties, the cellular uptake of nanoparticles together with their anti-infective cargo can be enhanced [91, 202].

In recent years bacterial molecules and even bacterial invasion systems have been explored as new strategies for active targeting. It has been demonstrated for example that *Salmonella*-like nanoparticles, obtained by coupling *Salmonella enteritidis* flagellin (the main component of the flagellar filament and normally used by this bacteria to colonise epithelial host cells) on nanoparticles, could overcome the gastrointestinal mucosal barrier and penetrate into the intestinal tissue in rats [203].

Proteins normally expressed on the surface of bacteria, and used by the bacteria themselves to overcome the mammalian mucosal barriers or to invade mammalian cells, have also been coupled on the surface of nanoparticles, to produce what are commonly known as bacteriomimetic systems [204]. Invasin for example, an invasion protein normally expressed on the surface of *Yersinia* spp., was one of the first bacterial proteins used in order to produce these bacteriomimetic systems, via coupling onto latex beads [90]. The uptake and the influence of the invasin concentration on the surface of beads were studied, showing the advantages of having such a protein on surface of the beads on the cellular uptake of the system. While these proteins can be used in their entirety, fragments of bacterial proteins may also be employed to enhance nanoparticulate system uptake. In this respect, it has been demonstrated that a C-terminal fragment of invasin, also known as InvA497 [60], can improve cellular uptake when covalently coupled onto liposomes or PLGA nanoparticles [90, 92, 205]. As demonstrated by Labouta *et al.*, liposomes with InvA497 covalently coupled onto



the surface showed promising results, improving the uptake of the liposomes in comparison with the formulation without InvA497 [90].

The bacteriomimetic systems produced so far, such as InvA497-functionalised liposomes or *Salmonella*-like nanoparticles, are able to mimic only the way in which bacteria penetrate inside mammalian cells (or in some cases, such as through the use of lipid-based particle systems, the composition of bacteria), however no studies on other nanoparticle parameters, such as shape, have been conducted. Although rod-like bacteria are quite common in nature, in particular in enteropathogenic bacteria such as *Yersinia* and *Shigella* spp. as well as *Escherichia coli*, to the best of the author's knowledge no studies have yet been conducted using aspherical particle systems with bacterial moieties on the surface, and it remains unknown whether any correlation between carrier system shape and the uptake mechanism typical of some bacteria exists.

In order to study and explore unsolved questions regarding the importance of shape on surface functionalised nanoparticle on uptake into epithelial cells, polymeric systems with an aspherical shape, functionalised with biomolecules have been recently produced and studied. Polymeric nanoparticles surface-functionalised with specific ligands, such as biotin or a trastuzumab antibody, have been recently prepared and studied for particular application [159]. These molecules were used as model proteins due to their well-known and well-characterised mechanism of action. Such studies have not however been extended to the employment of bacteria-derived molecules, like InvA497, in order to access intracellular pathogens.

The idea of using a bacteriomimetic system, which has an aspherical shape typical of some bacteria and penetrates inside the mammalian cells using the way of bacteria, could create an interesting outlook for developing innovative drug delivery systems which is able to kill intracellular bacteria.

Therefore, the following work was focused on the method for coupling InvA497 on the surface of aspherical and spherical nanoparticle and characterisation of such bacteriomimetic systems. Aspherical and spherical (as comparator) PLGA nanoparticles were functionalised with InvA497 using an optimised coupling procedure and afterwards characterised for their morphology. The surface functionalisation was optimised and the covalent coupling of InvA497 on the surface of both aspherical and spherical was probed using IR spectroscopy.

After measuring the size of aspherical and spherical systems, a 3D model was generated in order to study the InvA497 distribution on the surface of aspherical and spherical nanoparticles.

## **3.2 MATERIALS AND METHODS**

### **3.2.1 MATERIALS**

For the preparation of nanoparticles, PLGA Resomer RG 503 H (lactic/glycolic acid, 50/50 wt/wt; MW 40 300 Da; inherent viscosity 0.41 dl/g; from Evonik Industries AG, Darmstadt, Germany), fluoresceinamine isomer I and N'-(3-Dimethylaminopropyl)N-ethylcarbodiimide HCl (FA and EDC respectively, both from Sigma-Aldrich, Steinheim, Germany) were used.

PVA (Mowiol® 4–88, Kuraray Specialties Europe GmbH, Frankfurt, Germany), glycerol and mineral oil (both from Sigma-Aldrich, Steinheim, Germany) were used for the stretching procedure.

For the coupling procedure bovine serum albumin (BSA) and 4-(4,6-Dimethoxy-1,3,5-triazin-2-yl)-4-methylmorpholinium chloride (DMTMM) from Sigma-Aldrich (Steinheim, Germany) were used. To quantify the amount of InvA497 protein a bicinchoninic acid (BCA) kit was utilised (QuantiPro™; Sigma-Aldrich, Steinheim, Germany).

All the other solvents and chemicals used were of at least analytical grade, and distilled de-ionised water with conductivity of less than 18.2 MΩ/cm at 25 °C was employed.

### **3.2.2 PREPARATION OF FLUORESCENTLY LABELLED NANOPARTICLES**

To enable fluorescent labelling of nanoparticles, fluoresceinamine-PLGA (FA-PLGA) was prepared according to Weiss *et al.* and Horisawa *et al.* [206, 207]. Briefly 3.07 g of PLGA, 0.0583 g of FA and 0.0408 g of EDC were dissolved in 30 ml of acetonitrile and incubated at room temperature (RT) for 24 h. The resulting FA-PLGA was precipitated by addition of water and separated by centrifugation (20 min, 16 000 g, RT; Rotina 420R, Hettich Zentrifugen, Tuttlingen, Germany). The excess of FA and EDC was then removed by repeated dissolution of the mixture in acetone and precipitation in ethanol, followed by centrifugation (10 min, 16000 g, RT) in order to sediment the formed FA-PLGA. The final product was then lyophilised overnight and stored in the freezer at -20 °C.

Fluorescently labelled nanoparticles (spherical = S, aspherical = A) were then prepared as described in Chapter 2, using a mixture of FA-PLGA and PLGA (0.25: 0.75 weight ratio).

### **3.2.3 NANOPARTICLE SURFACE FUNCTIONALISATION**

PLGA nanoparticles were surface functionalised with InvA497, a 497 amino acid fragment of the C-terminus of invasin, an invasion protein of *Y. pseudotuberculosis*, which was extracted and purified from *E. coli* BL21 as described previously [90, 208]. BSA was however first used for optimisation of the coupling procedure, before employing InvA497 itself.

A similar stretching procedure to that described in Chapter 2 was employed for preparing aspherical BSA-functionalised nanoparticles (AB) or InvA497-functionalised nanoparticles (AI), with some modifications. Three different preparation and coupling procedures were tested:

- As illustrated in Figure 3.1a, 1 ml of aspherical nanoparticles (A), prepared as described in Chapter 2, was first diluted with 0.9 ml of water and then incubated for 2 h with 0.6 ml of a 5 mg/ml solution of the carboxyl group-activating agent DMTMM, at RT. Afterwards a solution of 1 mg/ml BSA was added in order to have a final concentration of 320 µg/ml,

and the dispersion was stirred overnight in an ice bath. The excess of DMTMM reagent and unbound BSA was then removed by centrifugation (using Centrisart<sup>®</sup> tubes 300 kDa MWCO, 1 605 g and 4 °C for 10 min, three cycles).

- As shown in Figure 3.1b, 1 ml of spherical nanoparticle dispersion was first diluted with 0.9 ml of water. The diluted dispersion was then incubated for 2 h with 0.6 ml of a 5 mg/ml solution of DMTMM, at RT. BSA was then added to a final concentration of 320 µg/ml, stirred overnight in an ice bath, and then subjected to centrifugation as described in method 1 in order to remove unbound BSA. The surface functionalised spherical nanoparticles were then immobilised into the PVA-glycerol film as described in Chapter 2; subsequent stretching of the nanoparticles, dissolution of films and removal of excess PVA were all conducted as also described in Chapter 2.
- As seen in Figure 3.1 c, 1 ml of spherical nanoparticle dispersion was incubated with DMTMM, as described above, and then immobilised in a PVA-glycerol film, as described in Chapter 2. Stretching of the immobilised nanoparticles, dissolution of films and removal of excess PVA were then all conducted as also described in Chapter 2. The produced aspherical nanoparticles were stirred overnight in ice bath with BSA or InvA497 (320 µg/ml). Unbound BSA or InvA497 was then removed by centrifugation as described in methods 1 and 2 (using Centrisart<sup>®</sup> tubes 300 kDa MWCO, 1 605 g and 4 °C for 10 min, three cycles).

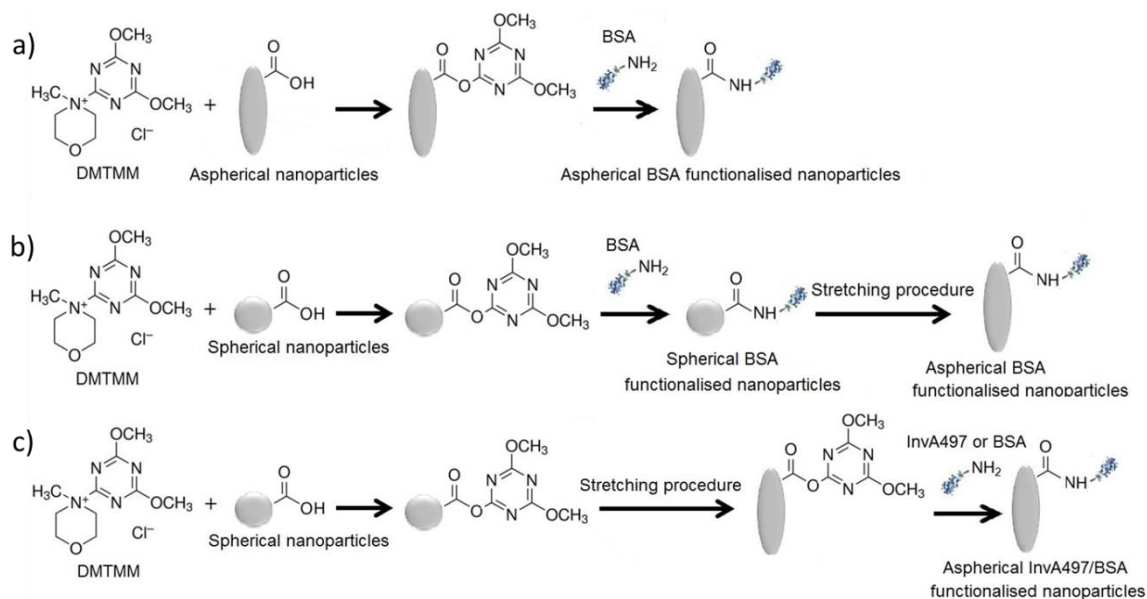


Figure 3.1 Schematic of aspherical nanoparticle surface functionalisation with InvA497.

a) In method 1, BSA was coupled on the surface of aspherical nanoparticles by first activating surface-exposed carboxyl groups with DMTMM, followed by the addition of BSA; b) in method 2, BSA was coupled on the surface of spherical nanoparticles by first activating surface-exposed carboxyl groups with DMTMM, followed by the addition of BSA and particle stretching; c) in method 3, surface coupling of BSA or InvA497 onto aspherical nanoparticles was performed by activating carboxyl groups of spherical nanoparticles and particle stretching, followed by incubation with BSA or InvA497.

In order to surface functionalise spherical nanoparticles (S), 1 ml of nanoparticle dispersion was first diluted with 0.9 ml of water. The diluted dispersion was then incubated for 2 h with 0.6 ml of a 5 mg/ml solution of DMTMM, at RT. Nanoparticle dispersions were then diluted with water (1:8, 1:4, 1:2, 2:3 or 1:1 water:nanoparticles; v:v), to a final volume of 2.5 ml. After dilution, BSA or InvA497 were added in order to have a final concentration of 320  $\mu\text{g/ml}$ , and the dispersion was stirred overnight in an ice bath. The excess of DMTMM reagent and unbound BSA or InvA497 was removed by carrying out three centrifugation cycles as described above. The resulting spherical, BSA- InvA497-functionalised nanoparticles are further referred to as SB or SI respectively.

### **3.2.4 PROTEIN QUANTIFICATION**

The amount of BSA or InvA497 coupled to the surface of SI and AI formulations was quantified using a BCA kit, in accordance with the manufacturer's instructions (QuantiPro™; Sigma-Aldrich, Steinheim, Germany) and as previously described [90, 209]. After preparing a calibration curve in accordance with the manufacturer's instruction, the concentration of BSA or InvA497 was calculated and after dividing the concentration for ml of nanoparticle solution the amount of coupled BSA or InvA497. From the amount of InvA497 coupled protein, the molecules of surface-bound InvA497 was calculated dividing for the amount for the molecular weight of InvA497 and multiplying for the Avogadro number.

### **3.2.5 IMAGING OF NANOPARTICLES**

The morphology of both SI and AI formulations was visualised using SEM (Zeiss EVO HD 15, Carl Zeiss AG, Oberkochen, Germany) at an accelerating voltage of 5 kV. Samples were diluted and dried overnight prior to imaging, and were sputter coated (Quorum Q150R ES, Quorum Technologies Ltd, Laughton, United Kingdom) with gold.

For the AI formulation, major and minor axis lengths as well as the AR were determined from SEM images using ImageJ software (Fiji).

### **3.2.6 NANOSIGHT ANALYSIS**

The number of nanoparticles for SI and AI was counted using nanoparticle tracking analysis (NTA, NanoSight LM 10, Malvern Instruments Ltd, Worcestershire, United Kingdom). The concentration of nanoparticles within appropriately diluted samples was first calculated by the NTA software. This was then converted into a number of nanoparticles in the total dispersion, dividing the concentration for the ml of solution. The previously found quantified molecules of surface-bound InvA497, previously found with BCA assay, was divided for the number of nanoparticles in the total dispersion in order to estimate the number of InvA497 molecules per nanoparticle for both SI and AI formulations.

### **3.2.7 FT-IR SPECTROSCOPY**

To confirm the formation of a covalent, amide bond between amine groups of InvA497 and the carboxyl group of PLGA molecules exposed on nanoparticle surfaces, sample of AI, SI and S formulations as well as InvA497 alone were freeze dried and afterwards the infrared spectra were collected, using a Fourier Transform Infrared (FT-IR) spectrometer (Perkin Elmer system 2000). Each spectrum was collected in a range between 4000 and 600  $\text{cm}^{-1}$  with a resolution of 1  $\text{cm}^{-1}$  (100 scans per sample).

### **3.2.8 DLS**

The size distribution of SI nanoparticle dispersions was determined by DLS using a Zetasizer Nano (Malvern Instruments Ltd, Worcestershire, United Kingdom), as described in Chapter 2.

### **3.2.9 CALCULATION OF SURFACE OCCUPANCY**

Using the estimated number of molecules per nanoparticle and the gyration radius of InvA497 [210], the total area occupied by InvA497 molecules was calculated. This was divided by the surface area of SI and AI nanoparticles, calculated using sphere and ellipsoid shape descriptors respectively, in order to obtain the total percentage of nanoparticle surface area occupied by InvA497 in each case (see appendix).

### **3.2.10 GENERATION OF 3D MODEL OF INVA497-FUNCTIONALISED NANOPARTICLES**

A 3D model of InvA497-functionalised SI and AI nanoparticles was generated via a self-written script for PovRay 3.7 (see appendix). In order to produce the model, X-ray coordinates of InvA497 (PDB ID: 1CWV) [65] were exported and scaled to the PovRay format using YASARA structure (YASARA Biosciences) [210]. After modelling of spherical and aspherical nanoparticle

shapes, the number of InvA497 molecules calculated to be present on each nanoparticle (as described above – 235 and 198 molecules for SI and AI respectively) were randomly distributed on the spherical and aspherical objects. The picture was rendered with subsurface light scattering turned on.

### **3.2.11 STATISTICAL ANALYSIS**

Where relevant, data are expressed as mean  $\pm$  standard error of the mean (SE). Also where appropriate, data was analysed using SigmaPlot Version 11 (Systat Software Inc., San Jose, CA, USA) for statistical significance. Comparisons between groups were performed using Student's t test (two-sided), or one-way ANOVA with post-hoc Bonferroni adjustment for experiments with more than two subgroups. Results were considered statistically significant at  $p$  values  $<0.05$ .

## **3.3 RESULTS AND DISCUSSIONS**

The surface of A and S nanoparticles was decorated with a fragment of the bacterial invasion protein invasin, known as InvA497, to produce formulation referred to as AI and SI respectively. In order to allow for visualisation of nanoparticles in later work (while still allowing for nanoparticle surface functionalisation), nanoparticles were prepared using PLGA mixed with a small amount of FA-PLGA.

InvA497 presents a receptor binding domain and three important amino acids involved in the receptor-mediated uptake (Phenylalanine 808, Aspartate 811 and Aspartate 911) [60] on the C-terminal part which must remain free in order to preserve the invasive properties. Moreover C-terminal part must also be direct through the outer part of the particle. Therefore, free PLGA carboxyl groups on the surface of AI and SI nanoparticles were used in the present study to couple to amine groups of InvA497 molecules. Due to the non-reactive nature of the PLGA carboxyl groups and the amine groups of InvA497, a coupling agent, DMTMM, was used. As with most commonly employed coupling methods, the reaction principle first involves the activation of the carboxyl group, followed by the interaction



between this activated group and an entity containing an amine group to form an amide bond.

In the case of the AI, the coupling method was first optimised in order to maintain the aspherical shape of the nanoparticles. In an initial approach (Method 1, Figure 3.1a), freshly prepared A nanoparticles were incubated with DMTMM and then with BSA protein (AB), a model protein with the same molecular weight of InvA497 and used in previous work for coupling optimisation and demonstrated in previous work to be an appropriate protein model for coupling optimisation. This strategy was employed due to the difficulties on produce and purifies InvaA497 compared with the commercial available BSA. Although more than 300  $\mu\text{g}$ , corresponding to a 50% functionalisation efficiency (data not showed) of BSA was found to be coupled to the surface of AB, SEM images showed reversion to a spherical shape due to the coupling procedure (Figure 3.2).

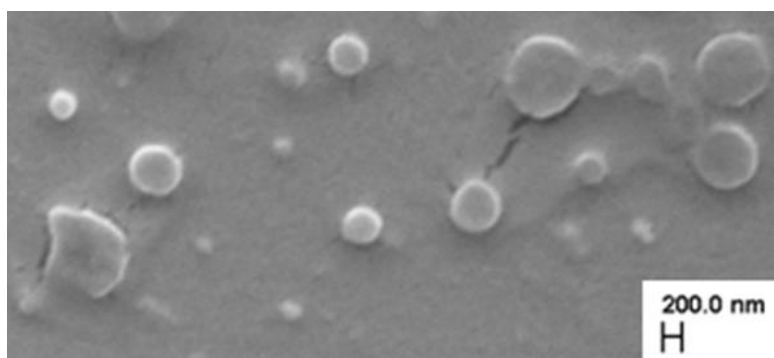


*Figure 3.2 Morphology of AB nanoparticles produced using coupling method 1.*

*SEM image of aspherical BSA-functionalised nanoparticles (AB) after direct functionalisation of aspherical nanoparticles (A) (as described in Figure 3.1a).*

As direct functionalisation of aspherical nanoparticles seemed to have a negative effect on the shape, two further coupling methods were trialled in order to produce AB. In both methods, carboxyl groups of spherical PLGA nanoparticles were activated with DMTMM, following which two different approach were employed: for method 2 BSA was first coupled and afterwards the particles were immobilised into PVA film and stretched (Figure 3.1b); for method 3 particles were first immobilised into PVA film and stretched, followed by BSA surface coupling (Figure 3.1c). During coupling reaction between the amine group of DMTMM and the carboxylic group of PLGA on the surface of the aspherical nanoparticles, a change of the interfacial tension of the nanoparticle occurs, which could induce a

recovery of the spherical shape. In both method 2 and 3, the first step of the functionalisation is performed before the stretching of the nanoparticles when the system still has a spherical shape.

As shown in Figure 3.3, the highest amount of coupled BSA was reached with method 3 (approximately 480  $\mu\text{g}$  of BSA coupled), in which the two steps of the functionalisation process (activation of PLGA carboxylic acid groups and final incubation with BSA) were interrupted by the particle stretching procedure.

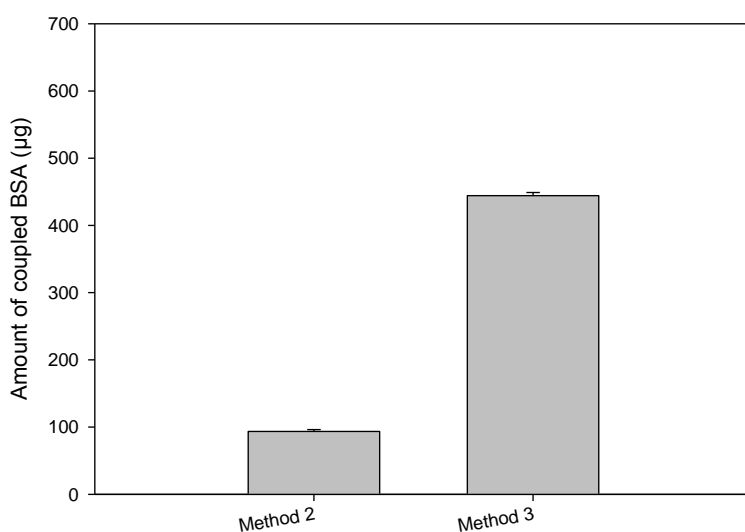


*Figure 3.3 Characterisation of BSA functionalised aspherical nanoparticles prepared via different coupling methods.*

*The amount of total coupled BSA on the surface of AB nanoparticles using two different preparations and coupling procedures. In both methods spherical nanoparticles were first incubated with DMTMM. In method 2 the nanoparticles were then incubated with BSA and afterwards stretched; in method 3, spherical nanoparticles were stretched and then incubated with BSA. Results represent the mean  $\pm$  SE ( $n=3$ ).*

An even higher amount of coupled protein was found when InvA497 was substituted for BSA using method 3, and the aspherical morphology of resulting AI was seen with SEM (Figure 3.4).

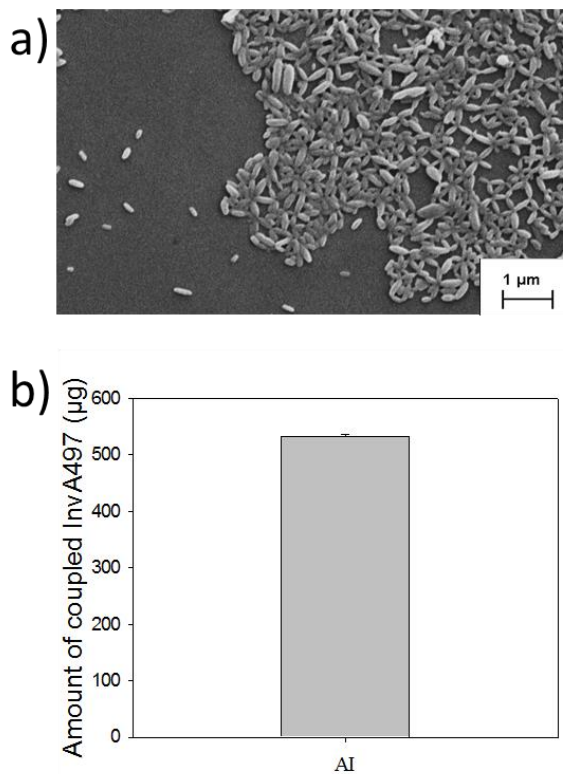
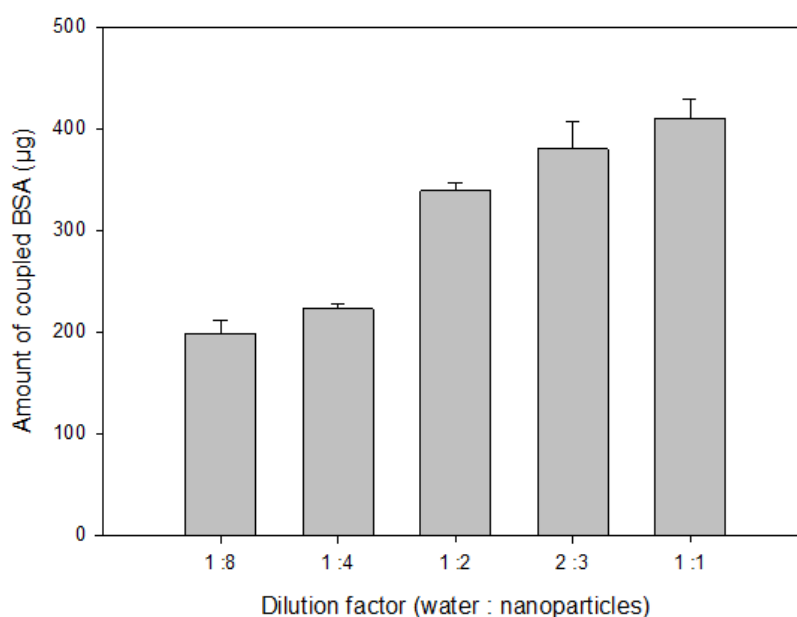


Figure 3.4 Morphology and coupling characterisation of AI.

a) SEM image of aspherical InvA497 functionalised nanoparticles (AI). b) The amount of total coupled InvA497 on the surface of AI nanoparticles was measured via the BCA assay. Results represent the mean  $\pm$  SE ( $n=3$ ).

As method 3 resulted in the production of aspherical nanoparticles with the highest amount of surface coupled BSA, and an even higher amount of coupled InvA497, this method was selected as an optimum preparation procedure for AI. Moreover comparing method 3 with method 2, as the stretching procedure is performed before the final step of the functionalisation, the protein coupled on the surface of the particle is not exposed to the harsh condition of the stretching method. The high temperature and the thermomechanical stress used during the production of aspherical nanoparticles could have led to a degradation and loss of activity of the BSA or InvA497 protein.

In order to produce a truly comparable spherical formulation with a similar amount of surface coupled protein to the optimised aspherical nanoparticles, the functionalisation procedure for production of SI was also optimised by first using BSA (SB). After incubating S with DMTMM, the nanoparticle dispersion was diluted to varying extents and then incubated with the same amount of BSA as used for coupling to AB (Figure 3.5).



*Figure 3.5 Coupling characterisation of SB.*

*Nanoparticle dispersions were diluted with water by dilution factors of 1:8, 1:4, 1:2, 2:3 and 1:1 (water:nanoparticles, v:v), following the carboxylic group activation. The amount of coupled BSA on the surface of spherical BSA functionalised nanoparticles (SB) was then measured with the BCA assay. Results represent the mean  $\pm$  SE (n=3).*

It was found that dilution of SB nanoparticle dispersions by factors of 2:3 and 1:1 prior to coupling had comparable amounts of surface coupled BSA to AB nanoparticles. A dilution factor of 2:3 was chosen for further use due to the similar amount of nanoparticles in the dispersion as AB formulation, as calculated by NTA (approximately  $2 \times 10^6$  nanoparticles).

After replacing BSA with InvA497 on the surface of spherical nanoparticles, the amount of InvA497 on the surface of AI and SI was compared (Figure 3.6). For both AI and SI, approximately 500  $\mu\text{g}$  of InvA497 in total was found to be bound to the surface of nanoparticles. The number of molecules of InvA497 per nanoparticle and the coupling density were then estimated, using the number of coupled molecules of InvA497, extrapolated from the measured amount of InvA497, and the number of nanoparticles in solution, extrapolated with the NTA and its software. Combining the total amount of surface-bound InvA497 together with NTA-measured nanoparticle numbers, it was further estimated that approximately 200 molecules of InvA497 were present on the surface of each SI or AI nanoparticle. Comparing the functionalisation of SI and AI with previously prepared

invasin-functionalised latex particles [211], where the authors show the optimal number of invasins complete protein per nanoparticles to reach the highest uptake, PLGA AI and SI formulation present a lower amount compared with first systems. Considering the already proven effective intracellular delivery of the aforementioned liposomal formulation with a relatively low number of InvA497 molecules, the approximate number of InvA497 molecules estimated to be on the surface of SI and AI was not considered to preclude InvA497-receptor mediated uptake and therefore internalisation of the current nanoparticle systems.

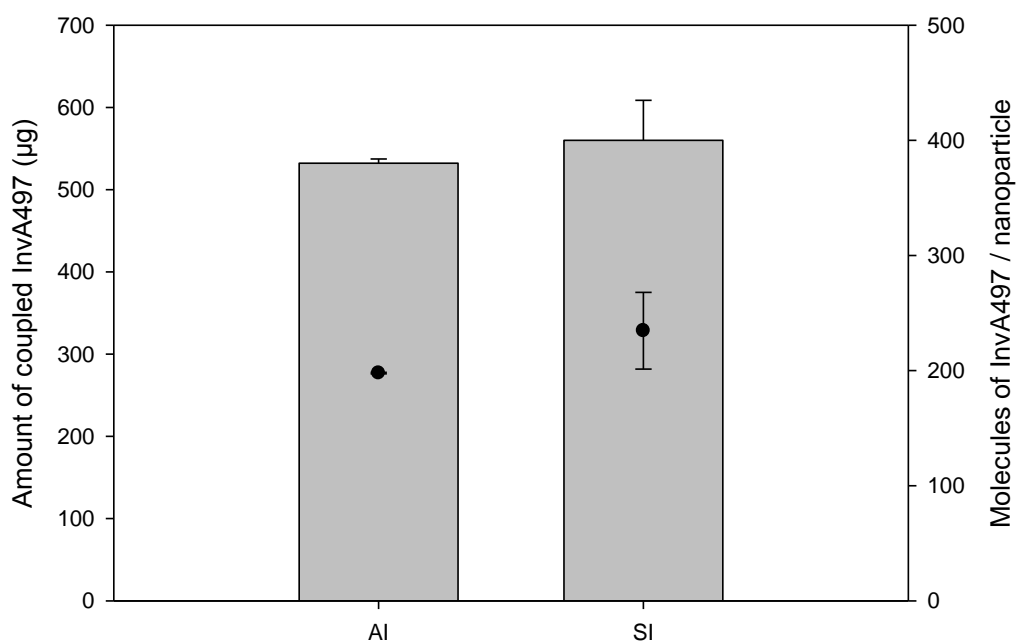


*Figure 3.6 Characterisation of InvA497 functionalisation on nanoparticle.*

*The amount of total coupled InvA497 (grey bars) on the surface of AI and SI nanoparticles was measured via the BCA assay, and afterwards molecules of InvA497 per nanoparticle (black points) were estimated using the number of nanoparticles (as determined using NTA). Results represent the mean  $\pm$  SE (n=3).*

To confirm the formation of an amide bond between the carboxyl group of PLGA and the amine group of InvA497, and therefore a successful coupling of InvA497 on the surface of AI and SI, IR spectra were collected for both functionalised nanoparticles and spherical non-functionalised nanoparticles alone (Figure 3.7).

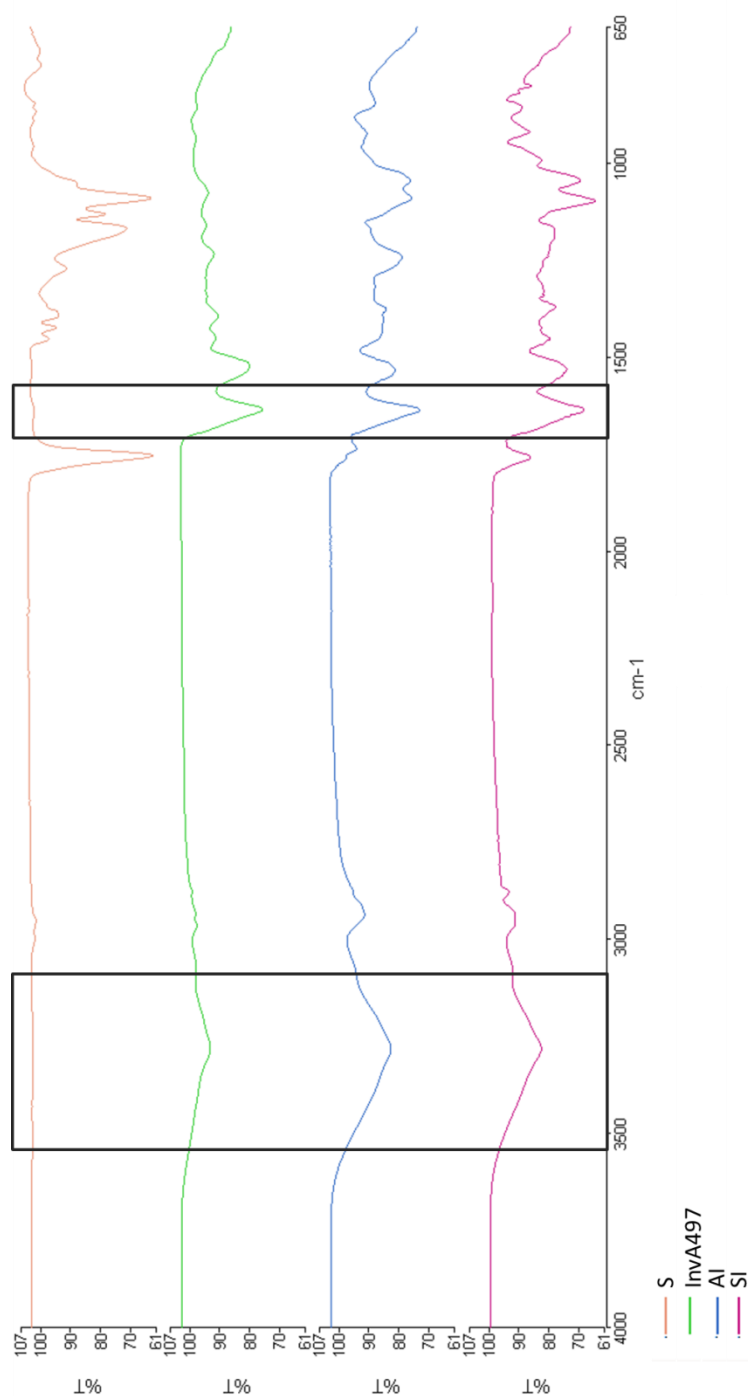


Figure 3.7: IR spectra of nanoparticles and InvA497.

IR spectra of non-functionalised spherical nanoparticles (S, pink line), InvA497 protein alone (green line) and functionalised aspherical (AI) and spherical (SI) nanoparticles (blue and pink lines respectively) were collected.

As shown in the IR spectra, the characteristic amide C=O peak (around  $1600\text{ cm}^{-1}$ ) and the amine band (between  $3000$  and  $3500\text{ cm}^{-1}$ ) were found only in

Al and SI, but not on the formulation without functionalisation. These spectra demonstrate therefore that InvA497 was successfully coupled on the surface of both Al and SI; however, additional adsorption of the protein fragment on the surface of Al and SI cannot be ruled out.

After demonstrating the continued presence of aspherical or spherical shape of nanoparticles following successful surface functionalisation, physical characterisation of both Al and SI was conducted. Size was measured using SEM image analysis for Al and DLS for SI, with values of 300 nm and 110 nm found for the major and minor axis length of Al, and a diameter of 180 nm measured for SI (Figure 3.8). These values were found to be comparable to respective A and S formulations, indicating no influence of surface functionalisation on the dimensions of either spherical or aspherical systems. The asphericity of the Al nanoparticles was further determined from measured major and minor axis lengths, by calculation of the nanoparticle AR – this was found to be approximately 2.6, a value which is comparable to the aspect ratio of *Yersinia* bacteria [212].

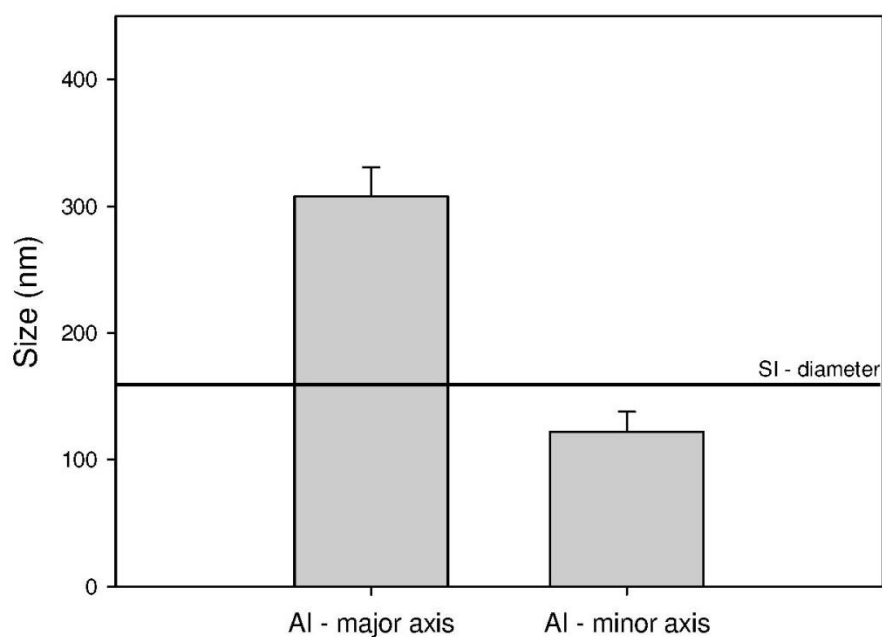


*Figure 3.8 Size of AI and SI nanoparticles.*

*The major and minor axis dimensions of AI were assessed and compared with the diameter of precursor SI (horizontal line). Major and minor axis measurements represent mean  $\pm$  SE ( $n = 98$ ).*

Illustrative 3D models of the surface-modified carrier systems were then generated (Figure 3.9), using the experimentally-determined dimensions of AI and SI and the amount of InvA497 on the surface, as determined by BCA assay, combined with published X-ray coordinates of InvA497 (PDB ID: 1CWV) [65].



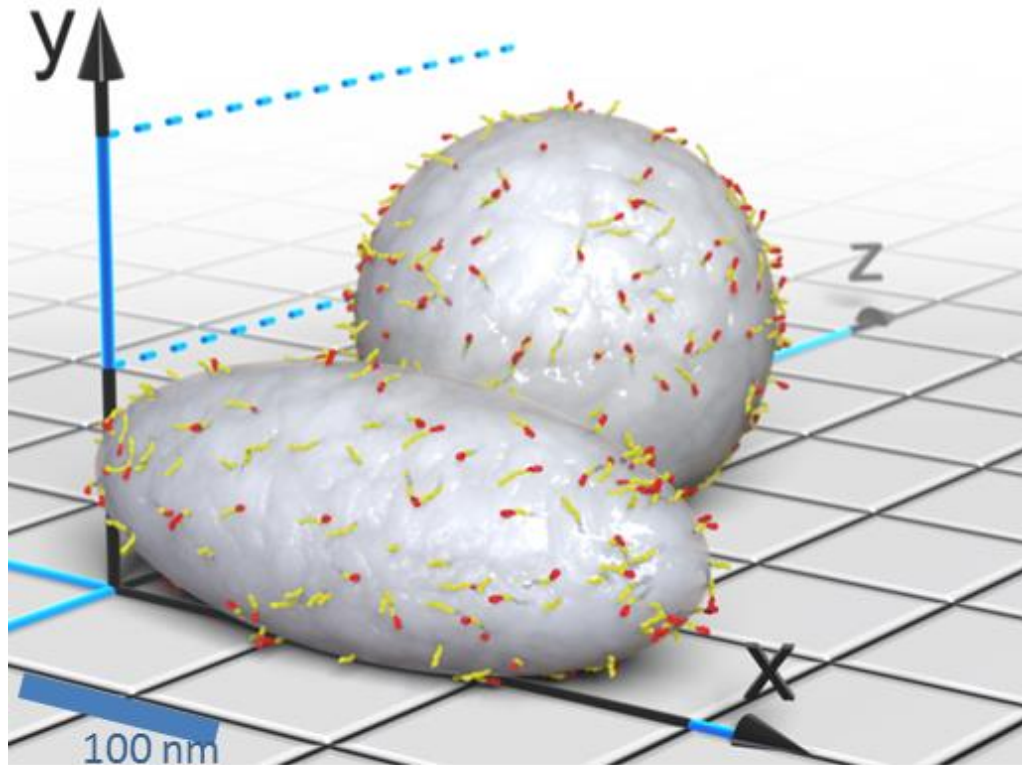


*Figure 3.9 3D model of AI and SI.*

*Particle surfaces are coloured grey and the randomly distributed InvA497 molecules are shown in yellow, with the C-terminal integrin-binding regions highlighted in red.*

As part of the model generation particle surface areas were assumed to be equivalent to a sphere for SI or to an ellipsoid for AI; it was also simulated that each InvA497 molecule occupies a circular area as dictated by its gyration radius. Using these approximations, the degree of particle surface coverage by InvA497 protein was estimated to be approximately 39% for both AI and SI nanoparticles (for calculation see Appendix). The protein fragments were randomly orientated on particle surfaces, with some InvA97 C-terminal regions (in red) directed externally, demonstrating coupling with the correct orientation on particle surfaces; others however have the integrin binding region aligned with the nanoparticle surface, and represent the fraction of surface-adsorbed protein likely to be present.

### *3.4 CONCLUSION*

In this chapter, spherical and aspherical nanoparticles surface-functionalised with InvA497 were prepared and characterised. In particular, a stretching procedure and coupling reaction were combined in order to obtain a system which can mimic the aspherical shape of bacteria as well as their natural invasion mechanism.

Characterisation of both morphology and coupled amount of InvA497 was conducted for both AI and SI formulations. On both AI and SI, InvA497 was coupled on nanoparticle surfaces using a coupling reaction between the carboxylic acid group of PLGA and the amine group of InvA497. The coupling procedure was optimised, first with BSA and then with InvA497, so that a similar total amount of invasin fragment was found to be present on the surface of both nanoparticle types. Approximately 200 molecules of protein were estimated to be present on the surface of each individual SI and AI nanoparticle. Afterwards the coupling of InvA497 with PLGA molecules was confirmed by measuring IR spectra, although the existence of a fraction of surface adsorbed InvA497 could not be excluded.

Using SEM image analysis and DLS, the produced functionalised nanoparticles were found to have dimensions of approximately 300 and 110 nm for the major and minor axes of AI respectively, and around 180 nm for the diameter of SI. Combining the produced dimension data and the quantified amount of coupled InvA497, a 3D model of the aspherical and spherical nanoparticles was generated. Such a model shows the distribution of InvA497 on the surface of AI and SI, as well as the likely orientation of the C-terminal region of InvA497.

So far, the current work has been focused on the development of bacteriomimetic nanoparticles, exhibiting an aspherical shape and InvA497 protein on the surface. The spherical corresponding formulation has also been prepared as a comparator and the two systems have been optimised in order to possess a similar amount of surface coupled InvA497. Further chapters in this thesis will focus on testing the uptake of both types of bacteriomimetic nanoparticles in an epithelial cell line, and determination of the influence of nanoparticle shape on this uptake.

# 4. UPTAKE OF INVASIN-FUNCTIONALISED BACTERIOMIMETIC NANOPARTICLES INTO HEP- 2 CELLS

Parts of this chapter have been published in *Pharmaceutical Research*, with the title "Aspherical and Spherical InvA497-functionalized Nanocarriers for Intracellular Delivery of Anti-infective Agents"

## 4.1 INTRODUCTION

The ability of bacteria to penetrate into and infect host cells is an important step in the infection cycle in many cases. For example, specific molecules, like invasins, expressed on the surface of some species of enteropathogenic bacteria, such as *Yersinia* spp, enhance the bacteria cellular permeation and the establishment of the intracellular infection in the GI tract [213]. Each enteropathogenic bacterial species has a different invasion mechanism, which involves specific host cell-bacteria interactions. As examples, both *Shigella* and *Salmonella* spp. use similar small actin regulatory proteins to invade M cells of the intestinal epithelium; however, *Shigella* spp. appears to be internalised without destroying the host cells, in contrast to *Salmonella* spp., which presents a more invasive mechanism [214, 215].

As a further example, *Yersinia* spp. express various monomeric invasins and adhesins, as well as highly sophisticated macromolecular machinery such as the commonly expressed type III secretion system, all of which facilitate interaction between the pathogen and host cells [216]. Invasin is one of these expressed invasive proteins, which plays an important role in the complex internalisation mechanism utilised by *Y. enterocolitica* and *Y. pseudotuberculosis* [217]. Invasin is an outer membrane protein which is normally expressed at the early stationary phase of bacterial growth [218]. It consists of 986 amino acids, however only the last 192 amino acids of the protein C-terminus are responsible for binding with  $\beta_1$  integrin receptors on the surface of M cells [60, 219]. Interaction between invasins and these receptors leads to a rearrangement of the cell cytoskeletal system and the consequent internalisation of the pathogen [217]. As  $\beta_1$  integrins are only expressed on the basolateral side of epithelial cells, binding and internalisation of bacteria can only occur when the integrity of the epithelial barrier is compromised, like a result of inflammation. Although only the last 192 amino acids are effectively involved with the binding procedure, it has been shown that an invasins fragment containing the last 197 amino acids of the parent protein C-terminus was not able to promote as effective an uptake of latex beads as a longer fragment, composed of 497 amino acids of the C-terminus, known as InvA497 [60].

Recently, an in-depth mechanistic study was published exploring the cellular interaction between a liposomal bacteriomimetic system decorated with InvA497, and two epithelial cell lines (HEp-2 and Caco2) [90]. In this work, Labouta *et al.* demonstrated that InvA497-functionalised liposomes were able to mimic the cellular uptake mechanism of invasin-expressing *Yersinia* spp., and could also be used to effectively kill two different species of intracellular enteropathogenic bacteria [90, 91]. The potential of bacterial invasion factors such as invasin is therefore clear; however the full capabilities of bacteriomimetic still remain to be explored. In particular, the role of other system parameters, including the shape of the carrier system itself, has not yet been systematically studied with respect to invasin-functionalised drug carriers, or in terms of other bacteriomimetic systems.

In general, the possible role of the carrier shape on the uptake of ligand functionalised nanoparticles has been mostly explored only with molecular modelling simulations. Different molecular dynamics simulation theories have been published in recent years, exploring the endocytosis of spheroid nanoparticles [220] as well as active uptake of ligand functionalised rod-like nanoparticles [221, 222]. Simulations of receptor–ligand binding and nanoparticle transport across cell membranes have been studied, keeping constant the volume and ligand density of spherical and various aspherical (long and short rods, discs) nanoparticles [222]. According to these simulations, aspherical nanoparticles first orient toward the cell membrane in such a manner so as to maximise contact between particle-associated ligands and corresponding cell surface receptors, leading to a second stage in which an invagination of the cell membrane occurs. The kinetic of this second stage depends on the shape and size of the nanoparticles, and on the release of free energy resulting from ligand-receptor binding [222].

Despite the conduction of such simulations and computational studies, the impact of particle shape on receptor mediated uptake has only been explored experimentally by Banerjee *et al* [188]. They were able to show that the presence of biotin functionalisation on the surface of aspherical nanoparticles enhanced uptake into human enterocytes [188]. The successful production and optimisation of aspherical InvA497-functionalised nanoparticles as detailed in the previous chapters therefore creates the possibility to answer these questions.

The following work was focused on exploring the uptake of aspherical InvA497-functionalised nanoparticles in comparison to spherical InvA497-functionalised nanoparticles. The HEp-2 cell line was used as an *in vitro* epithelial cell model, and both confocal imaging and fluorescence-activated cell sorting (FACS) analysis were employed to assess the uptake.

## **4.2 MATERIALS AND METHODS**

### **4.2.1 MATERIALS**

For the culturing of cells, Roswell Park Memorial Institute 1640 medium (RPMI 1640, Gibco, Carlsbad, USA) and foetal calf serum (FCS, Lonza, Cologne, Germany) were used.

For cytotoxicity assessment, Triton X-100, 3-(4,5-di-methylthiazol-2-yl)-2,5-diphenyltetrazolium bromide reagent (MTT) and dimethyl sulfoxide (DMSO) were all purchased from Sigma-Aldrich (Steinheim, Germany) and phosphate buffered saline (PBS) from Gibco (Gibco, Carlsbad, USA) was used.

Rhodamine-labeled Ricinus Communis Agglutinin I (Vector Laboratories, Inc., Burlingame, CA, USA), paraformaldehyde (Electron Microscopy Sciences, Hatfield, USA), 4',6-diamidino-2-phenylindole (DAPI, LifeTechnologies™, Darmstadt, Germany) and trypsin-EDTA (1x, Gibco, Carlsbad, USA), were employed to study the uptake.

### **4.2.2 PREPARATION OF NANOPARTICLES AND FUNCTIONALISATION**

Spherical and aspherical PLGA nanoparticles (A and S respectively) were prepared as described in Chapter 3 using double emulsion and film stretching methods.

Aspherical and spherical nanoparticles with InvA497 covalently coupled on the surface (AI and SI respectively) were also prepared, as described in Chapter 3.

### **4.2.3 CELL CULTIVATION**

Cells of the human larynx carcinoma-derived HEp-2 cell line were cultured in 75 cm<sup>2</sup> flasks with RPMI 1640 medium, supplemented with 10% FCS. Cells were incubated at 37 °C and 5% CO<sub>2</sub> and medium was changed every 2-3 days. Cells were split upon 80% confluency.

### **4.2.4 CYTOTOXICITY STUDIES**

The cytotoxicity of the various nanoparticle formulations was assessed using the MTT assay. HEp-2 cells were seeded in 96-well plates (seeding density 0.05x10<sup>6</sup> cells/well) three days before the experiment and were incubated with AI, SI, A or S (containing either 45 or 100 µg/ml of InvA497 in the case of AI and SI, and 1.06 or 0.63 mg/ml of PLGA/FA-PLGA) in RPMI 1640 medium, or with RPMI 1640 medium neat or containing 2% Triton X-100 as controls, for 4 h at 37 °C and 5% CO<sub>2</sub>. The supernatants were then removed from each well, and 10% (v/v) MTT reagent (5 mg/ml) in PBS was added and incubated with cells for a further 4 h. The medium was then removed. Formed formazan crystals were solubilised by incubation for 15 min in 100 µl of DMSO, and the absorbance of each well was measured with a plate reader (TECAN, Männedorf, Switzerland) at 550 nm. Measured absorbance values were then standardised to the employed positive control (2% Triton X-100 in RPMI 1640: 0% of cell viability) and cell viabilities were calculated in comparison to the used negative control (RPMI 1640 alone: 100% cell viability).

### **4.2.5 UPTAKE STUDIES**

HEp-2 cells were seeded on 24-well plates (seeding density 0.2x10<sup>6</sup> cells/well) the day before each experiment. After washing with PBS, cells were incubated with AI, SI, A, or S (containing 455 µg/ml of PLGA and, where appropriate, 60 µg/ml of InvA497 per sample) dispersed in RPMI 1640, for various intervals covering a total time period of 1-5 h. Nanoparticle uptake was then assessed as described in the following sections.

## **4.2.6 CONFOCAL IMAGING**

Cells treated with various nanoparticles for a period of 5 h were visualised using confocal imaging. After removing cell supernatants and washing with PBS to remove any extracellular nanoparticles, HEP-2 cell staining and fixing was carried out as follows. First, cell membranes were stained with 20 µg/ml Rhodamine-labeled Ricinus Communis Agglutinin I; cells were then fixed with 3% paraformaldehyde in PBS. As a final step, cell nuclei were stained with DAPI diluted 1:50 000 (from a stock solution of 1 mg/ml) in PBS. Samples were then imaged via confocal laser scanning microscopy (CLSM, Leica TCS SP 8; Leica, Mannheim, Germany) using LAS X software (Leica Application Suite X; Leica, Mannheim, Germany).

## **4.2.7 FACS ANALYSIS**

FACS analysis was used to quantify uptake of nanoparticles into HEP-2 cells following incubation periods of 1, 2, 3, 4 and 5 h. Supernatants containing the various employed nanoparticles were first removed from plate wells, and cells were washed with PBS to remove non-internalised nanoparticles. Cells were then detached from plate wells by incubating with 100 µl of 0.05% trypsin-EDTA (10 min at 37 °C). To stop the trypsinisation, 900 µl of 2% FCS in PBS was added and the cells were centrifuged at 257 g for 5 min at 4 °C (Rotina 420R, Hettich Zentrifugen, Tuttlingen, Germany). Afterwards, 600 µl of 2% FCS in PBS was used to resuspend the pellets, and cell suspensions were stored at 4 °C until FACS analysis. FACS was performed using a BD LSRFortessa™ (BD Biosciences, Heidelberg, Germany) employing BD FACSDiva™ Software v8.0.1. Using an untreated negative control sample for reference, forward scatter (FSC) and side scatter (SSC) parameters were collected for live cells within each sample. Green fluorescence data (ex: 488 nm, filter: 530/30) were then collected from these living subpopulations, for a minimum of 10 000 events (cells) per sample.

To determine the energy dependence of nanoparticle uptake, the same uptake study procedure and FACS analysis was applied, after incubating the nanoparticles with HEP-2 cells at 4 °C.



#### **4.2.8 STATISTICAL ANALYSIS**

Where appropriate, data are expressed as mean  $\pm$  SE. Also where appropriate, data was analysed using SigmaPlot Version 11 (Systat Software Inc., San Jose, CA, USA) for statistical significance. Comparisons between groups were performed using Student's t test (two-sided). Results were considered statistically significant at  $p$  values  $<0.05$ .

### ***4.3 RESULTS AND DISCUSSION***

As a preliminary test, the cytotoxicity of S, A, SI and AI formulations in a HEp-2 epithelial cell model was determined (Figure 4.1). Two concentrations were selected for testing - the highest concentration of InvA497 able to be administered without dilution (100  $\mu\text{g/ml}$ ), and a concentration same as the one employed in the case of the previously tested InvA497-functionalised liposome formulation (45  $\mu\text{g/ml}$ ) [91] – in order to encompass the possible working range for further studies. A small reduction of the cells viability was noticed for the lowest concentrations, instead a high cells toxicity was found when the undiluted nanoparticles were tested.

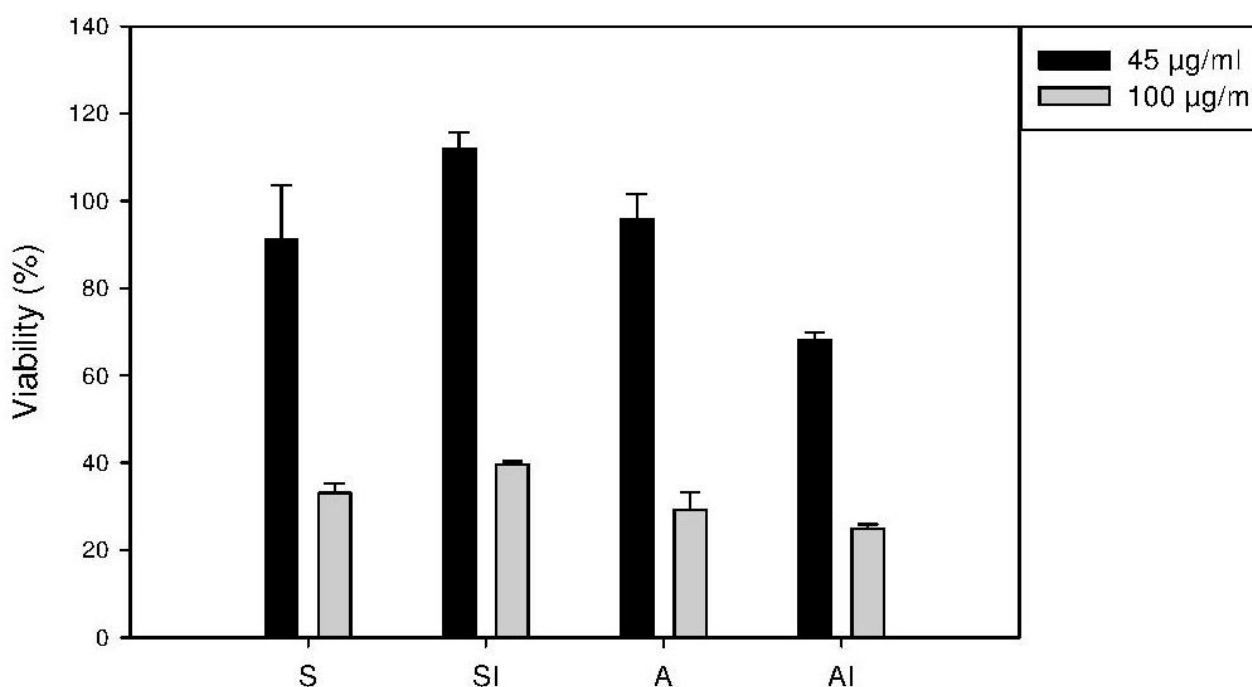


Figure 4.1: Cytotoxicity of nanoparticles.

Spherical nanoparticles without or with functionalisation (S and SI) and the corresponding aspherical formulations (A and AI) were incubated with HEP-2 cells and the viability was measured via MTT assay. Results represent the mean  $\pm$  SE (n=3).

After testing the cell toxicity, the influence of particle shape on cellular uptake was then determined by incubating a non-toxic concentration of each nanoparticle formulation with HEP-2 cells, followed by CLSM (Figure 4.2) and FACS analysis (4.3). The HEP-2 cell line was consistently used for all experiments as this epithelial line expresses the  $\beta_1$  integrin receptor necessary for InvA497-mediated uptake.

As it was expected from the previous liposome studies [90], InvA497 functionalisation was seen to enhance the uptake of both spherical and aspherical nanoparticles into HEP-2 cells. An increased uptake of SI and AI (Figures 4.2a and 4.2b respectively) in comparison to S and A formulations (Figure 4.2c and 4.2d) at the 5 h endpoint of uptake studies was demonstrated, as noted from the increased presence of green fluorescence localised inside the cells in the case of SI and AI compared to S and A. Surprisingly for these last two formulations no appreciable uptake was seen due to the absence of InvA497 on the surface, in contrast with

the results obtained by other authors who tested uptake of spherical PLGA nanoparticles into Hep-2 cells [223, 224]. However as these uptake studies were done with PLGA particles marked with fluorescent molecules not covalently bounded to the polymeric core, the possible leakage of these fluorescent molecules out of the nanoparticle might have influenced and misled the uptake study.

The cross sections, shown in Figures 4.2a and 4.2b, demonstrate that SI and AI nanoparticles are able to penetrate inside the HEp-2 cells and not only adhere to cell surfaces. The green SI and AI nanoparticles are localised between the red cell membrane and the blue nucleus.

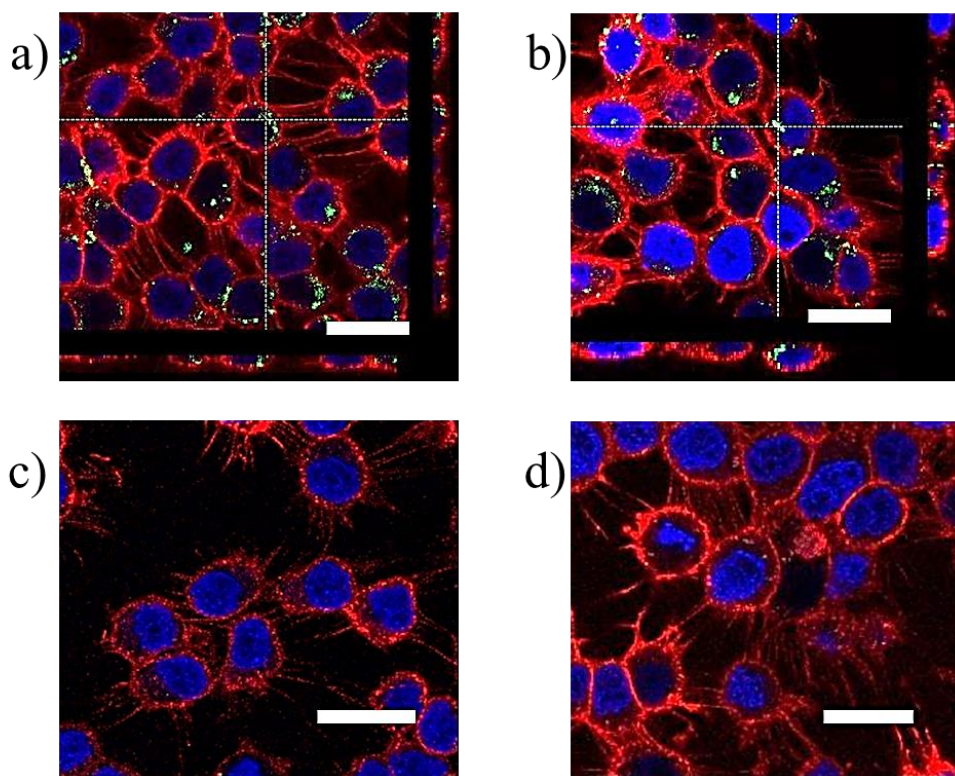


*Figure 4.2: Confocal microscopy images of the cellular uptake of nanoparticles.*

*Uptake of aspherical ('AI', a) and spherical ('SI', b) nanoparticles functionalised with InvA497, as well as non-functionalised aspherical ('A', c) and spherical ('S', d) control nanoparticles into HEp-2 cells is shown after 5 h of incubation at 37 °C. Cross sections for a and b are also shown, demonstrating the internalisation of the nanoparticles inside the HEp-2 cells. Red: HEp-2 cell membranes, green: nanoparticles, blue: HEp-2 cell nuclei (scale bar: 20 µm).*

As quantification of particle uptake and assessment of uptake kinetics could not be performed using the confocal instrument setup, FACS analysis was further employed (Figure 4.3).

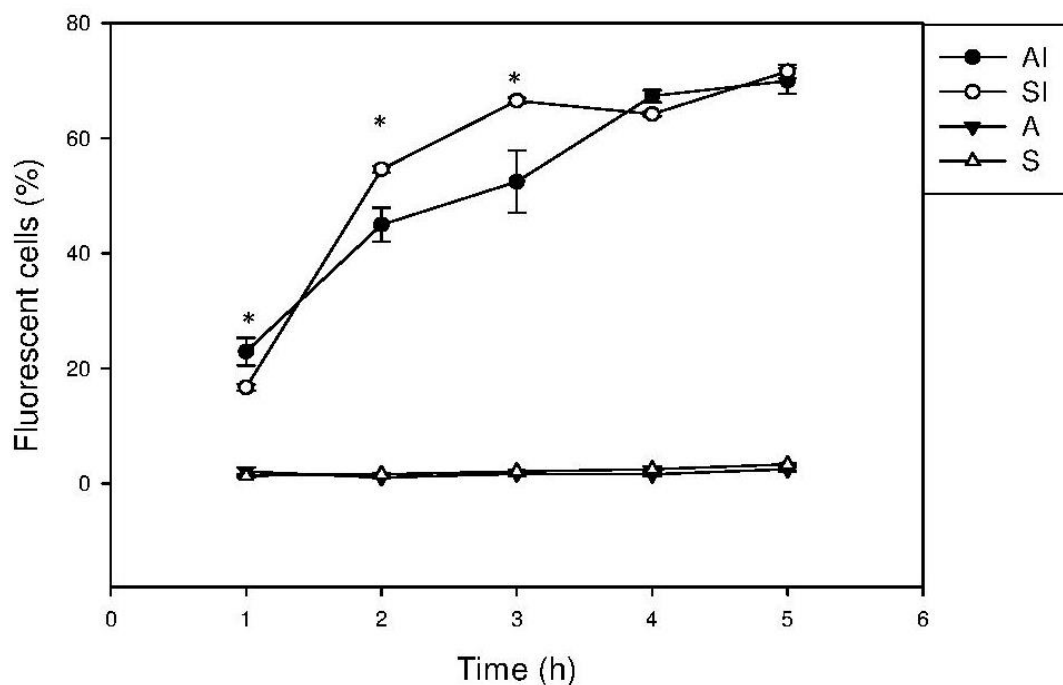


Figure 4.3: Quantification of intracellular uptake of nanoparticles into HEp-2 cells.

The uptake of aspherical and spherical nanoparticles with or without InvA497 functionalisation (AI, SI, A and S) was tested at different time points, for a total period of 5 h. Results represent the mean  $\pm$  SE (n=3); \* indicates p value < 0.05

Looking at the total extent of the particle uptake, internalisation of InvA497-functionalised nanoparticles was found to be independent from nanoparticles shape. In particular, AI particles showed a slightly faster uptake compared to SI in the first hour. However the uptake ratio levelled out after 4 h, at approximately the same value of 66%. This levelling out appears to correspond to the plateau phase typically indicative of saturation of uptake-mediating receptors [225]. The uptake of InvA497-functionalised nanoparticles seems therefore not to be influenced from particle shape, as only a small difference in the kinetic of SI and AI cellular uptake was seen. Similar results were found for worm or rod-shaped particles, where the uptake into alveolar rat macrophages was lower compared with the spherical control [176].

In accordance with the confocal study, no appreciable uptake was noted for both A and S nanoparticles. Within the first 3 h, internalisation of AI and SI formulations was found to be significantly greater than A and S, independent of particle shape.

In order to confirm that the uptake of the nanoparticles occurs through an energy dependent endocytosis uptake mediated by  $\beta_1$  integrin receptor, the uptake of the various nanoparticles into HEP-2 cells at 37 °C was compared with the uptake at 4 °C (Figure 4.4). As shown in literature, the energy-dependent uptake of functionalised nanoparticles at 4 °C is generally greatly reduced in comparison to uptake at physiological temperatures [90, 100].

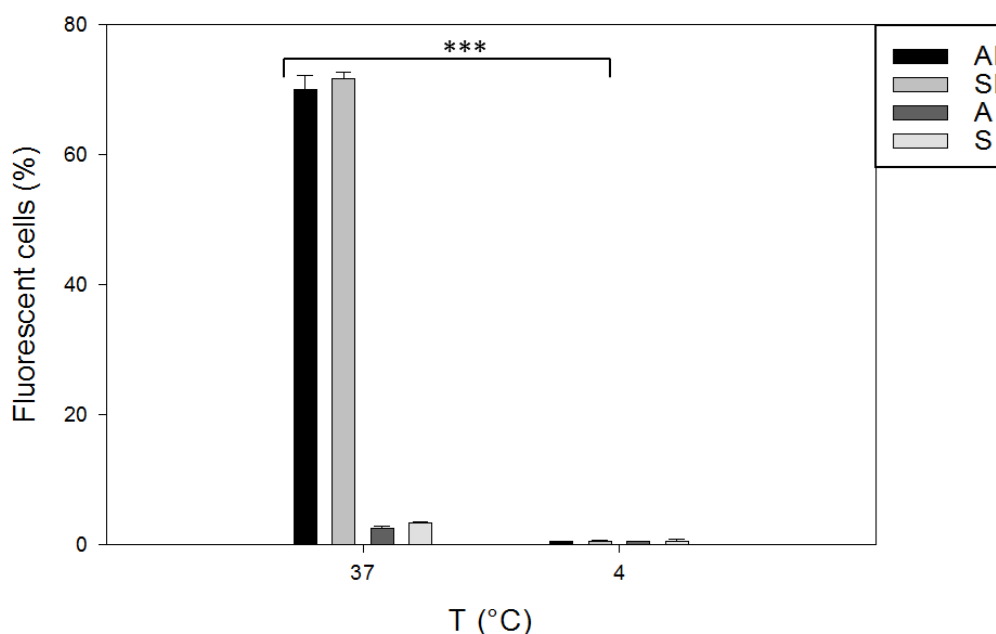


Figure 4.4 Energy dependent uptake of nanoparticles on Hep-2 cells.

Percentage of fluorescent HEP-2 cells after incubation of aspherical and spherical nanoparticles with or without InvA497 functionalisation (AI, SI, and A and S) with HEP-2 cells at 37° C and at 4° C was compared. Results represent the mean  $\pm$  SE (n=3). \*\*\* indicates p value < 0.001

As also previously shown for liposomes functionalised with InvA497 [90], a significant reduction in the percentage of nanoparticle-containing, fluorescent cells were observed for both AI and SI at 4° C compared with 37 °C. This suggests that both AI and SI are taken up via an energy-dependent mechanism due to the presence of InvA497 on the particle surface, as this internalisation pathway is

generally reduced at low temperature [100]. This also demonstrates the success of the coupling reaction between InvA497 proteins and terminal groups of PLGA, as only the correct oriented proteins are able to bind with the integrin protein on the surface of HEP-2 cells and penetrate via an energy-dependent mechanism.

#### *4.4 CONCLUSION*

The uptake of aspherical and spherical PLGA nanoparticles functionalised with InvA497, developed and optimised as detailed in chapter 3, was assessed in order to explore the influence of shape on receptor-mediated uptake and on normal uptake.

After establishing a non-cytotoxic concentration of InvA497-functionalised nanoparticles, nanoparticles were incubated for a total time period of 5 h with HEP-2 epithelial cells, and both confocal imaging and FACS analysis were conducted. It was noted using both measures that InvA497-functionalised aspherical and spherical nanoparticles exhibited a greater uptake compared with the non-functionalised A and S formulations. Moreover, looking at the total kinetic uptake studies using FACS, internalisation of InvA497-functionalised nanoparticles was found to be independent on nanoparticle shape. In studies conducted at 4 °C no uptake of AI and SI into HEP-2 cells was noted, indicating that both aspherical and spherical InvA497 functionalised nanoparticles are taken up via an active energy dependent mechanism - in agreement with the natural mechanism by which invasin mediates bacterial uptake into host cells.

This current work represents one of the first investigations into the influence of shape on cellular uptake of bacteriomimetic nanoparticles. Although the results obtained from the uptake of bacteriomimetic nanoparticles into epithelial cells are a somewhat unexpected result, the internalisation is only one of the factors which can influence the effectiveness of the system. Other nanoparticle characteristics can influence the efficacy against intracellular bacteria, including drug loading capacity and release behaviour. Therefore, to further investigate the influence of shape on bacteriomimetic systems, experiments with drug-loaded nanoparticles are required and will be discussed in the next chapter.

## 5.EFFICACY STUDIES OF BACTERIOMIMETIC NANOPARTICLES

Parts of this chapter have been published in Pharmaceutical Research, with the title "Aspherical and Spherical InvA497-functionalized Nanocarriers for Intracellular Delivery of Anti-infective Agents"

## 5.1 INTRODUCTION

Although new antibiotics are being identified every day, the ability of pathogens to escape the immune system and resist the action of commonly used antibiotic drugs is continually evolving. Bacteria are normally divided into two groups depending on their localisation within a host: namely, extracellular and intracellular bacteria [226, 227]. For the first group, *Streptococcus pyogenes* and *P. aeruginosa* are the most common examples [226]. Classical examples of intracellular pathogens are *S. flexneri*, *Listeria monocytogenes*, *M. tuberculosis* and *Salmonella enterica*. This latter type of bacteria has the ability to invade into cells, like mammalian cells, and hide from the host immune system [21, 47]. Bacteria such as *Yersinia* spp. for example, are able to invade into M cells of the intestinal epithelium, to shelter inside membrane-bound vacuoles. This bacterium is then able to persist and multiply within the intestinal epithelial barrier, or infect distant mesenteric lymph nodes [228]. Other bacteria like *S. flexneri*, after penetrating through the host cell membrane, are able to escape from the vacuoles within which they are internalised and proliferate in the cell cytosol [22].

The hydrophilic nature of many antibiotics presents a major limitation to their efficacy against intracellular bacteria [229]. A classic example in this respect is gentamicin, a broad spectrum aminoglycoside antibiotic. While its broad spectrum of action creates the potential to utilise gentamicin as antibiotic therapy for a variety of infections, its highly hydrophilic nature prevents permeation across mammalian cell membranes [230]. Its clinical use is therefore limited to the treatment of intracellular bacterial infections, such as *S. flexneri* [231, 232].

Improvement in the nanoparticle field and studies on nanoparticle uptake could overcome the low permeation into the mammalian cells of hydrophilic antibiotics, like gentamicin. Moreover, active targeting could give a positive contribution to these 'hard-to-treat' infections. As discussed previously, the efficacy of bacteriomimetic nanoparticles against intracellular infections has been achieved by mimicking a  $\beta_1$  integrin-mediated uptake system from bacteria. Menina *et al.* [91] proved that liposomes functionalised with InvA497 and loaded with gentamicin were able to kill bacteria hidden inside HEp-2 cells, namely *S. enterica* and *Y. pseudotuberculosis*. This opens the possibility to explore the world of bacteriomimetic systems and their potential against intracellular infections.



The role of the physical characteristics of nanoparticles in drug delivery, as for example their shape, has not yet been systematically studied to the best of the author's knowledge. There is clear evidence of the importance of the shape of colloidal structures in biological interactions, including the shape variation of bacteria themselves [94-96]. Modelling the bacterial shape variation in a bacteriomimetic system was therefore considered to be a logical yet largely un-investigated step.

As discussed in previous chapters a well-known technique was adapted in order to prepare polymeric nanoparticles with an aspherical shape; InvA497 was then coupled onto particle surfaces. The following work will be focused on the drug loading of this bacteriomimetic system with a lipophilic preparation of gentamicin, and efficacy testing of this system in an epithelial cell model infected with the common intracellular bacterium, *S. flexneri*. The efficacy of the aspherical bacteriomimetic system will be evaluated as throughout this thesis in comparison to drug-loaded bacteriomimetic nanoparticles composed of PLGA and also with InvA497 surface functionalisation, but which are spherical in shape.

## 5.2 MATERIALS AND METHODS

### 5.2.1 MATERIALS

For nanoparticle preparation and characterisation, gentamicin sulphate, bis(2-ethylhexyl) sulfosuccinate sodium salt (AOT), sodium acetate, potassium chloride, calcium chloride, o-Phthaldialdehyde reagent (OPA), methanol, boric acid, 2-mercaptoethanol and potassium hydroxide were all purchased from Sigma-Aldrich (Steinheim, Germany).

For the anti-infective efficacy study and bacteria culture, RPMI 1640 (Gibco, Carlsbad, USA), PBS (Gibco, Carlsbad, USA), FCS (Lonza, Cologne, Germany), tryptic soy broth (TSB) medium (BD, Difco, Maryland), tryptic soy broth agar (TSA, BD, Difco, Maryland) and congo red (Fisher Chemical, Waltham, Massachusetts, USA) were used.

For microbiological investigations and cytotoxicity assessment, Triton X-100 (Sigma-Aldrich, Steinheim, Germany), a lactate dehydrogenase (LDH) activity cytotoxicity detection kit (Roche, Mannheim, Germany), RPMI 1640 medium

without phenol red (Gibco, Carlsbad, USA), fluorescein diacetate (FDA) and propidium iodide (both from Sigma-Aldrich, Steinheim, Germany) were employed.

### **5.2.2 AOT-GENTAMICIN PREPARATION**

Gentamicin bis(2-ethylhexyl) sulfosuccinate sodium salt (AOT-gentamicin) was prepared according to Elizondo *et al.* [233] and Imbuluzqueta *et al.* [234]. For this process, 5 mol of the surfactant AOT was stoichiometrically complexed with the 5 ionisable amino groups of gentamicin via a hydrophobic ion pairing method (ionic complex molar ratio gentamicin:AOT 1:5). Briefly, 800 ml of a solution of AOT in dichloromethane (12.55 mg/ml) was mixed vigorously with a buffered aqueous solution (10 mM sodium acetate, 10 mM potassium chloride, 10 mM calcium chloride, pH 5.0) of gentamicin (4 mg/mL) for 3 h. The two formed phases were then separated by centrifugation (3 136 *g*, 5 min, RT; Rotina 420R, Hettich Zentrifugen, Tuttlingen, Germany), and, after evaporation of the organic phase (under vacuum for 15 min), AOT-gentamicin was recovered.

### **5.2.3 FT-IR SPECTROSCOPY**

To compare the produced AOT-gentamicin with literature data from Imbuluzqueta *et al.* [234], a FT-IR spectrometer (Perkin Elmer system 2000) was used. For the measurements, dry AOT-gentamicin was employed and analysed. Spectra of dry AOT-gentamicin were collected in a range between 4000 and 650  $\text{cm}^{-1}$  with a resolution of 1  $\text{cm}^{-1}$  (100 scans per sample).

### **5.2.4 PREPARATION OF DRUG-LOADED NANOPARTICLES**

Spherical and aspherical PLGA nanoparticles loaded with AOT-gentamicin without InvA497 (SG and AG respectively) were produced as control groups. For SG, 3 mg of the ionic AOT-gentamicin complex was dissolved with the PLGA solution in ethyl acetate and the oil in water emulsion with PLGA was prepared as described in chapter 3. The excess of non-encapsulated AOT-gentamicin was then removed from formed nanoparticles using centrifugation (12 544 *g* for 12 min at 12 °C). AG were prepared by stretching of SG nanoparticles, as described previously.

Where required, InvA497 was then coupled on the surface of spherical and aspherical AOT-gentamicin-loaded nanoparticles, also as described in chapter 2, to produce formulations denoted SIG and AIG respectively.

The amount of AOT-gentamicin encapsulated in SG, AG, SIG and AIG nanoparticles was quantified as described by Imbuluzqueta *et al.* [234] using a fluorometric method based on the use of OPA reagent.

Briefly, 0.2 g of OPA was first dissolved in 1 ml of methanol, 19 ml boric acid (0.4 M, pH 10.4) and 0.4 ml of 2-mercaptoethanol (14.3 M). After adjusting the pH to 10.4 using potassium hydroxide, 2 ml of this solution was mixed with 16 ml of methanol in order to have the final OPA solution. Standards were prepared using 1 ml of AOT-gentamicin solution in boric acid ranging in concentration from 0 to 40 µg/ml, adjusted to pH 7.4. For nanoparticle samples, AOT-gentamicin was first extracted from the nanoparticles by stirring 0.5 ml of particle solution with 0.5 ml of hydrochloric acid (0.1 M) for 8 h. The pH of the sample solutions was adjusted to pH 7.4 using potassium hydroxide and diluted to a volume of 1 ml with water. For the quantification, 1 ml solutions of standards and samples was mixed with 0.6 ml of methanol and 0.9 ml of the reagent solution (0.1 ml OPA reagent solution and 0.8 ml methanol) and then incubated for 10 min in dark. Afterwards the fluorescence was measured in a plate reader (TECAN, Männedorf, Switzerland) with an excitation of 344 nm and emission of 450 nm.

The quantified amount of encapsulated AOT-gentamicin together with the initial amount of AOT-gentamicin used during nanoparticle preparation was used to calculate an encapsulation efficiency (EE%). After determining the dry mass of nanoparticle samples using the freeze dried (Alpha 2-4 LSC, Christ, Osterode am Harz, Germany), the loading capacity (LC%) was calculated as the amount of encapsulated drug related to the total sample weight.

### **5.2.5 ZETA POTENTIAL**

The zeta potential of all aspherical and spherical formulations – functionalised and not-functionalised, drug loaded and empty – was determined by measurement of electrophoretic mobility using a Zetasizer Nano (Malvern Instruments Ltd, Worcestershire, United Kingdom).

### **5.2.6 RELEASE TEST OF AOT-GENTAMICIN**

In order to achieve sink conditions and allow for determination of the release kinetics of AOT-gentamicin from various nanoparticle formulations, multiple samples of each formulation (containing 69.36 µg/ml of AOT-gentamicin) were centrifuged and resuspended in 7 ml of PBS pH 7.4. Samples were then incubated at 37 °C with stirring for a total of 24 h. At various intervals during this time, 2 samples of each nanoparticle formulation were taken and centrifuged (1 680 g, 10 min). After centrifuging, the amount of released AOT-gentamicin in the produced supernatant was measured using the aforementioned fluorometric method [234].

At the 2 h timepoint of release studies, samples of aspherical nanoparticle formulations were also taken and analysed for their shape using SEM (Zeiss EVO HD 15, Carl Zeiss AG, Oberkochen, Germany) at an accelerating voltage of 5 kV. Samples were imaged after drying overnight and following sputter coating (Quorum Q150R ES, Quorum Technologies Ltd, Laughton, United Kingdom) with gold.

### **5.2.7 CELL CULTIVATION**

As described in chapter 4, cells of the human larynx carcinoma-derived HEp-2 cell line were cultured in 75 cm<sup>2</sup> flasks using RPMI 1640 medium, supplemented with 10% FCS. Cells were incubated at 37 °C and 5% CO<sub>2</sub> and medium was changed every 2-3 days. Cells were split upon 80% confluency.

## **5.2.8 CYTOTOXICITY OF AOT-GENTAMICIN LOADED NANOPARTICLES AND AOT-GENTAMICIN ALONE**

An LDH cytotoxicity detection kit was used to assess the viability of HEp-2 cells following treatment with AG, SG, AIG and SIG as well as AOT-gentamicin alone, in accordance with the manufacturer's instructions. This kit measures the activity of the LDH enzyme, which catalyses the interconversion of pyruvate and lactate. The activity of this enzyme is high when there is cell damage, for example as a result of exposure to a toxic agent.

Briefly, HEp-2 cells were seeded in a 96-well plate (seeding density  $0.05 \times 10^6$  cells/well), cultured for 72 hours and, after washing with PBS, incubated for 4 h (at 37 °C and 5% CO<sub>2</sub>) with different concentrations of nanoparticle formulations (concentration of AOT-gentamicin 5-120 µg/ml, corresponding concentration of InvA497 12-50 µg/ml) dispersed in RPMI 1640 medium without phenol red. As controls, cells incubated with RPMI 1640 medium alone (negative control) and RPMI with 2% Triton X-100 (positive control) were used. Cell supernatants were then removed and incubated with the provided LDH reagent for 3 min at RT. The absorbance of cell supernatants, indicative of LDH activity, was then read with a plate reader (TECAN, Männedorf, Switzerland) at a wavelength of 490 nm. To calculate cell viability, the absorbance measured in each sample supernatant was standardised to that of the positive control (Triton X-100) and calculated in comparison to that of a negative control (RPMI-treated cells).

## **5.2.9 BACTERIA CULTURE**

*S. flexneri* (strain M90T, kindly supplied by the Department of Molecular Infection Biology, HZI, Braunschweig, Germany) bacteria were stored on sterile TSA agar plates supplemented with 0.08% (w/v) congo red at 4 °C. Before each experiment, virulence factor-expressing colonies of *S. flexneri* had been cultured and incubated in glass tubes containing 10 ml of TSB overnight at 37 °C, with shaking to reach the stationary growth phase.

### **5.2.10 INVASION ASSAY OPTIMISATION**

The virulence of *S. flexneri* bacteria in different growth phases was first tested, in order to find parameters that would provide an optimal balance between rate of invasion of Hep-2 cells and used bacterial inoculum. Bacteria had been cultured as described above in order to reach the stationary phase and, before infecting cells, bacteria in exponential phase were prepared by incubating a freshly diluted culture of *S. flexneri* in TSB medium at 37 °C for 2 h. Both bacteria in stationary phase (overnight culture) and in exponential phase (2 h culture) were used to infect previously cultured HEp-2 cells in a 24-well plate (seeding density  $0.2 \times 10^6$  cells/well) after resuspending both cultures in RPMI 1640 medium. Different multiplicities of infection (MOI - bacteria:HEp-2 cell ratio) were also investigated. To enhance bacteria sedimentation onto the HEp-2 cells, plates were centrifuged (6 708 *g* for 5 min) following addition of bacteria, and were afterwards incubated for 2 h in a humidified incubator at 37 °C and 5% CO<sub>2</sub> atmosphere, in order to allow for bacterial adhesion and cellular invasion. Cells were then washed with PBS to remove the excess of bacteria. In order to kill any remaining extracellular bacteria, cells were further incubated for 2 h with RPMI medium containing 50 µg/ml of gentamicin. Killed extracellular bacteria were then removed by washing of cells with PBS. Intracellular bacteria were counted after lysing the infected HEp-2 cells with 0.01% Triton X-100, and plating the cell lysate in serial dilutions in sterile agar plates. Plates were incubated overnight at 37 °C to allow for bacterial growth, before counting the final number of bacterial colony forming units (CFU). After multiplying by relevant dilution factors, the CFU of *S. flexneri* were expressed as a percentage of the number of colonies from the inoculum, termed the percentage of invasion.

### **5.2.11 CYTOTOXICITY OF INFECTED HEP-2 AFTER NANOPARTICLES TREATMENT**

Confocal imaging was used to assess the continued viability of infected HEp-2 cells after treatment with AIG, SIG, AG, SG, AI, SI, A and S, as well as AOT-gentamicin alone. After seeding and culturing HEp-2 cells in a 24-well culture plate for imaging for 24 h (seeding density  $0.2 \times 10^6$  cells/well), the cells were

infected with *S. flexneri* in the exponential phase and at an MOI of 25:1 dispersed in RPMI 1640 medium. After washing with PBS, the infected cells were incubated for 2 h with RPMI medium containing 50 µg/ml of gentamicin for extracellular bacteria killing, as described above. After washing with PBS to remove dead extracellular bacteria, cells were incubated with loaded and unloaded spherical and aspherical nanoparticles, with or without InvA497-functionalisation. (120 µg/ml of AOT-gentamicin, 49 µg/ml of InvA497 and 3.7 mg/ml of PLGA/FA-PLGA where appropriate – standardised by employing drug-free functionalised or drug-free non-functionalised nanoparticles of corresponding shape where necessary) for 3 h at 37 °C and 5 % CO<sub>2</sub>. As controls AOT-gentamicin alone was used, as well as RPMI 1640 medium alone, and RPMI with 2% Triton X-100. Following incubation with formulations, HEp-2 cells were washed twice with PBS and then incubated with a 20 µg/ml solution of FDA (stock solution 1 mg/ml in acetone) and 40 µg/ml propidium iodide (stock solution 1 mg/ml) in PBS. The two substances stained respectively live cells (green) and dead cells (red). CLSM (Leica TCS SP 8; Leica, Mannheim, Germany) was employed for imaging of cell samples. The negative control (infected cells without treatment and incubated with RPMI medium) and positive control (2% Triton X-100) samples were used to give a qualitative comparison of cell viability.

### **5.2.12 EFFICACY STUDY**

The efficacy of the InvA497-functionalised, AOT-gentamicin loaded nanoparticle systems in killing of intracellular *S. flexneri* was tested. After seeding HEp-2 cells on 24 well plates (seeding density  $0.2 \times 10^6$  cells/well), infecting these with *S. flexneri* and killing the extracellular bacteria as described in section 5.2.10, different types of nanoparticles (AIG, SIG, AG, SG, AI, SI, A and S) as well as ATO-gentamicin alone were added and incubated for 3 h. Concentrations used were the same as those described in the LDH-based cytotoxicity assay (section 5.2.8). After washing twice with PBS, HEp-2 cells were incubated with 0.01 % Triton X-100 in order to lyse the cells. Dilutions of the cell lysate were plated in sterile TSB-agar plates and the plates were incubated overnight at 37 °C. The CFU of *S. flexneri* were counted and, after multiplying by relevant dilution factors, the percentage of remaining intracellular bacteria (expressed as CFU from each

cell lysate relative to the CFU of bacteria used for initial infection – the inoculum) was calculated. The efficacy was expressed as percentage of bacteria killing, using the values for each formulation treatment group normalised to the percentage of remaining intracellular bacteria in untreated cell samples.

### **5.2.13 STATISTICAL ANALYSIS**

Where appropriate, data are expressed as mean  $\pm$  SE. Also where appropriate, data was analysed using SigmaPlot Version 11 (Systat Software Inc., San Jose, CA, USA) for statistical significance. Comparisons between groups were performed using Student's t test (two-sided) or one-way ANOVA with post-hoc Bonferroni adjustment for experiments with more than two subgroups. Results were considered statistically significant at  $p$  values  $<0.05$ .

## **5.3 RESULTS AND DISCUSSIONS**

AOT-gentamicin was prepared according to Elizondo *et al.* [233] and Imbuluzqueta *et al.* [234] and loaded into spherical and aspherical nanoparticles. This lipophilic preparation of gentamicin was used to overcome the low encapsulation of unmodified gentamicin found to occur within PLGA nanoparticles, due to the hydrophilic nature of the drug. Simple mixing of gentamicin and the surfactant AOT, followed by solvent evaporation, leads to formation of a highly lipophilic preparation, as a result of electrostatic interaction between the sulfonate part of AOT and the five amine groups present within each gentamicin molecule, (Figure 5.1a and b respectively). The successful formation of the AOT-gentamicin preparation was confirmed by comparing IR spectra obtained in the current work, with that of Imbuluzqueta *et al.* [234] (Figure 5.1c).



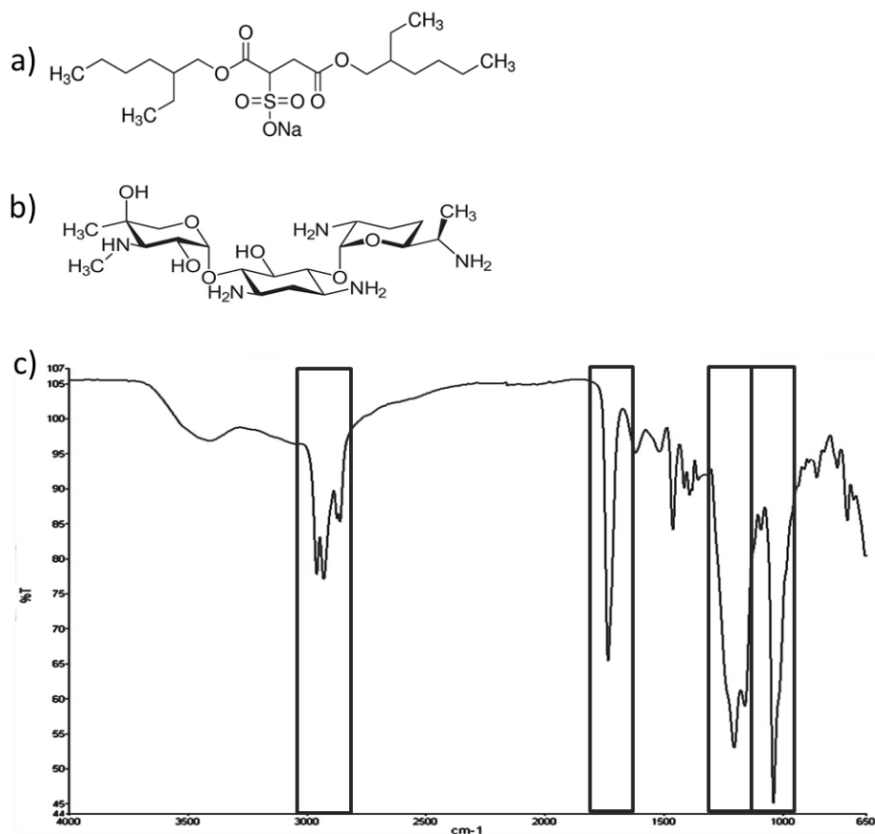


Figure 5.1: Chemical structure and IR spectrum of AOT-gentamicin.

Chemical structure of AOT (a) and gentamicin (b) molecules used to form AOT-gentamicin complex. c) IR spectrum showing typical peaks and bands (black boxes) due to the presence of the surfactant AOT as well as gentamicin were observed in the formed AOT-gentamicin complex.

Typical peaks and bands were recognised in obtained IR spectra of the AOT-gentamicin complex, when comparing to the results of Imbuluzqueta *et al.* In particular: a band between 3000 and 2800  $\text{cm}^{-1}$  denoting alkyl chain vibrations; bands at 1734, 1201 and 1157  $\text{cm}^{-1}$ , indicative of the AOT ester groups; and a band at 1036  $\text{cm}^{-1}$ , for the presence of sulfonyl group. The same bands were found by Imbuluzqueta *et al.* [234], demonstrating the successful formation of the ion-complex AOT-gentamicin.

For the preparation of SG and AG nanoparticles, freshly prepared AOT-gentamicin was included in the organic solvent solution with PLGA and standard particle preparation as described in previous chapters was then conducted. InvA497 was then coupled to the surface of SG and AG to produce SIG and AIG respectively. For all loaded formulations, the amount of encapsulated AOT-gentamicin was determined and the EE% and LC% was calculated (Figure 5.2).

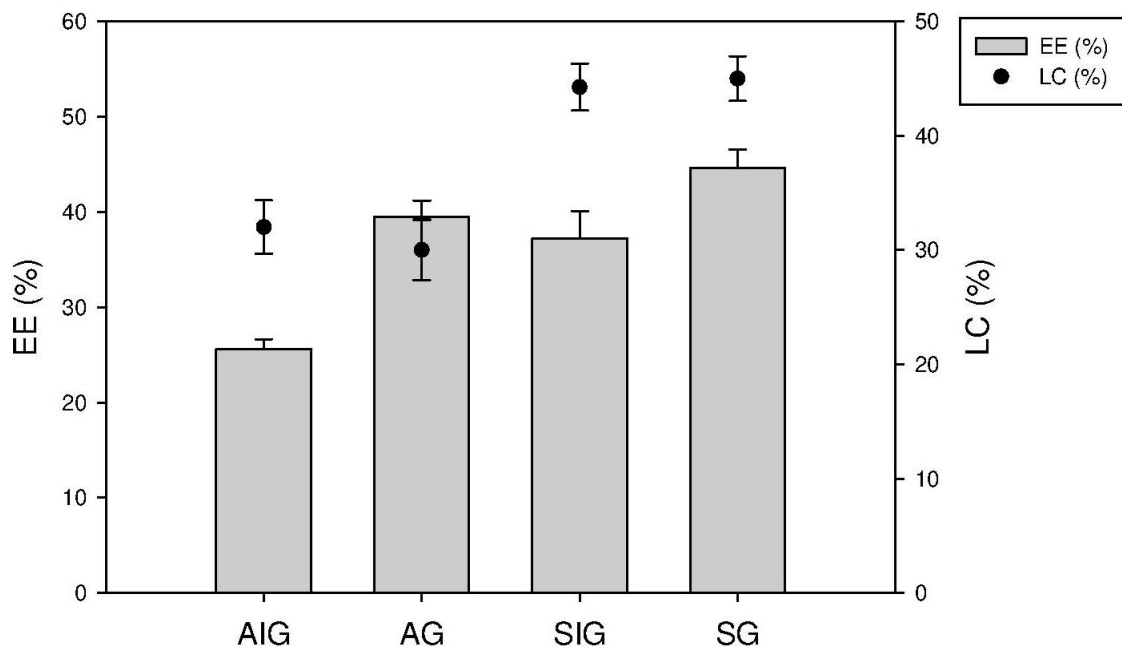
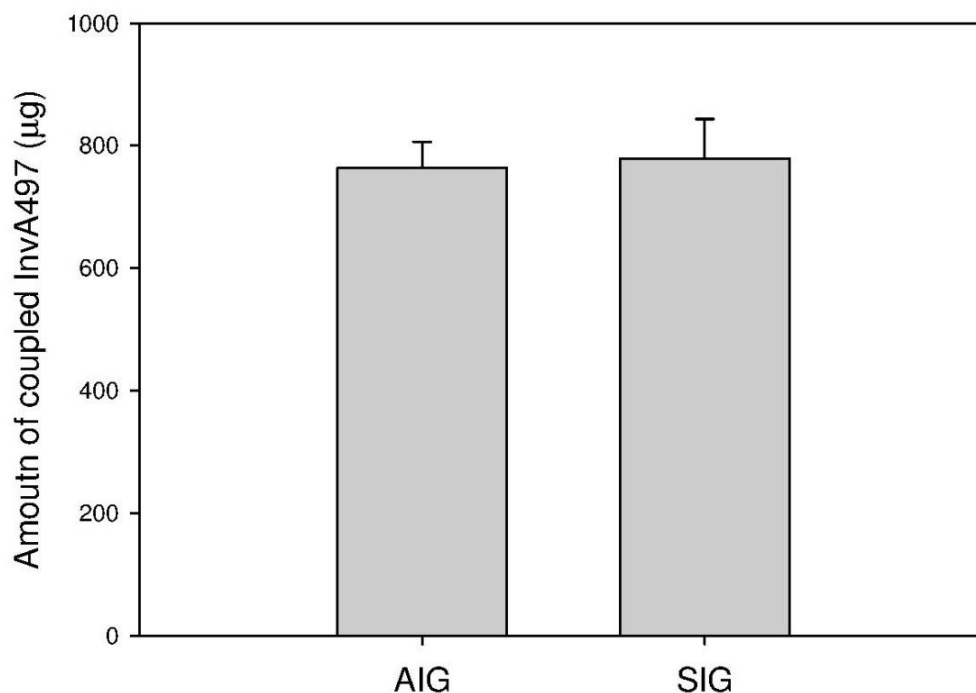


Figure 5.2 Chemical characterisation of drug-loaded nanoparticles.

(a) The encapsulation efficiency (EE%) and loading capacity (LC%) of AIG and SIG, as well as AG and SG is shown. Results represent the mean  $\pm$  SE (n=3).

A reduction of approximately 10% with respect to the EE% of AIG (approximately 26%) and AG (approximately 38%) formulations was observed relative to their spherical counterparts (around 37% for SIG and 45% for SG) most likely as a result of the stretching procedure and the numerous washing steps done during the preparation procedure. A drop of approximately 15% was also observed in terms of LC%. Even with this reduction however, aspherical nanoparticle formulations still demonstrate a good ability to incorporate AOT-gentamicin, with an EE% more than 25% and LC% higher than 35%.

Despite the small differences in amount of encapsulated drug, the amount of InvA497 functionalisation for AIG and SIG was found to be slightly higher than for the AI and SI formulations (Figure 5.3) (see chapter 3). The amount of InvA497 on AIG and SIG might have been due to an increase of the absorbed fraction of protein on the nanoparticles surface - caused by the presence of AOT-gentamicin inside the PLGA layer - more than a higher number of covalently bounded InvA497.



*Figure 5.3 InvA497 functionalisation for drug-loaded nanoparticles.*

*The amount of InvA497 coupled to the surface of AIG and SIG formulations was shown to be comparable. Results represent the mean  $\pm$  SE (n=3).*

The encapsulation of AOT-gentamicin within both aspherical and spherical formulations also had an effect on the surface charge (Figure 5.4). The zeta potential of drug-loaded formulations was found to be significantly higher than that of the empty formulations, while no difference was found between the surface charge of functionalised and non-functionalised nanoparticles. This difference in surface charge between the loaded nanoparticles (AIG and SIG) and the empty formulations (AI and SI) could provide a possible explanation for the different amounts of InvA497 coupled on the surface of these two formulation types. The decrease in the magnitude of surface charge found for drug-loaded formulations (AIG and SIG) could have led to a higher amount of the adsorbed InvA497 protein on the surface compared with the empty formulation.

Surprisingly no difference in the zeta potential was found between aspherical and spherical formulations, indicating that the shape of these PLGA nanoparticles does not have an impact on surface charge.

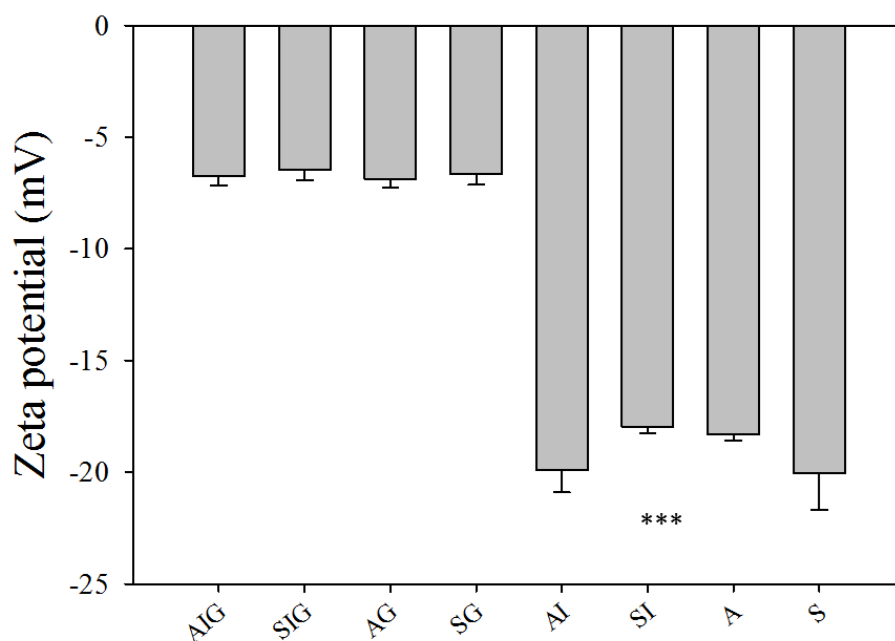


Figure 5.4 Zeta potential of bacteriomimetic nanoparticles.

The zeta potential of aspherical and spherical *InvA497*-functionalised nanoparticles loaded with AOT-gentamicin (AIG and SIG respectively), aspherical and spherical nanoparticles loaded with AOT-gentamicin (AG and SG), aspherical and spherical *InvA497*-functionalised nanoparticles (AI and SI) and aspherical and spherical nanoparticles (A and S), was measured by electrophoretic mobility. \*\*\* indicates statistical significance with a *p* value < 0.001 for AIG, SIG, AG and SG versus AI, SI, A and S. Data shows the mean  $\pm$  SE (*n*=9).

The *in vitro* release profiles of AOT-gentamicin from AIG, SIG, AG and SG were also measured at a pH of 7.4 (Figure 5.5).

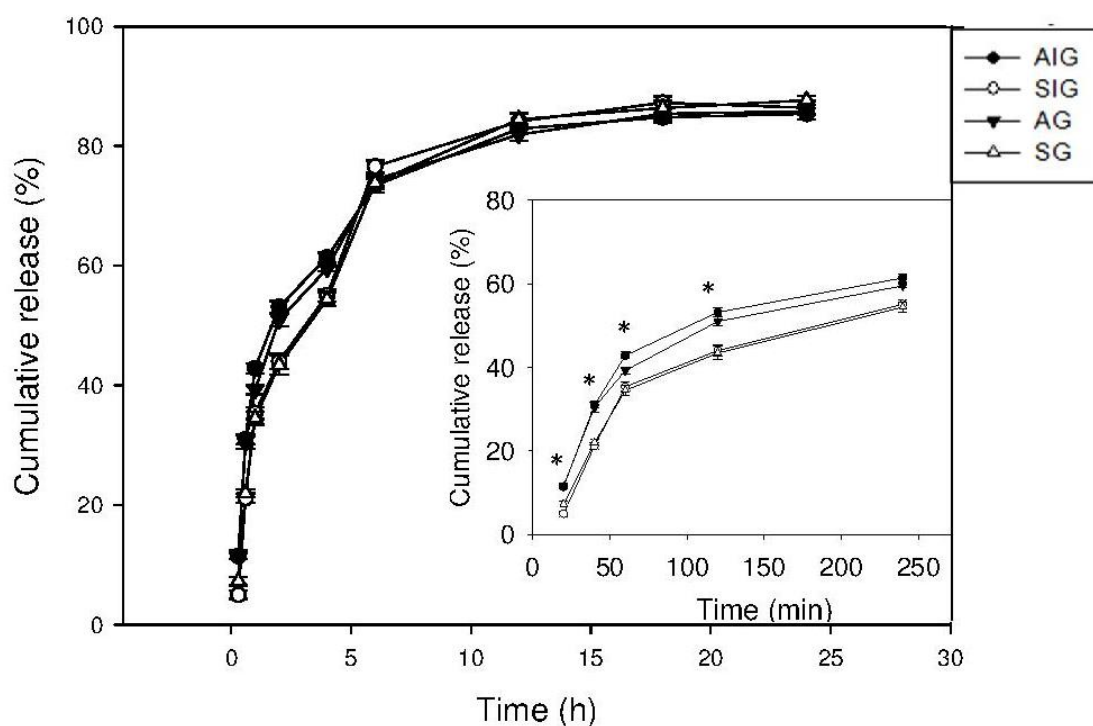
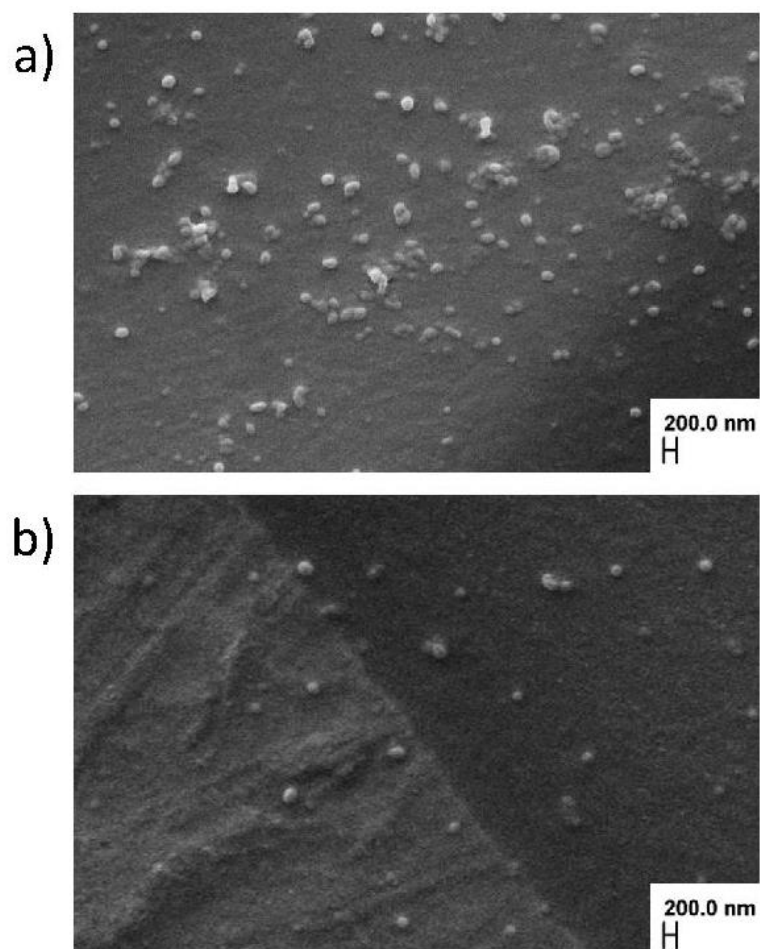


Figure 5.5 In vitro release kinetics.

AOT-gentamicin release was measured from AIG, SIG, AG and SG over 24 h in PBS at 37 °C. The insert graph shows release over the first 250 min. \*Indicates statistical significance with  $p$  value < 0.05 for AIG or AG versus SIG or SG. Results represent the mean  $\pm$  SE of three independent experiments, each with duplicate samples.

Within the first two hours, a slightly greater burst release was noted from AG and AIG compared to SIG and SG. Although this small difference was noted in the early time points, the overall release profile seems to be independent from the shape. Moreover the presence of InvA497 on the surface of both aspherical and spherical nanoparticles doesn't influence the drug release. This observed difference in the kinetics could potentially be explained by an accompanying change in shape of aspherical nanoparticles during this time period, as observed using SEM imaging (Figure 5.6).



*Figure 5.6 Morphology of asphercial nanoparticles during the release study.*

*Representative SEM images of AIG (a) and AG (b) after 2 h of incubation at 37 °C during drug release studies are shown.*

The observed recovery of the original spherical geometry seen for both AIG and AG nanoparticles could potentially have induced an initial faster release of AOT-gentamicin from these nanoparticles. This slightly accelerated release profile is unlikely to be an effect of degradation [235]. Shape recovery, and therefore the faster drug release, might be caused by the change of the surface tension of the nanoparticles, which is influenced by the shift of pH from 6 to 7.4 and the addition of PBS salt. A similar shape change of non-spherical nanoparticles was previously reported by Yoo *et al.* [157] as a result of a reduction in pH, who however did not test drug release from such particles. Moreover such shape change in constant pH condition was never observed and the associated release was not seen in other

formulations. The implications of this shape-dependent release on the later efficacy study need to be further investigated.

In order to determine a suitable dose of AOT-gentamicin alone as well as incorporated in nanoparticles for later efficacy studies, the cytotoxicity of AIG, SIG, AG and SG nanoparticles and as well AOT-gentamicin alone (G) was tested in HEp-2 cells using an LDH assay (Figure 5.7).

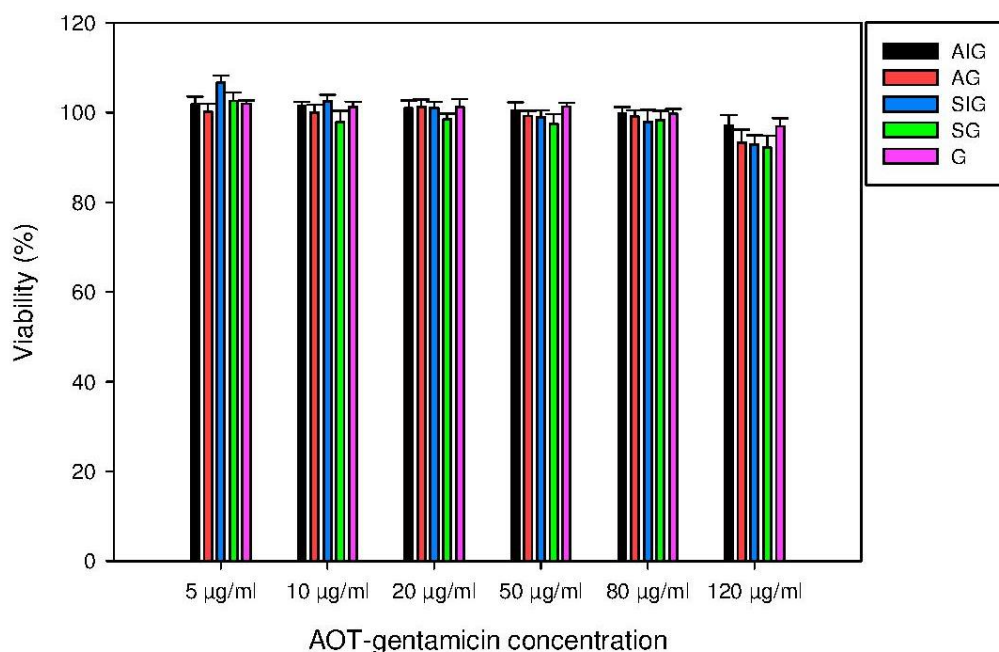


Figure 5.7 Cytotoxicity of drug-loaded nanoparticles.

Viability of HEp-2 cells after 4 h treatment with AIG, AG, SIG and SG was tested, as well as after treatment with free AOT-gentamicin (G) as control. Results represent the mean  $\pm$  SE (n=3).

For both nanoparticles and free drug, cytotoxicity was tested over a range of AOT-gentamicin concentrations, which encompassed the concentration of gentamicin contained within the previously tested InvA497-functionalised liposomes (50 µg/ml of gentamicin) [91]. No toxic effect on HEp-2 viability was found at any of the tested concentrations, with treatment at all concentrations showing a reduction in HEp-2 viability of less than 5%. Surprisingly no difference in cytotoxicity was found between aspherical and spherical formulations. From this data, formulations containing 30 µg/ml, 60 µg/ml and 120 µg/ml of AOT-gentamicin were selected for testing in efficacy studies.

After nanoparticle characterisation and preliminary cytotoxicity *in vitro* study, the anti-infective efficacy of bacteriomimetic nanoparticles against intracellular *S. flexneri* was evaluated.

First an *in vitro* model of HEp-2 cells infected with *S. flexneri* was established and optimised, in order to provide an optimal balance between bacterial invasion percentage and used bacterial inoculum. In particular the invasion capacity of *S. flexneri* bacteria in different growth phases and at various MOI was tested, in order to guarantee the highest invasion percentage with the lowest possible amount of bacteria and to avoid HEp-2 cell damage. Therefore *S. flexneri* cultures were grown to the exponential or stationary growth phase and afterwards HEp-2 cells were infected for 2 h with varying MOI. Following the infection stage, extracellular bacteria were killed using free gentamicin, which, due to its poor cell permeability, cannot penetrate inside the cells. As described previously [230], gentamicin is commonly used for this purpose in the establishment of *in vitro* cell models containing intracellular bacteria, as it guarantees killing of only extracellular bacteria and the survival of the intracellular fraction. The infection percentage of intracellular bacteria resulting from incubation with *S. flexneri* at different growth phases and at different MOI was then determined (Figure 5.8).



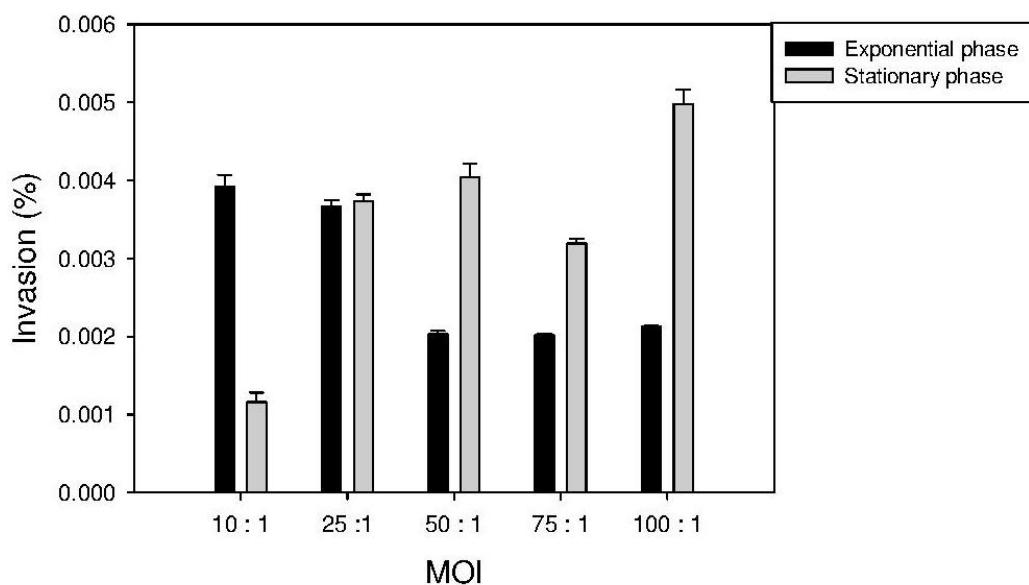


Figure 5.8 Optimisation of the infection of Hep-2 cells with *S. flexneri*

Percentage of infection after 4 h incubation of *S. flexneri* with HEp-2 cells with different MOI, using bacteria in either the exponential phase or stationary phase, is shown. Results represent the mean  $\pm$  SE ( $n=6$ ).

Bacteria in the exponential phase and at an MOI of 25:1 were determined to provide the optimal conditions for promoting uptake of intracellular bacteria, resulting in a reproducible number of intracellular bacteria while also giving the highest actual number of intracellular CFU (approximately 1800). Therefore these infection parameters were employed for the following efficacy studies.

After establishing the optimal conditions for intracellular infection of HEp-2 cells with *S. flexneri*, the viability of HEp-2 cells following both bacterial infection and treatment with various nanoparticle formulations and free drug was tested using a live-dead viability assay and confocal imaging (Figure 5.8). The highest concentration of AOT-gentamicin (120  $\mu\text{g/ml}$ ) found to be non-toxic in the previous LDH assay, was employed. Due to the presence of intracellular *S. flexneri* and therefore the inability to use conventional cytotoxicity methods (such as LDH assay or MTT method) to selectively measure the viability of HEp-2 cells, a qualitative method with calcein AM and ethidium homodimer-1 was employed to indicate the viability of infected Hep-2 cells after nanoparticles treatment. In this method, the

green dye calcein AM is able to stain only healthy cells and the red dye ethidium homodimer-1 is able to stain the nuclei exposed in damaged cells.

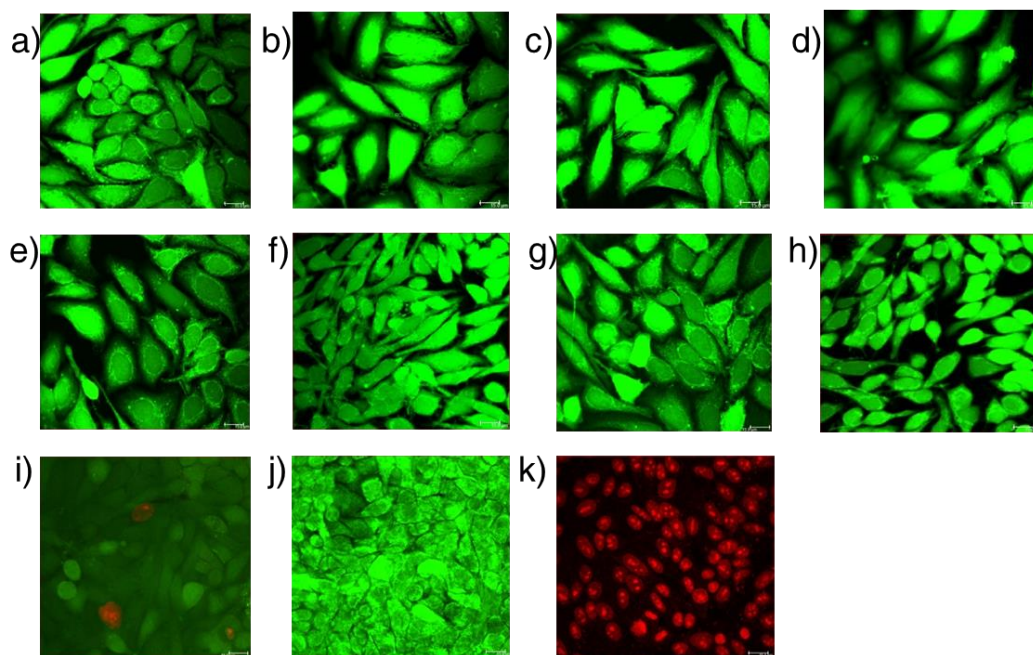


*Figure 5.9 Viability of S. flexneri infected cells after nanoparticles treatment.*

*Hep-2 cells infected with S. flexneri were treated for 3 h with AIG (a), AI (b), AG (c), A (d), SIG (e), SI (f), SG (g), S (h) and G (i) followed by live-dead staining and confocal microscopy imaging in order to visualise continued cell viability. Cell viabilities were observed in comparison to negative control (infected cells without treatment) (j) and a positive control (infected cells treated with 2% Triton X-100) (k). Green=live cells; red=dead cells.*

No effect on HEp-2 cell viability following both infection with *S. flexneri* and treatment with various nanoparticle formulations was seen, due to the presence of clear green stained cells; however, a slight toxic effect, evident from the red colour of some cells and the duller green appearance of other cells (Figure 5.9 i), was observed when infected cells were treated with free AOT-gentamicin. Incorporation of AOT-gentamicin into nanoparticles seems therefore to have a protective effect. Despite the slight cytotoxicity of the free drug and considering the comparable safety of all the nanoparticles formulations on epithelial cells, in efficacy studies, infected cells were treated with three different doses of free AOT-gentamicin as well as AOT-gentamicin encapsulated inside nanoparticles (30 µg/ml, 60 µg/ml and 120 µg/ml) (Figure 5.9).

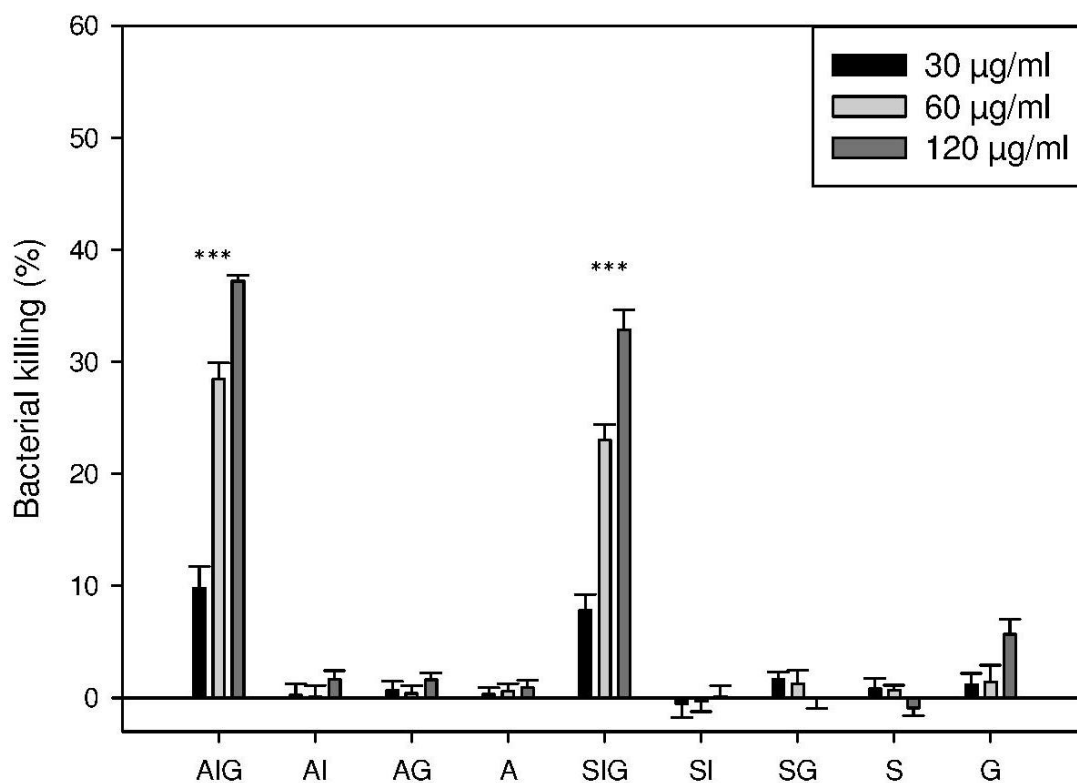


Figure 5.10: Efficacy study of nanoparticles against intracellular *S. flexneri*.

Percentage of killing of intracellular *S. flexneri* after 2 h treatment with the aspherical (AIG, AI, AG, A) and spherical (SIG, SI, SG, S) formulations, as well as free drug (G) using three different drug doses (30 µg/ml, 60 µg/ml and 120 µg/ml) is shown. \*\*\* indicates statistical significance with a *p* value < 0.001 for AIG versus AI, AG, A, and G, and SIG versus SI, SG, S and G. Data shows the mean ± SE of 3 independent experiments, each employing duplicate samples.

For the efficacy study, HEP-2 cells infected with intracellular *S. flexneri* bacteria were treated with freshly prepared AOT-gentamicin-loaded and InvA497-functionalised nanoparticles, of both aspherical and spherical shape (AIG and SIG). For comparison, formulations which were not loaded with drug but were surface functionalised (AI and SI) as well as drug-loaded formulations without surface InvA497 (AG and SG) and empty, non-functionalised formulations (A and S) were tested. Free AOT-gentamicin (G) was also employed. In the case of both AIG and SIG, a dose dependent reduction in the number of intracellular bacteria was observed. As expected from their poor cell-penetrating ability in the previous uptake study [91], formulations without InvA497 functionalisation (AG and SG) were not able to effectively kill intracellular *S. flexneri*; as expected, nor were control formulations without drug (AI and SI, as well as A and S). Surprisingly,

lipophilic free AOT-gentamicin was also not able to kill intracellular *S. flexneri*, as probably a high degree of lipophilicity is not the only characteristic controlling penetration into mammalian cells.

Comparing AIG and SIG, the trend in the percentage of intracellular killed bacteria was found to be dependent on the concentration. The higher concentration (120 µg/ml of AOT-gentamicin) of the bacteriomimetic nanoparticles leads to a greater killing comparing with the other two tested concentrations. Moreover a small but significant difference in bacteria killing was also found between the AIG and SIG formulations at the highest tested drug concentration - at which AIG systems led to a higher killing of intracellular bacteria in comparison to spherical bacteriomimetic nanocarriers (Figure 5.10).

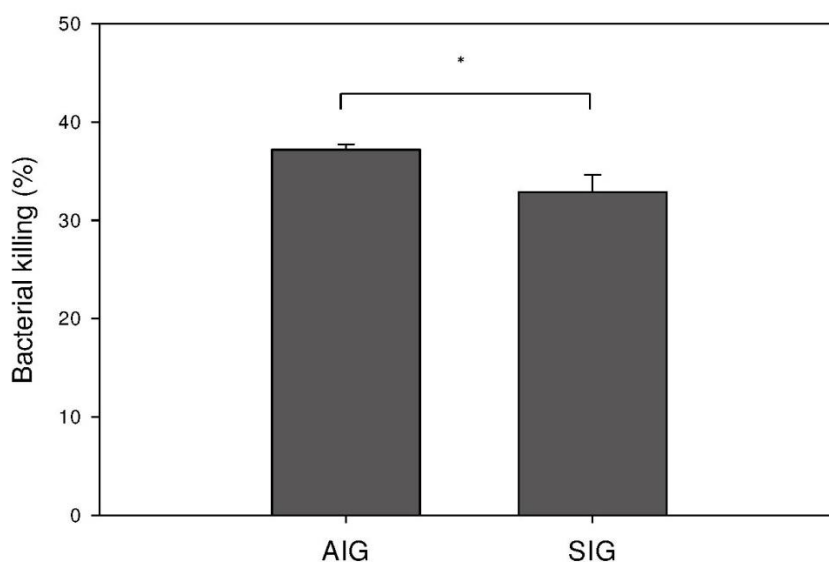


Figure 5.11: Direct comparison of bacterial killing of AIG and SIG.

Bacteria killing resulting from the treatment of *S. flexneri*-infected HEP-2 cells with AIG and SIG at a 120 µg/ml dose of AOT-gentamicin is shown. \* indicates  $p$  value < 0.05. Data shows the mean  $\pm$  SE of 3 independent experiments, each employing duplicate samples

The slightly higher beneficial effect of the aspherical nanoparticles could be explained with the initial burst release of the AOT-gentamicin from the AIG polymeric systems (see Figure 5.5), however the extent of the difference between the percentage of killed bacteria of AIG and SIG is too modest for evaluating the effect of the shape.

However this difference still indicates a promising application of aspherical systems functionalised with InvA497 systems for treating intracellular infection.

Independently by the shape, nanoparticles functionalised with InvA497 seem to represent a delivery system suitable for reaching and killing intracellular *S. flexneri*.

## 5.4 CONCLUSION

Aspherical and spherical nanoparticles loaded with a lipophilic preparation of gentamicin were prepared and functionalised with InvA497 in order to investigate the efficacy of the bacteriomimetic systems. Chemical characterisation of aspherical and spherical formulations showed an EE% and LC% higher than 25% and 35% respectively for the aspherical nanoparticles and higher than 35% and 50% for the spherical ones. Surprisingly the *in vitro* release profile of AOT-gentamicin from aspherical and spherical nanoparticles showed an initial burst release from both InvA497-functionalised and non-functionalised aspherical systems within the first two hours, which was hypothesised to be a result of the shape recovery of aspherical nanoparticles, observed to occur within the same time frame.

After establishing a non-toxic range of concentrations of the drug-loaded systems, and optimising the procedure for infecting HEp-2 cells with *S. flexneri*, the aspherical and spherical nanoparticles, with or without functionalisation and drug loaded or unloaded were tested in such an infection model. A dose dependent killing effect was found for both AIG and SIG, which additionally showed killing greater ability to kill intracellular *S. flexneri* comparing with all the other formulations. Moreover, comparing the efficacy of AIG and SIG at the highest employed dose, a significantly greater killing of intracellular *S. flexneri* was noted for the aspherical drug-loaded functionalised nanoparticles. However the modest magnitude of this difference highlights the considerable remaining scope for carrier system development and probing of shape effects – namely, optimisation of aspect ratio and maintenance of asphericity - in order to further enhance intracellular bacterial killing

Taken together, these results demonstrate that the presence of InvA497 on the surface of nanoparticles in combination with encapsulation of AOT-gentamicin

is able to increase the ability of PLGA-based delivery systems to effectively treat of infected epithelial cells. Moreover, nanoparticles with aspherical shape seem to be a promising candidate for intracellular delivery of anti-infective against bacteria.

## 6. OVERALL CONCLUSION AND OUTLOOK

The objectives of the presented study were related to the question: what is the potential in drug delivery of a bacteriomimetic system with an aspherical shape and InvA497 protein conjugated on the surface? The work was focused on investigating the influence of shape on the physico-chemical characteristics of bacteriomimetic systems, using InvA497-functionalised polymeric nanoparticles with spherical and aspherical morphology, and on evaluating the potential of both spherical and aspherical drug-loaded systems for accessing and killing intracellular bacteria.

The current work represents the first in-depth study into the impact of modifying the surface of nanoparticulate delivery systems through the use of bacteria-derived invasion molecules, in combination with changing their shape from spherical to non-spherical.

In the first part of the thesis, suitable methods for the preparation of spherical and, in particular, aspherical nanoparticles were selected. With respect to aspherical nanoparticles, the film stretching method was chosen as a more reproducible and suitable method for the present work. After designing a stretching apparatus and testing and optimising preparation conditions, PLGA nanoparticles with an aspherical shape were successfully obtained. In parallel, a strong focus was placed on the physical and chemical characterisation of the aspherical particles, with specific areas of interest being imaging of the particles using SEM and confocal microscopy, and on evaluation of different methods for determining particle dimensions and shape, such as SEM and AF4. Analysis of the size distribution of major and minor axes of the aspherical nanoparticles was conducted using these techniques.

The second part of this work was focused on the surface functionalisation of both spherical and aspherical nanoparticles with the bacterial invasion protein fragment InvA497, followed by preliminary *in vitro* uptake studies. Particularly for aspherical nanoparticles, the method of particle preparation was further adapted in order to achieve a high number of InvA497 molecules on the surface of nanoparticles, without changing their aspherical shape. With an appropriate quantification method, the amount of coupled InvA497 and the molecules of InvA497 per nanoparticle were measured. Moreover, a 3D model of aspherical and spherical nanoparticles functionalised with InvA497 was generated.



Afterwards the uptake of both bacteriomimetic systems (spherical and aspherical) was tested in HEP-2 cells, and compared with the non-functionalised polymeric nanoparticles. It was found that InvA497-functionalised nanoparticles were internalised better than the systems without InvA497. The presence of the protein on the surface of the nanoparticles was therefore able to enhance the particle uptake. Comparing the two bacteriomimetic formulations, a small difference was observed in the uptake, however considering the general uptake profile, the two shapes didn't exhibit differences in receptor-mediated uptake.

In the last part of this work, the aspherical and spherical systems were loaded with an anti-infective agent, AOT-gentamicin. After characterisation of both types of nanoparticles and functionalisation of the surface with InvA497, the *in vitro* release of AOT-gentamicin from the nanoparticles was tested. Although a small difference was found in the kinetic release of the aspherical and spherical nanoparticle, considering the general release profile, the two shapes didn't exhibit a substantial difference. After testing the *in vitro* cytotoxicity of the drug-loaded systems and developing an intracellular infection model of *S. flexneri*, the efficacy of aspherical and spherical InvA497-functionalised nanoparticles against intracellular bacteria was investigated. When loaded with an anti-infective and tested for their efficacy in an intracellular infection model, bacteriomimetic systems had a markedly improved killing effect in comparison to non-functionalised systems. Instead the shape of bacteriomimetic systems was found to have a small influence on the efficacy against intracellular *S. flexneri*. This last aspect is of great interest for future work.

Bacteriomimetic systems mimicking the invasive surface functionality as well as the shape of numerous intracellular bacteria therefore appear to be a promising approach for delivering anti-infective drugs into infected cells, combating such intracellular pathogens by mimicking their own infection pathway.

The demonstrated promise of these systems creates interesting perspectives for controlling a number of intracellular pathogens of the gastrointestinal tract. Further work should be focus on the optimisation of these systems for the respective pathogens and diseases typical of such specific routes of administration. The killing efficacy of the bacteriomimetic systems should be tested using a more specific model, which can represent better the intestinal barrier - like

a triple culture model that mimics the intestinal barrier and has the integrin receptor exposed – or against other enteropathogenic bacteria - like *Yersinia* or *Listeria*.

On the other hand the potential of bacteriomimetic delivery systems to kill intracellular infections might as well be explored in other types of bacteria, which infect different epithelial tissues and organs, such as the pulmonary epithelium.

Moreover a more deep mechanistic evaluation, looking at the intracellular pathway of the InvA497-functionalised nanoparticles, should be conducted in order to study the interaction between bacteria and nanoparticles.

From the preparation point of view, the orientation and distribution of InvA497 on the surface of both spherical and aspherical nanoparticles should be explored. These are important parameters for the InvA497-dependent uptake and for the interaction with the integrin receptor. Although the data are not showed in the present thesis, different techniques were already employed for this purpose (TEM, ESEM and Raman microscopy), using also InvA497-specific antibody, without positive results. In particular, changing the distribution of InvA497 on the surface of aspherical nanoparticles (protein concentrated in certain areas) and studying its influence on intracellular uptake and antibacterial effect would be an interesting future prospective.

## 7. APPENDIX

### 7.1 CALCULATION OF SURFACE OCCUPANCY

gyration radius of InvA497= 5.5mm (Yasara[210])

#### aspherical (spheroid)

r1 (b) = 151.5 nm

r2 (a) = 60.35 nm

Surface formula:

$$A = 2\pi a \left( a + \frac{c^2}{\sqrt{c^2 - a^2}} \arcsin \left( \frac{\sqrt{c^2 - a^2}}{c} \right) \right) .$$

A(spheroid)= 95603.7676 nm<sup>2</sup>

A(InvA497)= n(InvA497) \* 2πr(gyration)<sup>2</sup>

n(InvA497)= 198

A(InvA497)=37633.1384 nm<sup>2</sup>

A/A= 0.39 (= occupancy)

#### spherical (sphere)

r1= 95.6 nm

Surface formula:

$$A_O = 4\pi r^2 = \pi d^2 = \frac{dV}{dr}$$

A(sphere)= 114848.585 nm<sup>2</sup>

A(InvA497)=n(InvA497)\*2πr(gyration)<sup>2</sup>

n(InvA497)= 235

A(InvA497)= 44665.5936 nm<sup>2</sup>

A/A= 0.39 (=occupancy)

### 7.2 SCRIPT FOR POV-Ray 3.7

The following script was written for PovRay 3.7 to be used as an \*.inc file:

```
//----- random functions standard include file-----  
#include "rand.inc" //random functions provided by PovRay  
#include "invasin_tex.inc" //appearance of invasin molecules  
#include "invasin_surf03.inc" //coordinates of invasin surface vertices,  
generated as an export file from YASARA using pdb entry 1CWV  
#declare Random_1 = seed (124323); //initializing random coordinate #1  
#declare Random_2 = seed (1335); //initializing random coordinate #2
```

```

#declare NP_fin_01 = finish {ambient 0 emission 0 diffuse 1 brilliance 1
subsurface { translucency <4.69, 3.69, 2.69> }specular 0.15 roughness 0.5}
//appearance of particles

#declare NP_tex_03 = texture {pigment {granite colour_map {[0.0, srgb
<0.6,0.6,0.61>] [1.0, srgb <0.8,0.8,0.81>]}} normal { granite 0.1 } finish {NP_fin_01}
scale 0.1} texture {pigment {color srgbt<1,1,1,1>} normal { granite 0.5 } finish
{ambient 0 emission 0 diffuse 0 brilliance 1 specular 0.5 roughness 0.01} scale
0.1} //layered texture of particles

#declare invasin_tex_01 = texture {pigment {rgb <0.6,0.7,0.5>} finish
{phong 0.4}} //appearance of the space occupied by invasins – only seen when
included as an object

//INVASINS=====
=====

#declare inv_scaled = object {invasin_surf scale 0.000001163 translate
<0.0007,0,-0.033>} //model of invasin molecule, scaled to PovRay units

#declare inv_vol = cylinder{ <-0.0186/2,0,0>, <0.0186/2,0,0> ,0.00342
texture {invasin_tex_01}} //Volume which invasins occupy

//ASPHERICAL_NP=====
=====

#declare NP_basic_shape01 = //-----
-----

object{ //Spheroid(CenterVector, RadiusVector Rx,Ry,Rz )
Spheroid(<0,0,0>, <0.303/2,0.1207/2,0.1207/2> )
texture{ NP_tex_03} scale<1,1,1> rotate<0, 0,0>
translate<0,0.00,0>
} //shape of the aspherical naoparticle

#declare NP_surface01 = difference {object {NP_basic_shape01 scale
1.01} object {NP_basic_shape01 scale 1.005}} //Volume in which invasins are
placed

#declare invasins_rand01 = merge {
#local Nr = 0; // start
#local EndNr = 198; // number of invasins on surface
#while (Nr< EndNr)
object {inv_scaled

```

```

        rotate VRand_On_Sphere(Random_2)*180
        translate VRand_In_Obj( NP_surface01, Random_1)*1
        texture{ invasin_tex_01 } //interior_texture { PA_tex_01int } // end of
texture
    } // end of object
    #local Nr = Nr + 1; // next Nr
    #end
}
//SPHERICAL_NP=====
=====
    #declare NP_basic_shape02 = sphere {<0,0,0>, 0.1912/2 texture{
NP_tex_03} scale<1,1,1> rotate<0, 0,0> translate<0,0.00,0>} //shape of the
spherical naoparticle
    #declare NP_surface02 = difference {object {NP_basic_shape02 scale
1.01} object {NP_basic_shape02 scale 1.005}} //Volume in which invasins are
placed
    #declare invasins_rand02 = merge {
        #local Nr = 0; // start
        #local EndNr = 235; // number of invasins on surface
        #while (Nr< EndNr)
            object {inv_scaled
                rotate VRand_On_Sphere(Random_2)*180
                translate VRand_In_Obj( NP_surface02, Random_1)*1
                texture{ invasin_tex_01 } //interior_texture { PA_tex_01int } // end of
texture
            } // end of object
            #local Nr = Nr + 1; // next Nr
        #end
    }

```

## REFERENCES

1. Zhu, X., *et al.*, Nanomedicine in the management of microbial infection – Overview and perspectives. *Nano Today*, 2014. **9**(4): p. 478-498.
2. Yang, D.C., K.M. Blair, and N.R. Salama, Staying in Shape: the Impact of Cell Shape on Bacterial Survival in Diverse Environments. *Microbiol Mol Biol Rev*, 2016. **80**(1): p. 187-203.
3. Huh, A.J. and Y.J. Kwon, “Nanoantibiotics”: A new paradigm for treating infectious diseases using nanomaterials in the antibiotics resistant era. *J Control Release*, 2011. **156**(2): p. 128-145.
4. Zazo, H., C.I. Colino, and J.M. Lanao, Current applications of nanoparticles in infectious diseases. *J Control Release*, 2016. **224**: p. 86-102.
5. Michael, C.A., D. Dominey-Howes, and M. Labbate, The Antimicrobial Resistance Crisis: Causes, Consequences, and Management. *Front Public Health*, 2014. **2**: p. 145.
6. Rios, A.C., *et al.*, Alternatives to overcoming bacterial resistances: State-of-the-art. *Microbiol Res*, 2016. **191**: p. 51-80.
7. Carlet, J. and J.L. Mainardi, Antibacterial agents: back to the future? Can we live with only colistin, co-trimoxazole and fosfomycin? *Clin Microbiol Infect*, 2012. **18**(1): p. 1-3.
8. Rather, I.A., *et al.*, Self-medication and antibiotic resistance: Crisis, current challenges, and prevention. *Saudi J Biol Sci*, 2017. **24**(4): p. 808-812.
9. System, A.r.f.t.N., National Nosocomial Infections Surveillance (NNIS) System Report, data summary from January 1992 through June 2004, issued October 2004. *Am J Infect Control*, 2004. **32**(8): p. 470-485.
10. Edmond, M.B., *et al.*, Nosocomial Bloodstream Infections in United States Hospitals: A Three-Year Analysis. *Clin Infect Dis*, 1999. **29**(2): p. 239-244.
11. Tenover, F.C., Mechanisms of antimicrobial resistance in bacteria. *Am J Infect Control*, 2006. **34**(5, Supplement): p. S3-S10.
12. Munita, J.M. and C.A. Arias, Mechanisms of Antibiotic Resistance. *Microbiol Spectr*, 2016. **4**(2): p. 10.1128/microbiolspec.VMBF-0016-2015.
13. Ventola, C.L., The antibiotic resistance crisis: part 1: causes and threats. *P T*, 2015. **40**(4): p. 277-83.

14. Sykes, R., The 2009 Garrod Lecture: The evolution of antimicrobial resistance: a Darwinian perspective. *J Antimicrob Chemother*, 2010. **65**(9): p. 1842-1852.
15. Neu, H.C., The crisis in antibiotic resistance. *Science*, 1992. **257**(5073): p. 1064-73.
16. Alekshun, M.N. and S.B. Levy, Molecular mechanisms of antibacterial multidrug resistance. *Cell*, 2007. **128**(6): p. 1037-50.
17. Wilson, D.N., Ribosome-targeting antibiotics and mechanisms of bacterial resistance. *Nat Rev Microbiol*, 2014. **12**(1): p. 35-48.
18. Pages, J.M., C.E. James, and M. Winterhalter, The porin and the permeating antibiotic: a selective diffusion barrier in Gram-negative bacteria. *Nat Rev Microbiol*, 2008. **6**(12): p. 893-903.
19. Nikaido, H., Molecular basis of bacterial outer membrane permeability revisited. *Microbiol Mol Biol Rev*, 2003. **67**(4): p. 593-656.
20. Poole, K., Efflux-mediated antimicrobial resistance. *J Antimicrob Chemother*, 2005. **56**(1): p. 20-51.
21. Sansonetti, P., Bacterial pathogens, from adherence to invasion: comparative strategies. *Med Microbiol Immunol*, 1993. **182**(5): p. 223-232.
22. Phalipon, A. and P.J. Sansonetti, *Shigella's* ways of manipulating the host intestinal innate and adaptive immune system: a tool box for survival? *Immunol Cell Biol*, 2007. **85**(2): p. 119-29.
23. Erhardt, M. and P. Dersch, Regulatory principles governing *Salmonella* and *Yersinia* virulence. *Front Microbiol*, 2015. **6**: p. 949.
24. Cossart, P. and P.J. Sansonetti, Bacterial Invasion: The Paradigms of Enteroinvasive Pathogens. *Science*, 2004. **304**(5668): p. 242-248.
25. Briones, E., C.I. Colino, and J.M. Lanao, Delivery systems to increase the selectivity of antibiotics in phagocytic cells. *J Control Release*, 2008. **125**(3): p. 210-27.
26. Abed, N. and P. Couvreur, Nanocarriers for antibiotics: A promising solution to treat intracellular bacterial infections. *Int J Antimicrob Agents*, 2014. **43**(6): p. 485-496.
27. Barrios-Payan, J., et al., Extrapulmonary locations of *mycobacterium tuberculosis* DNA during latent infection. *J Infect Dis*, 2012. **206**(8): p. 1194-205.

28. Bäumler, A.J., *et al.*, *Salmonella typhimurium* loci involved in survival within macrophages. *Infect Immun*, 1994. **62**(5): p. 1623-1630.
29. Santos, R.L. and A.J. Bäumler, Cell tropism of *Salmonella enterica*. *Int J Med Microbiol*, 2004. **294**(4): p. 225-233.
30. Baldwin, C.L. and A.J. Winter, Macrophages and *Brucella*. *Immunol Ser*, 1994. **60**: p. 363-80.
31. Vázquez-Boland, J.A., *et al.*, *Listeria* Pathogenesis and Molecular Virulence Determinants. *Clin Microbiol Rev*, 2001. **14**(3): p. 584-640.
32. Amedei, A., *et al.*, Role of immune response in *Yersinia pestis* infection. *J Infect Dev Ctries*, 2011. **5**(9): p. 628-39.
33. Bokil, N.J., *et al.*, Intramacrophage survival of uropathogenic *Escherichia coli*: Differences between diverse clinical isolates and between mouse and human macrophages. *Immunobiology*, 2011. **216**(11): p. 1164-1171.
34. Porto, P.D., *et al.*, Dysfunctional CFTR Alters the Bactericidal Activity of Human Macrophages against *Pseudomonas aeruginosa*. *PLOS ONE*, 2011. **6**(5): p. e19970.
35. Horwitz, M.A. and S.C. Silverstein, Legionnaires' Disease Bacterium (*Legionella pneumophila*) Multiplies Intracellularly in Human Monocytes. *J Clin Invest*, 1980. **66**(3): p. 441-450.
36. Yancey, R.J., M.S. Sanchez, and C.W. Ford, Activity of antibiotics against *Staphylococcus aureus* within polymorphonuclear neutrophils. *Clin Microbiol Infect*, 1991. **10**(2): p. 107-113.
37. Finlay, B.B. and P. Cossart, Exploitation of Mammalian Host Cell Functions by Bacterial Pathogens. *Science*, 1997. **276**(5313): p. 718-725.
38. Sturgill-Koszycki, S., *et al.*, Lack of acidification in *Mycobacterium* phagosomes produced by exclusion of the vesicular proton-ATPase. *Science*, 1994. **263**(5147): p. 678-681.
39. Horwitz, M.A., Formation of a novel phagosome by the Legionnaires' disease bacterium (*Legionella pneumophila*) in human monocytes. *J Exp Med*, 1983. **158**(4): p. 1319-1331.
40. High, N., *et al.*, IpaB of *Shigella flexneri* causes entry into epithelial cells and escape from the phagocytic vacuole. *EMBO J*, 1992. **11**(5): p. 1991-1999.



41. Bielecki, J., *et al.*, *Bacillus subtilis* expressing a haemolysin gene from *Listeria monocytogenes* can grow in mammalian cells. *Nature*, 1990. **345**: p. 175.
42. Garzoni, C. and W.L. Kelley, *Staphylococcus aureus*: new evidence for intracellular persistence. *Trends Microbio*, 2009. **17**(2): p. 59-65.
43. Scott, C.C., R.J. Botelho, and S. Grinstein, Phagosome Maturation: A Few Bugs in the System. *J Membr Biol*, 2003. **193**(3): p. 137-152.
44. W., H.D., Trafficking of the *Salmonella* Vacuole in Macrophages. *Traffic*, 2002. **3**(3): p. 161-169.
45. Cesare, M., P. Emanuele, and S. Giampietro, Bacterial protein toxins penetrate cells via a four-step mechanism. *FEBS Lett*, 1994. **346**(1): p. 92-98.
46. Reis, R. and F. Horn, Enteropathogenic *Escherichia coli*, *Samonella*, *Shigella* and *Yersinia*: Cellular aspects of host-bacteria interactions in enteric diseases. Vol. 2. 2010. 8.
47. Sansonetti, P.J., War and peace at mucosal surfaces. *Nat Rev Immunol*, 2004. **4**(12): p. 953-964.
48. Sansonetti, P.J., D.J. Kopecko, and S.B. Formal, Involvement of a plasmid in the invasive ability of *Shigella flexneri*. *Infect Immun*, 1982. **35**(3): p. 852-860.
49. Isberg, R., Discrimination between intracellular uptake and surface adhesion of bacterial pathogens. *Science*, 1991. **252**(5008): p. 934-938.
50. Galán, J.E., *Salmonella* entry into mammalian cells: different yet converging signal transduction pathways? *Trends Cell Biol*, 1994. **4**(6): p. 196-199.
51. Carayol, N. and G. Tran Van Nhieu, Tips and tricks about *Shigella* invasion of epithelial cells. *Curr Opin Microbiol*, 2013. **16**(1): p. 32-37.
52. Veenendaal, A.K.J., *et al.*, The type III secretion system needle tip complex mediates host cell sensing and translocon insertion. *Mol Microbiol*, 2007. **63**(6): p. 1719-1730.
53. Blocker, A., *et al.*, The Tripartite Type III Secretion of *Shigella flexneri* Inserts Ipab and Ipac into Host Membranes. *J Cell Biol*, 1999. **147**(3): p. 683-693.
54. Hachani, A., *et al.*, IpgB1 and IpgB2, two homologous effectors secreted via the Mxi-Spa type III secretion apparatus, cooperate to mediate polarized cell invasion and inflammatory potential of *Shigella flexneri*. *Microbes Infect*, 2008. **10**(3): p. 260-8.

55. Mounier, J., *et al.*, The IpaC carboxyterminal effector domain mediates Src-dependent actin polymerization during *Shigella* invasion of epithelial cells. *PLoS Pathog*, 2009. **5**(1): p. e1000271.
56. Barreau, F. and J.P. Hugot, Intestinal barrier dysfunction triggered by invasive bacteria. *Curr Opin Microbiol*, 2014. **17**: p. 91-98.
57. Singer, M. and P.J. Sansonetti, IL-8 Is a Key Chemokine Regulating Neutrophil Recruitment in a New Mouse Model of *Shigella*-Induced Colitis. *J Immunol*, 2004. **173**(6): p. 4197-4206.
58. Kotloff, K.L., *et al.*, Shigellosis. *Lancet*, 2018. **391**(10122): p. 801-812.
59. Wiedemann, A., *et al.*, *Yersinia enterocolitica* invasin triggers phagocytosis via beta1 integrins, CDC42Hs and WASp in macrophages. *Cell Microbiol*, 2001. **3**(10): p. 693-702.
60. Dersch, P. and R.R. Isberg, A region of the *Yersinia pseudotuberculosis* invasin protein enhances integrin-mediated uptake into mammalian cells and promotes self-association. *EMBO J*, 1999. **18**(5): p. 1199-1213.
61. Isberg, R.R. and J.M. Leong, Multiple  $\beta$ 1 chain integrins are receptors for invasin, a protein that promotes bacterial penetration into mammalian cells. *Cell*, 1990. **60**(5): p. 861-871.
62. Isberg, R.R., D.L. Voorhis, and S. Falkow, Identification of invasin: A protein that allows enteric bacteria to penetrate cultured mammalian cells. *Cell*, 1987. **50**(5): p. 769-778.
63. Kochut, A. and P. Dersch, Bacterial invasion factors: tools for crossing biological barriers and drug delivery? *Eur J Pharm Biopharm*, 2013. **84**(2): p. 242-50.
64. Isberg, R.R. and J.M. Leong, Cultured mammalian cells attach to the invasin protein of *Yersinia pseudotuberculosis*. *Proc Natl Acad Sci U S A*, 1988. **85**(18): p. 6682-6.
65. Hamburger, Z.A., *et al.*, Crystal Structure of Invasin: A Bacterial Integrin-Binding Protein. *Science*, 1999. **286**(5438): p. 291-295.
66. Hamzaoui, N., *et al.*, Expression and distribution of  $\beta$ 1 integrins in in vitro-induced M cells: implications for *Yersinia* adhesion to Peyer's patch epithelium. *Cell Microbiol*, 2004. **6**(9): p. 817-828.

67. Alrutz, M.A. and R.R. Isberg, Involvement of focal adhesion kinase in invasin-mediated uptake. *Proc Natl Acad Sci U S A*, 1998. **95**(23): p. 13658-63.
68. Uliczka, F., *et al.*, Cell invasion of *Yersinia pseudotuberculosis* by invasin and YadA requires protein kinase C, phospholipase C-gamma1 and Akt kinase. *Cell Microbiol*, 2009. **11**(12): p. 1782-801.
69. Armstead, A.L. and B. Li, Nanomedicine as an emerging approach against intracellular pathogens. *Int J Nanomedicine*, 2011. **6**: p. 3281-93.
70. Barrett, J. and C.N. Fhogartaigh, Bacterial gastroenteritis. *Medicine*, 2017. **45**(11): p. 683-689.
71. Weir, E., *et al.*, The use of nanoparticles in anti-microbial materials and their characterization. *Analyst*, 2008. **133**(7): p. 835-845.
72. Zhang, L., *et al.*, Development of Nanoparticles for Antimicrobial Drug Delivery. *Curr Med Chem*, 2010. **17**(6): p. 585-594.
73. Pinto-Alphandary, H., A. Andremont, and P. Couvreur, Targeted delivery of antibiotics using liposomes and nanoparticles: research and applications. *Int J Antimicrob Agents*, 2000. **13**(3): p. 155-168.
74. Zhang, L., *et al.*, Nanoparticles in Medicine: Therapeutic Applications and Developments. *Clinical Pharmacology & Therapeutics*, 2008. **83**(5): p. 761-769.
75. Couvreur, P. and C. Vauthier, Nanotechnology: intelligent design to treat complex disease. *Pharm Res*, 2006. **23**(7): p. 1417-50.
76. Schiffelers, R., G. Storm, and I. Bakker-Woudenberg, Liposome-encapsulated aminoglycosides in pre-clinical and clinical studies. *J Antimicrob Chemother*, 2001. **48**(3): p. 333-44.
77. Fattal, E., *et al.*, Treatment of experimental salmonellosis in mice with ampicillin-bound nanoparticles. *Antimicrob Agents Chemother*, 1989. **33**(9): p. 1540-3.
78. Fattal, E., *et al.*, Liposome-entrapped ampicillin in the treatment of experimental murine listeriosis and salmonellosis. *Antimicrob Agents Chemother*, 1991. **35**(4): p. 770-2.
79. Mansour, H.M., Y.S. Rhee, and X. Wu, Nanomedicine in pulmonary delivery. *Int J Nanomedicine*, 2009. **4**: p. 299-319.

80. Sosnik, A., *et al.*, New old challenges in tuberculosis: potentially effective nanotechnologies in drug delivery. *Adv Drug Deliv Rev*, 2010. **62**(4-5): p. 547-59.
81. Amin, M.L., *et al.*, Surface modification and local orientations of surface molecules in nanotherapeutics. *J Control Release*, 2015. **207**: p. 131-142.
82. Vasir, J.K. and V. Labhasetwar, Biodegradable nanoparticles for cytosolic delivery of therapeutics. *Adv Drug Deliv Rev*, 2007. **59**(8): p. 718-28.
83. Saraogi, G.K., *et al.*, Mannosylated gelatin nanoparticles bearing isoniazid for effective management of tuberculosis. *J Drug Target*, 2011. **19**(3): p. 219-27.
84. Gajbhiye, V., *et al.*, Synthesis, characterization and targeting potential of zidovudine loaded sialic acid conjugated-mannosylated poly(propyleneimine) dendrimers. *Eur J Pharm Sci*, 2013. **48**(4-5): p. 668-79.
85. van Riet, E., *et al.*, Combatting infectious diseases; nanotechnology as a platform for rational vaccine design. *Adv Drug Deliv Rev*, 2014. **74**: p. 28-34.
86. Marasini, N., M. Skwarczynski, and I. Toth, Oral delivery of nanoparticle-based vaccines. *Expert Rev Vaccines*, 2014. **13**(11): p. 1361-1376.
87. Hurdle, J.G., *et al.*, Targeting bacterial membrane function: an underexploited mechanism for treating persistent infections. *Nat Rev Microbiol*, 2011. **9**(1): p. 62-75.
88. Salman, H.H., *et al.*, Micro-organism-like nanoparticles for oral antigen delivery. *J Drug Deliv Sci Technol*, 2008. **18**(1): p. 31-39.
89. Gabor, F., A. Bernkop-Schnürch, and G. Hamilton, Bioadhesion to the intestine by means of *E. coli* K99-fimbriae: Gastrointestinal stability and specificity of adherence. *Eur J Pharm Sci*, 1997. **5**(4): p. 233-242.
90. Labouta, H.I., *et al.*, Bacteriomimetic invasin-functionalized nanocarriers for intracellular delivery. *J Control Release*, 2015. **220**(Pt A): p. 414-424.
91. Menina, S., *et al.*, Invasin-functionalized liposome nanocarriers improve the intracellular delivery of anti-infective drugs. *RSC Advances*, 2016. **6**(47): p. 41622-41629.
92. Dawson, G.F. and G.W. Halbert, The in vitro cell association of invasin coated polylactide-co-glycolide nanoparticles. *Pharm Res*, 2000. **17**(11): p. 1420-5.

93. Hussain, N. and A.T. Florence, Utilizing bacterial mechanisms of epithelial cell entry: Invasin-induced oral uptake of latex nanoparticles. *Pharm Res*, 1998. **15**(1): p. 153-156.
94. Brakhage, A.A., *et al.*, Interaction of phagocytes with filamentous fungi. *Curr Opin Microbiol*, 2010. **13**(4): p. 409-415.
95. Justice, S.S., *et al.*, Morphological plasticity as a bacterial survival strategy. *Nat Rev Microbiol*, 2008. **6**(2): p. 162-168.
96. Young, K.D., Bacterial morphology: why have different shapes? *Curr Opin Microbiol*, 2007. **10**(6): p. 596-600.
97. Merkel, T.J., *et al.*, Scalable, Shape-Specific, Top-Down Fabrication Methods for the Synthesis of Engineered Colloidal Particles. *Langmuir*, 2009. **26**(16): p. 13086-13096.
98. Mathaes, R., *et al.*, Non-spherical micro- and nanoparticles: fabrication, characterization and drug delivery applications. *Expert Opin Drug Deliv*, 2015. **12**(3): p. 481-92.
99. Venkataraman, S., *et al.*, The effects of polymeric nanostructure shape on drug delivery. *Adv Drug Deliv Rev*, 2011. **63**(14-15): p. 1228-46.
100. Herd, H., *et al.*, Nanoparticle Geometry and Surface Orientation Influence Mode of Cellular Uptake. *ACS Nano*, 2013. **7**(3): p. 1961-1973.
101. Möhwald, M., *et al.*, Aspherical, Nanostructured Microparticles for Targeted Gene Delivery to Alveolar Macrophages. *Adv Healthc Mater* 2017. **6**(20): p. 1700478-n/a.
102. Petros, R.A., P.A. Ropp, and J.M. DeSimone, Reductively Labile PRINT Particles for the Delivery of Doxorubicin to HeLa Cells. *J Am Chem Soc*, 2008. **130**(15): p. 5008-5009.
103. Glangchai, L.C., *et al.*, Nanoimprint lithography based fabrication of shape-specific, enzymatically-triggered smart nanoparticles. *J Control Release*, 2008. **125**(3): p. 263-72.
104. Dendukuri, D., *et al.*, Continuous-flow lithography for high-throughput microparticle synthesis. *Nat Mater*, 2006. **5**(5): p. 365-369.
105. Glotzer, S.C. and M.J. Solomon, Anisotropy of building blocks and their assembly into complex structures. *Nat Mater*, 2007. **6**(8): p. 557-62.
106. Milliron, D.J., *et al.*, Colloidal nanocrystal heterostructures with linear and branched topology. *Nature*, 2004. **430**(6996): p. 190-5.

107. Chithrani, B.D., A.A. Ghazani, and W.C. Chan, Determining the size and shape dependence of gold nanoparticle uptake into mammalian cells. *Nano Lett*, 2006. **6**(4): p. 662-8.

108. Afrooz, A.R.M.N., *et al.*, Spheres vs. rods: The shape of gold nanoparticles influences aggregation and deposition behavior. *Chemosphere*, 2013. **91**(1): p. 93-98.

109. Herd, H.L., A. Malugin, and H. Ghandehari, Silica nanoconstruct cellular toleration threshold in vitro. *J Control Release*, 2011. **153**(1): p. 40-8.

110. Tritschler, U., *et al.*, 50th Anniversary Perspective: Functional Nanoparticles from the Solution Self-Assembly of Block Copolymers. *Macromolecules*, 2017. **50**(9): p. 3439-3463.

111. Karayianni, M. and S. Pispas, Fluorescence Studies of Polymer Containing Systems. 1 ed. Springer Series on Fluorescence. Vol. 16. 2016: Springer International Publishing. 302.

112. Lepeltier, E., *et al.*, Self-Assembly of Squalene-Based Nucleolipids: Relating the Chemical Structure of the Bioconjugates to the Architecture of the Nanoparticles. *Langmuir*, 2013. **29**(48): p. 14795-14803.

113. Cao, G. and D. Liu, Template-based synthesis of nanorod, nanowire, and nanotube arrays. *Adv Colloid Interface Sci*, 2008. **136**(1-2): p. 45-64.

114. Martin, C.R., Nanomaterials: a membrane-based synthetic approach. *Science*, 1994. **266**(5193): p. 1961-6.

115. Martin, C.R., Membrane-Based Synthesis of Nanomaterials. *Chem Mater*, 1996. **8**(8): p. 1739-1746.

116. Rolland, J.P., *et al.*, Direct Fabrication and Harvesting of Monodisperse, Shape-Specific Nanobiomaterials. *J Am Chem Soc*, 2005. **127**(28): p. 10096-10100.

117. Daum, N., *et al.*, Novel approaches for drug delivery systems in nanomedicine: effects of particle design and shape. *Wiley Interdiscip Rev Nanomed Nanobiotechnol*, 2012. **4**(1): p. 52-65.

118. Caldorera-Moore, M., *et al.*, Designer nanoparticles: incorporating size, shape and triggered release into nanoscale drug carriers. *Expert Opin Drug Deliv*, 2010. **7**(4): p. 479-495.

119. Dendukuri, D. and P.S. Doyle, The Synthesis and Assembly of Polymeric Microparticles Using Microfluidics. *Adv Mater*, 2009. **21**(41): p. 4071-4086.
120. Liu, Z.-M., *et al.*, Advances in Droplet-Based Microfluidic Technology and Its Applications. *Chinese Journal of Analytical Chemistry*, 2017. **45**(2): p. 282-296.
121. Ma, J., *et al.*, Controllable synthesis of functional nanoparticles by microfluidic platforms for biomedical applications - a review. *Lab Chip*, 2017. **17**(2): p. 209-226.
122. Doshi, N. and S. Mitragotri, Designer Biomaterials for Nanomedicine. *Adv Funct Mater*, 2009. **19**(24): p. 3843–3854.
123. Champion, J.A., Y.K. Katare, and S. Mitragotri, Making polymeric micro- and nanoparticles of complex shapes. *Proc Natl Acad Sci U S A*, 2007. **104**(29): p. 11901-4.
124. Mathaes, R., *et al.*, Application of different analytical methods for the characterization of non-spherical micro- and nanoparticles. *Int J Pharm*, 2013. **453**(2): p. 620-9.
125. Kohler, D., *et al.*, Template-Assisted Polyelectrolyte Encapsulation of Nanoparticles into Dispersible, Hierarchically Nanostructured Microfibers. *Adv Mater*, 2011. **23**(11): p. 1376-1379.
126. Yin, Y. and Y. Xia, Self-Assembly of Monodispersed Spherical Colloids into Complex Aggregates with Well-Defined Sizes, Shapes, and Structures. *Adv Mater*, 2001. **13**(4): p. 267-271.
127. Möhwald, M., *et al.*, Aspherical, Nanostructured Microparticles for Targeted Gene Delivery to Alveolar Macrophages. *Adv Healthc Mater*, 2017. **6**(20): p. 1700478-n/a.
128. Hou, S., J. Wang, and C.R. Martin, Template-Synthesized Protein Nanotubes. *Nano Letters*, 2005. **5**(2): p. 231-234.
129. Tscheka, C., *et al.*, Macrophage uptake of cylindrical microparticles investigated with correlative microscopy. *Eur J Pharm Biopharm*, 2015. **95**: p. 151-155.
130. Xia, Y. and G.M. Whitesides, Soft Lithography. *Angew Chem Int Ed Engl*, 1998. **37**(5): p. 550-575.

131. Tao, L., *et al.*, Lithographically defined uniform worm-shaped polymeric nanoparticles. *Nanotechnology*, 2010. **21**(9): p. 095301.
132. Buyukserin, F., *et al.*, Fabrication of Polymeric Nanorods Using Bilayer Nanoimprint Lithography. *Small*, 2009. **5**(14): p. 1632-1636.
133. Agarwal, R., *et al.*, Scalable Imprinting of Shape-Specific Polymeric Nanocarriers Using a Release Layer of Switchable Water Solubility. *ACS Nano*, 2012. **6**(3): p. 2524-31.
134. Kelly, J.Y. and J.M. DeSimone, Shape-Specific, Monodisperse Nano-Molding of Protein Particles. *J Am Chem Soc*, 2008. **130**(16): p. 5438-5439.
135. Canelas, D.A., K.P. Herlihy, and J.M. DeSimone, Top-down particle fabrication: control of size and shape for diagnostic imaging and drug delivery. *Wiley Interdiscip Rev Nanomed Nanobiotechnol*, 2009. **1**(4): p. 391-404.
136. Gratton, S.E.A., *et al.*, The effect of particle design on cellular internalization pathways. *Proc Natl Acad Sci U S A*, 2008. **105**(33): p. 11613-11618.
137. Galloway, A.L., *et al.*, Development of a nanoparticle-based influenza vaccine using the PRINT® technology. *Nanomedicine*, 2013. **9**(4): p. 523-531.
138. Wack, A., *et al.*, Combination adjuvants for the induction of potent, long-lasting antibody and T-cell responses to influenza vaccine in mice. *Vaccine*, 2008. **26**(4): p. 552-561.
139. Hwang, D.K., D. Dendukuri, and P.S. Doyle, Microfluidic-based synthesis of non-spherical magnetic hydrogel microparticles. *Lab Chip*, 2008. **8**(10): p. 1640-1647.
140. Nisisako, T., T. Torii, and T. Higuchi, Droplet formation in a microchannel network. *Lab Chip*, 2002. **2**(1): p. 24-26.
141. Serra, C.A. and Z. Chang, Microfluidic-Assisted Synthesis of Polymer Particles. *Chem Eng Technol*, 2008. **31**(8): p. 1099-1115.
142. Anna, S., N. Bontoux, and H. A. Stone, Formation of Dispersions Using 'Flow-Focusing' in Microchannels. *Appl Phys Lett*, 2002.
143. Kenis, P.J.A., R.F. Ismagilov, and G.M. Whitesides, Microfabrication Inside Capillaries Using Multiphase Laminar Flow Patterning. *Science*, 1999. **285**(5424): p. 83-85.
144. Shepherd, R.F., *et al.*, Microfluidic Assembly of Homogeneous and Janus Colloid-Filled Hydrogel Granules. *Langmuir*, 2006. **22**(21): p. 8618-8622.



145. Dendukuri, D., *et al.*, Controlled Synthesis of Nonspherical Microparticles Using Microfluidics. *Langmuir*, 2005. **21**(6): p. 2113-2116.
146. Xu, S., *et al.*, Generation of Monodisperse Particles by Using Microfluidics: Control over Size, Shape, and Composition. *Angew Chem Int Ed Engl*, 2005. **44**(5): p. 724-728.
147. Dendukuri, D., T.A. Hatton, and P.S. Doyle, Synthesis and Self-Assembly of Amphiphilic Polymeric Microparticles. *Langmuir*, 2007. **23**(8): p. 4669-4674.
148. Nie, Z., *et al.*, Polymer Particles with Various Shapes and Morphologies Produced in Continuous Microfluidic Reactors. *J Am Chem Soc*, 2005. **127**(22): p. 8058-8063.
149. Hakimi, N., *et al.*, One-Step Two-Dimensional Microfluidics-Based Synthesis of Three-Dimensional Particles. *Adv Mater*, 2014. **26**(9): p. 1393-1398.
150. Ma, J., Y. Wang, and J. Liu, Biomaterials Meet Microfluidics: From Synthesis Technologies to Biological Applications. *Micromachines*, 2017. **8**(8): p. 255.
151. Ho, C.C., *et al.*, Preparation of monodisperse ellipsoidal polystyrene particles. *Colloid Polym Sci*, 1993. **271**(5): p. 469-479.
152. Sharma, G., *et al.*, Polymer particle shape independently influences binding and internalization by macrophages. *J Control Release*, 2010. **147**(3): p. 408-12.
153. Mathaes, R., *et al.*, Influence of particle geometry and PEGylation on phagocytosis of particulate carriers. *Int J Pharm*, 2014. **465**(1-2): p. 159-64.
154. Wischke, C. and A. Lendlein, Method for preparation, programming, and characterization of miniaturized particulate shape-memory polymer matrices. *Langmuir*, 2014. **30**(10): p. 2820-7.
155. Wischke, C., M. Schossig, and A. Lendlein, Shape-memory effect of micro-/nanoparticles from thermoplastic multiblock copolymers. *Small*, 2014. **10**(1): p. 83-7.
156. Friess, F., *et al.*, Polymer Micronetworks with Shape-Memory as Future Platform to Explore Shape-Dependent Biological Effects. *Adv Healthc Mater*, 2014. **3**(12): p. 1986-1990.
157. Yoo, J.W. and S. Mitragotri, Polymer particles that switch shape in response to a stimulus. *Proc Natl Acad Sci U S A*, 2010. **107**(25): p. 11205-10.

158. Kolhar, P., *et al.*, Using shape effects to target antibody-coated nanoparticles to lung and brain endothelium. *Proc Natl Acad Sci U S A*, 2013. **110**(26): p. 10753-10758.
159. Barua, S., *et al.*, Particle shape enhances specificity of antibody-displaying nanoparticles. *Proc Natl Acad Sci U S A*, 2013. **110**(9): p. 3270-3275.
160. Truong, N.P., *et al.*, The importance of nanoparticle shape in cancer drug delivery. *Expert Opin Drug Deliv*, 2015. **12**(1): p. 1-14.
161. Decuzzi, P., *et al.*, Size and shape effects in the biodistribution of intravascularly injected particles. *J Control Release*, 2010. **141**(3): p. 320-7.
162. Decuzzi, P., *et al.*, A Theoretical Model for the Margination of Particles within Blood Vessels. *Ann Biomed Eng*, 2005. **33**(2): p. 179-190.
163. Niidome, T., *et al.*, PEG-modified gold nanorods with a stealth character for in vivo applications. *J Control Release*, 2006. **114**(3): p. 343-347.
164. Arnida, *et al.*, Geometry and surface characteristics of gold nanoparticles influence their biodistribution and uptake by macrophages. *Eur J Pharm Biopharm*, 2011. **77**(3): p. 417-423.
165. Toy, R., *et al.*, The effects of particle size, density and shape on margination of nanoparticles in microcirculation. *Nanotechnology*, 2011. **22**(11): p. 115101.
166. Akiyama, Y., *et al.*, The effects of PEG grafting level and injection dose on gold nanorod biodistribution in the tumor-bearing mice. *J Control Release*, 2009. **139**(1): p. 81-84.
167. Geng, Y., *et al.*, Shape effects of filaments versus spherical particles in flow and drug delivery. *Nat Nanotechnol*, 2007. **2**(4): p. 249-55.
168. Christian, D.A., *et al.*, Flexible Filaments for in Vivo Imaging and Delivery: Persistent Circulation of Filomicelles Opens the Dosage Window for Sustained Tumor Shrinkage. *Mol Pharm*, 2009. **6**(5): p. 1343-1352.
169. Chambers, E. and S. Mitragotri, Long circulating nanoparticles via adhesion on red blood cells: mechanism and extended circulation. *Vol. 232*. 2007. 958-66.
170. Anselmo, A.C., *et al.*, Exploiting shape, cellular-hitchhiking and antibodies to target nanoparticles to lung endothelium: Synergy between physical, chemical and biological approaches. *Biomaterials*, 2015. **68**: p. 1-8.

171. Toy, R., *et al.*, Shaping cancer nanomedicine: the effect of particle shape on the in vivo journey of nanoparticles. *Nanomedicine*, 2013. **9**(1): p. 121-134.
172. Muro, S., *et al.*, Control of Endothelial Targeting and Intracellular Delivery of Therapeutic Enzymes by Modulating the Size and Shape of ICAM-1-targeted Carriers. *Molecular Therapy*, 2008. **16**(8): p. 1450-1458.
173. Gratton, S.E.A., *et al.*, Nanofabricated particles for engineered drug therapies: A preliminary biodistribution study of PRINT™ nanoparticles. *J Control Release*, 2007. **121**(1–2): p. 10-18.
174. Agarwal, R., *et al.*, Mammalian cells preferentially internalize hydrogel nanodiscs over nanorods and use shape-specific uptake mechanisms. *Proc Natl Acad Sci U S A*, 2013. **110**(43): p. 17247-17252.
175. Champion, J.A., A. Walker, and S. Mitragotri, Role of particle size in phagocytosis of polymeric microspheres. *Pharm Res*, 2008. **25**(8): p. 1815-21.
176. Champion, J.A. and S. Mitragotri, Role of target geometry in phagocytosis. *Proc Natl Acad Sci U S A*, 2006. **103**(13): p. 4930-4.
177. Champion, J.A. and S. Mitragotri, Shape induced inhibition of phagocytosis of polymer particles. *Pharm Res*, 2009. **26**(1): p. 244-9.
178. Qiu, Y., *et al.*, Surface chemistry and aspect ratio mediated cellular uptake of Au nanorods. *Biomaterials*, 2010. **31**(30): p. 7606-7619.
179. Zhang, K., *et al.*, Shape Effects of Nanoparticles Conjugated with Cell-Penetrating Peptides (HIV Tat PTD) on CHO Cell Uptake. *Bioconjug Chem*, 2008. **19**(9): p. 1880-1887.
180. Gratton, S.E.A., *et al.*, The Pursuit of a Scalable Nanofabrication Platform for Use in Material and Life Science Applications. *Acc Chem Res*, 2008. **41**(12): p. 1685-1695.
181. Hinde, E., *et al.*, Pair correlation microscopy reveals the role of nanoparticle shape in intracellular transport and site of drug release. *Nat Nanotechnol*, 2017. **12**(1): p. 81-89.
182. Li, D., *et al.*, Influence of Particle Geometry on Gastrointestinal Transit and Absorption following Oral Administration. *ACS Appl Mater Interfaces*, 2017. **9**(49): p. 42492-42502.

183. Huang, X., *et al.*, The shape effect of mesoporous silica nanoparticles on biodistribution, clearance, and biocompatibility in vivo. *ACS Nano*, 2011. **5**(7): p. 5390-9.
184. Cooley, M., *et al.*, Influence of particle size and shape on their margination and wall-adhesion: implications in drug delivery vehicle design across nano-to-micro scale. *Nanoscale*, 2018. **10**(32): p. 15350-15364.
185. Park, J.-H., *et al.*, Systematic Surface Engineering of Magnetic Nanoworms for In vivo Tumor Targeting. *Small*, 2009. **5**(6): p. 694-700.
186. Dalhaimer, P., *et al.*, Targeted Worm Micelles. *Biomacromolecules*, 2004. **5**(5): p. 1714-1719.
187. Accardo, A., *et al.*, Peptide-Containing Aggregates as Selective Nanocarriers for Therapeutics. *ChemMedChem*, 2008. **3**(4): p. 594-602.
188. Banerjee, A., *et al.*, Role of nanoparticle size, shape and surface chemistry in oral drug delivery. *J Control Release*, 2016. **238**: p. 176-85.
189. Petros, R.A. and J.M. DeSimone, Strategies in the design of nanoparticles for therapeutic applications. *Nat Rev Drug Discov*, 2010. **9**(8): p. 615-27.
190. Champion, J.A., Y.K. Katare, and S. Mitragotri, Particle shape: A new design parameter for micro- and nanoscale drug delivery carriers. *J Control Release*, 2007. **121**(1–2): p. 3-9.
191. Mitragotri, S., In Drug Delivery, Shape Does Matter. *Pharm Res*, 2009. **26**(1): p. 232-234.
192. Simone, E.A., T.D. Dziubla, and V.R. Muzykantov, Polymeric carriers: role of geometry in drug delivery. *Expert Opin Drug Deliv*, 2008. **5**(12): p. 1283-300.
193. Martin, C.R., *Nanomaterials: A Membrane-Based Synthetic Approach*. Science, 1994. **266**(5193): p. 1961-1966.
194. Cao, G. and D. Liu, Template-based synthesis of nanorod, nanowire, and nanotube arrays. *Adv Colloid Interface Sci*, 2008. **136**(1–2): p. 45-64.
195. Iijima, S., Helical microtubules of graphitic carbon. *Nature*, 1991. **354**(6348): p. 56-58.
196. Raber, A.S., *et al.*, Quantification of nanoparticle uptake into hair follicles in pig ear and human forearm. *J Control Release*, 2014. **179**: p. 25-32.

197. Haque, S., *et al.*, Suggested Procedures for the Reproducible Synthesis of Poly(d,l-lactide-co-glycolide) Nanoparticles Using the Emulsification Solvent Diffusion Platform. *Curr Nanosci*, 2018. **14**(5): p. 448-453.

198. Passerini, N. and D.Q.M. Craig, An investigation into the effects of residual water on the glass transition temperature of polylactide microspheres using modulated temperature DSC. *J Control Release*, 2001. **73**(1): p. 111-115.

199. Gunes, D.Z., *et al.*, Flow-induced orientation of non-spherical particles: Effect of aspect ratio and medium rheology. *J Nonnewton Fluid Mech*, 2008. **155**(1–2): p. 39-50.

200. Gajdos, L.J. and H. Brenner, Field-Flow Fractionation: Extensions to Nonspherical Particles and Wall Effects. *Sep Sci Technol*, 1978. **13**(3): p. 215-240.

201. Johann, C., *et al.*, A novel approach to improve operation and performance in flow field-flow fractionation. *J Chromatogr A*, 2011. **1218**(27): p. 4126-4131.

202. Haltner, E., J.H. Easson, and C.-M. Lehr, Lectins and bacterial invasion factors for controlling endo- and transcytosis of bioadhesive drug carrier systems. *Eur J Pharm Biopharm*, 1997. **44**(1): p. 3-13.

203. Salman, H.H., *et al.*, Salmonella-like bioadhesive nanoparticles. *J Control Release*, 2005. **106**(1-2): p. 1-13.

204. Easson, J., E. Haltner, and D. Jahn, Bacterial Invasion Factors and Lectins as Second-Generation Bioadhesives, in *Bioadhesive Drug Delivery Systems*. 1999, CRC Press. p. 409-431.

205. Florence, A.T. and N. Hussain, Transcytosis of nanoparticle and dendrimer delivery systems: evolving vistas. *Adv Drug Deliv Rev*, 2001. **50**, **Supplement 1**(0): p. S69-S89.

206. Weiss, B., *et al.*, Nanoparticles made of fluorescence-labelled Poly(L-lactide-co-glycolide): preparation, stability, and biocompatibility. *J Nanosci Nanotechnol*, 2006. **6**(9-10): p. 3048-56.

207. Horisawa, E., *et al.*, Size-dependency of DL-lactide/glycolide copolymer particulates for intra-articular delivery system on phagocytosis in rat synovium. *Pharm Res*, 2002. **19**(2): p. 132-9.

208. Dersch, P. and R.R. Isberg, An immunoglobulin superfamily-like domain unique to the *Yersinia pseudotuberculosis* invasin protein is required for

stimulation of bacterial uptake via integrin receptors. *Infect Immun*, 2000. **68**(5): p. 2930-8.

209. Smith, P.K., *et al.*, Measurement of protein using bicinchoninic acid. *Anal Biochem*, 1985. **150**(1): p. 76-85.

210. Krieger, E., G. Koraimann, and G. Vriend, Increasing the precision of comparative models with YASARA NOVA--a self-parameterizing force field. *Proteins*, 2002. **47**(3): p. 393-402.

211. Lehr, C. and E. Mathiowitz, *Bioadhesive Drug Delivery Systems*, ed. D. Chickering III. 1999: Boca Raton: CRC Press.

212. Hoekstra, A., V. Maltsev, and G. Videen, *Optics of Biological Particles*. 2007: Springer Netherlands.

213. Sonnenberg, M.S., Pathogenic strategies of enteric bacteria. *Nature*, 2000. **406**(6797): p. 768-74.

214. Sansonetti, P.J., G.T. Van Nhieu, and C. Égile, Rupture of the Intestinal Epithelial Barrier and Mucosal Invasion by *Shigella flexneri*. *Clin Infect Dis*, 1999. **28**(3): p. 466-475.

215. Jensen, V.B., J.T. Harty, and B.D. Jones, Interactions of the Invasive Pathogens *Salmonella typhimurium*, *Listeria Infection* and Immunity monocytophenes, and *Shigella flexneri* with M Cells and Murine Peyer's Patches., 1998. **66**(8): p. 3758-3766.

216. Salmond, G.P. and P.J. Reeves, Membrane traffic wardens and protein secretion in gram-negative bacteria. *Trends Biochem Sci*, 1993. **18**(1): p. 7-12.

217. Grassl, G.A., *et al.*, Interaction of *Yersinia enterocolitica* with epithelial cells: invasin beyond invasion. *Int J Med Microbiol*, 2003. **293**(1): p. 41-54.

218. Nagel, G., A. Lahrz, and P. Dersch, Environmental control of invasin expression in *Yersinia pseudotuberculosis* is mediated by regulation of RovA, a transcriptional activator of the SlyA/Hor family. *Mol Microbiol*, 2001. **41**(6): p. 1249-1269.

219. Isberg, R.R. and G.T. Van Nhieu, Two mammalian cell internalization strategies used by pathogenic bacteria. *Annu Rev Genet*, 1994. **28**: p. 395-422.

220. Vacha, R., F.J. Martinez-Veracoechea, and D. Frenkel, Receptor-mediated endocytosis of nanoparticles of various shapes. *Nano Lett*, 2011. **11**(12): p. 5391-5.

221. Kettler, K., *et al.*, Cellular uptake of nanoparticles as determined by particle properties, experimental conditions, and cell type. *Environ Toxicol Chem*, 2014. **33**(3): p. 481-492.

222. Li, Y., *et al.*, Molecular modeling of the relationship between nanoparticle shape anisotropy and endocytosis kinetics. *Biomaterials*, 2012. **33**(19): p. 4965-4973.

223. Masloub, S.M., *et al.*, Comparative evaluation of PLGA nanoparticle delivery system for 5-fluorouracil and curcumin on squamous cell carcinoma. *Arch Oral Biol*, 2016. **64**: p. 1-10.

224. Patel, J., *et al.*, Targeted delivery of monoclonal antibody conjugated docetaxel loaded PLGA nanoparticles into EGFR overexpressed lung tumour cells. *J Microencapsul*, 2018. **35**(2): p. 204-217.

225. de Diesbach, P., *et al.*, Receptor-mediated endocytosis of phosphodiester oligonucleotides in the HepG2 cell line: evidence for non-conventional intracellular trafficking. *Nucleic Acids Res*, 2002. **30**(7): p. 1512-21.

226. Silva, M.T., Classical Labeling of Bacterial Pathogens According to Their Lifestyle in the Host: Inconsistencies and Alternatives. *Front Microbiol*, 2012. **3**: p. 71.

227. Salouti, M. and A. Ahangari, Nanoparticle based Drug Delivery Systems for Treatment of Infectious Diseases. *Application of Nanotechnology in Drug Delivery*. 2014.

228. Falkow, S., R.R. Isberg, and D.A. Portnoy, The interaction of bacteria with mammalian cells. *Annu Rev Cell Biol*, 1992. **8**: p. 333-63.

229. Abed, N. and P. Couvreur, Nanocarriers for antibiotics: a promising solution to treat intracellular bacterial infections. *Int J Antimicrob Agents*, 2014. **43**(6): p. 485-96.

230. Elsinghorst, E.A., Measurement of invasion by gentamicin resistance, in *Methods in Enzymology*. 1994, Academic Press. p. 405-420.

231. Sansonetti, P.J., Shigellosis: An Old Disease in New Clothes? *PLoS Med*, 2006. **3**(9): p. e354.

232. Kotloff, K.L., *et al.*, Global burden of *Shigella* infections: implications for vaccine development and implementation of control strategies. *Bulletin of the World Health Organization*, 1999. **77**(8): p. 651-666.

233. Elizondo, E., *et al.*, High loading of gentamicin in bioadhesive PVM/MA nanostructured microparticles using compressed carbon-dioxide. *Pharm Res*, 2011. **28**(2): p. 309-21.

234. Imbuluzqueta, E., *et al.*, Novel bioactive hydrophobic gentamicin carriers for the treatment of intracellular bacterial infections. *Acta Biomaterialia*, 2011. **7**(4): p. 1599-608.

235. Park, T.G., Degradation of poly(lactic-co-glycolic acid) microspheres: effect of copolymer composition. *Biomaterials*, 1995. **16**(15): p. 1123-30.



## ABBREVIATIONS

A	aspherical nanoparticles
AAO	anodised aluminum oxide
AB	aspherical BSA-functionalised nanoparticles
AF4	asymmetric flow field flow fractionation
AG	aspherical AOT-gentamicin-loaded nanoparticles
AI	aspherical InvA497-functionalised nanoparticles
AIG	aspherical AOT-gentamicin-loaded, InvA497-functionalised nanoparticles
AOT-gentamicin	gentamicin bis(2-ethylhexyl) sulfosuccinate sodium salt
AR	aspect ratio
BCA	bicinchoninic acid kit
BSA	bovine serum albumin
CDC	Centers for Disease Control and Prevention
CFU	colony forming units
DAPI	4',6-diamidino-2-phenylindole
DLS	dynamic light scattering
DMSO	dimethyl sulfoxide
DMTMM chloride	4-(4,6-Dimethoxy-1,3,5-triazin-2-yl)-4-methylmorpholinium chloride
ECDC	European Centre for Disease Prevention and Control
EDC	N'-(3-Dimethylaminopropyl)N-ethylcarbodiimid HCl
EE%	encapsulation efficiency
EtAch	ethyl acetate
FA	fluoresceinamine
FACS	fluorescence-activated cell sorting
FCS	foetal calf serum
FDA	fluorescein diacetate
FSC	forward scatter
FT-IR	fourier transform infrared spectroscopy
HEp-2 cells	Human epithelial type 2l cells - HeLa contaminant
InvA497 invasin	fragment of the last 497 aminoacid of the C-terminal region of invasin

ICAM-1	intercellular adhesion molecule
HA	influenza virus antigen
MALLS	multi-angle laser light scattering
LC%	loading capacity
LDH	lactate dehydrogenase
MWCO	molecular weight cut off
MOI	multiplicity of infection
MTT	3-(4,5-di-methylthiazol-2-yl)-2,5-diphenyltetrazolium bromide
NTA	nanoparticle tracking analysis
OPA	o-phthaldialdehyde
PBS	phosphate-buffered saline
PDI	polydispersity index
PEG	polyethylene glycol
PFPE mold	perfluoropolyether
PLGA	poly (D,L-lactic-co-glycolic acid)
PRINT®	Particle Replication in Non-wetting Templates
PVA	polyvinyl alcohol
RAC	Ras-related C3 botulinum toxin
RPMI	Roswell Park Memorial Institute
RT	room temperature
QELS	Quasi-Elastic-Light-Scattering
S	spherical nanoparticles
SD	standard deviation
SDS	sodium dodecyl sulfate
SE	standard error of the mean
SEM	scanning electron microscopy
SB	spherical BSA-functionalised nanoparticles
SG	spherical AOT-gentamicin-loaded nanoparticles
SI	spherical InvA497-functionalised nanoparticles
SIG	spherical AOT-gentamicin-loaded, InvA497-functionalised nanoparticles
SSC	side scatter
spp.	species
TSB	tryptic soy broth

$T_g$	transition temperature
UV	ultraviolet
WHO	World Health Organization

## LIST OF FIGURES

Figure 1.1 Shighella invasion of epithelial cells[51].	19
Figure 1.2 Structure of the extracellular binding domain of invasin [63].	21
Figure 1.3 Examples of aspherical systems produced by different preparation methods.	27
Figure 1.4 Schematic representation of the template-assisted method.	29
Figure 1.5 Differences between traditional imprint lithography and PRINT® technology.	32
Figure 1.6 Uptake of particles into macrophages depending on the shape and orientation.	38
Figure 1.7 Interaction of particles with different shape and with target moieties with the cells.	41
Figure 2.1 Schematic picture of the stretching machine.	49
Figure 2.2 Schematic representation of the aspherical nanoparticle preparation procedure.	50
Figure 2.3 Schematic representations of the shape descriptors used to characterise aspherical nanoparticles .	51
Figure 2.4 Comparative morphology of spherical and aspherical nanoparticles.	54
Figure 2.5 Size and PDI of aspherical and spherical PLGA nanoparticles.	55
Figure 2.6 Distribution of shape descriptors.	58
Figure 2.7 AF4 chromatograms of spherical and aspherical nanoparticles, and comparison of shape descriptors measured with AF4 and SEM image analysis.	60
Figure 3.1 Schematic of aspherical nanoparticle surface functionalisation with InvA497.	69
Figure 3.2 Morphology of AB nanoparticles produced using coupling method 1.	73

Figure 3.3 Characterisation of BSA functionalised aspherical nanoparticles prepared via different coupling methods. ....	74
Figure 3.4 Morphology and coupling characterisation of AI.....	75
Figure 3.5 Coupling characterisation of SB. ....	76
Figure 3.6 Characterisation of InvA497 functionalisation on nanoparticle.....	77
Figure 3.7: IR spectra of nanoparticles and InvA497. ....	78
Figure 3.8 Size of AI and SI nanoparticles. ....	80
Figure 3.9 3D model of AI and SI.....	81
Figure 4.1: Cytotoxicity of nanoparticles.....	90
Figure 4.2: Confocal microscopy images of the cellular uptake of nanoparticles. ....	91
Figure 4.3: Quantification of intracellular uptake of nanoparticles into HEP-2 cells. ....	92
Figure 4.4 Energy dependent uptake of nanoparticles on Hep-2 cells. ....	93
Figure 5.1: Chemical structure and IR spectrum of AOT-gentamicin. ....	105
Figure 5.2 Chemical characterisation of drug-loaded nanoparticles. ....	106
Figure 5.3 InvA497 functionalisation for drug-loaded nanoparticles. ....	107
Figure 5.4 Zeta potential of bacteriomimetic nanoparticles.....	108
Figure 5.5 In vitro release kinetics. ....	109
Figure 5.6 Morphology of aspherical nanoparticles during the release study.....	110
Figure 5.7 Cytotoxicity of drug-loaded nanoparticles. ....	111
Figure 5.8 Optimisation of the infection of Hep-2 cells with <i>S. flexneri</i> ....	113
Figure 5.9 Viability of <i>S. flexneri</i> infected cells after nanoparticles treatment. ....	114
Figure 5.10: Efficacy study of nanoparticles against intracellular <i>S. flexneri</i> . ....	115

Figure 5.11: Direct comparison of bacterial killing of AIG and SIG.  
.....116

# LIST OF PUBLICATIONS

## Research papers:

2018 A.Castoldi et al., **Aspherical and Spherical InvA497-functionalized Nanocarriers for Intracellular Delivery of Anti-infective Agents**, Pharmaceutical Research, 2018 Dec 5;36(1):22. doi: 10.1007/s11095-018-2521-3.

09/2016 A. Castoldi et al., **Calcifediol-loaded liposomes for local treatment of pulmonary bacterial infections**, European Journal of Pharmaceutics and Biopharmaceutics, 2016 Nov 22. pii: S0939-6411(16)30853-0

## Patent:

02/2016 C.-M. Lehr, H. I. Labouta, S. Gordon, A. Castoldi, S. Menina, R. Geyer, A. Kochut, P. Dersch, **Methods and compositions of carrier systems for the purpose of intracellular drug targeting**, WO2016024008 A1

## Posters:

June 29th, 2016 **6<sup>th</sup> HIPS Symposium 2016** (Saarbrücken, DE) - "Pseudobacterial Nanocarriers for Intracellular Delivery of Anti-infective Drugs"

April 12th-15th, 2016 **14<sup>th</sup> European Symposium on Controlled Drug Delivery** (Egmond aan Zee, NL) - "Bacteria Meet Nanoparticles: an Innovative Delivery Strategy as Treatment for Intracellular Bacterial Infections"

March 7th-9th, 2016 **11<sup>th</sup> International Symposium on Biological Barriers** (Saarbrücken, DE) - "Pseudobacterial Nanocarriers: a Bacteria-derived Delivery Strategy for Combating Intracellular Infections"

- July 26th-29th, 2015      **42<sup>nd</sup> Controlled Released Society Annual Meeting**  
(Edinburgh, UK) - "Development of Aspherical Nanoparticles Functionalised with Invasion Moieties for Studying the Influence of Particle Shape on Cellular Uptake"
- April 13th-14th, 2015      **1<sup>st</sup> European Conferences on Pharmaceutics** (Reims, FR) - "Aspherical Nanoparticles for Drug Delivery Application"
- Aug. 27th-30th, 2014      **10<sup>th</sup> Globalization of Pharmaceutics Education Network** (Helsinki, FI) - "Shape-modified Nanocarriers for Intracellular Drug Delivery"



# CURRICULUM VITAE

## Personal Data

---

Date of birth 09.03.1989

Birthplace Milan

## Actual position

---

03/2018 - today **Essers Italy – Quality unit, Siziano (IT)**

Responsible person quality Italy and technical director of Siziano unit

## Jobs

---

03/2017 – 02/2018 **Doppel farmaceutici – Solid Dosage Form Unit, Rozzano (IT)**

Supervisor of production

## Doctoral studies

---

09/2013 – 11/2016 **Helmholtz Institute for Pharmaceutical Research Saarland (HIPS), Helmholtz Center for Infection Research (HZI), Department of Drug Delivery (Head: Prof. Dr. Claus-Michael Lehr), Saarbrücken (DE)**

Title: Development of pseudobacterial nanocarriers for intracellular delivery of anti-infectives

## Internships

---

10/2011 – 03/2012 **Farmacia Villani, Pavia (IT)**

As part of the mandatory pharmacy internship

07/2011 – 09/2011 **Istituto Clinico Humanitas, Rozzano (IT)**

As part of the mandatory pharmacy internship

Education

---

11/2013	<b>Pharmacist Licensure - State exam</b>
10/2008 – 07/2013	<b>Università degli Studi di Pavia – Pavia (IT)</b> Studies of Pharmaceutical Chemistry and Technology – Faculty of Pharmacy
01/2013 – 06/2013	<b>Universität des Saarlandes, Saarbrücken (DE)</b> Research Period Aimed to the Preparation of Graduation Thesis
09/2003 – 07/2008	<b>Liceo Classico con Annessa Sezione Liceo Scientifico B. Cairoli (High School), Vigevano (IT)</b>
09/2000 – 06/2003	<b>Scuola Media Europea (Secondary School), Abbiategrasso (IT)</b>
09/1995 – 06/2000	<b>Istituto Figlie di Betlem (Primary School), Abbiategrasso (IT)</b>

## ACKNOWLEDGEMENT/ RINGRAZIAMENTI

This PhD thesis is not only a book full of picture and graphs, but it also represents a long journey started on the 16<sup>th</sup> of January 2013 by a small Italian Erasmus student, lost in Saarbrücken. Since that day I learned how to become a scientist, how to drink beer and that, without some people, I would not be on my couch writing the acknowledgement.

First and foremost, I would like to thank my supervisor (Doktorvater) Prof. Dr. Claus-Michael Lehr for giving me the chance to join his working group and to build my scientific skills. You helped me growing professionally and personally, and never failed to encourage me when things were getting rough.

Second, Dr. Sarah C. Gordon (the small boss and the Doktormother) who supported me in this work more than anyone. To be honest no words can express my gratitude. Thank you for everything and every time that you didn't give up on me, the work and my bad English (the red pen can now rest). Your door was always open for me and I'm grateful for that. Team Gordon rules!!! (cit. Florian's thesis).

I would like to thank Rudolf Richter from the Physics Department of Saarland University for the help with the stretching machine and Dr. Martin Empting from the Drug Design and Optimisation department of HIPS for the 3d model.

I would like to thank all the "old" and "new" PhD students from the HIPS (Hanzey, Sara, Jing, Chrissi, Ankit, JD, Nico, Ana, Adrieli, Steffy, Kieth, Carlos, Salem, Branko, Christina and many more), master students, Postdoc (Brigitta, Nicole and Cristiane) and technicians that I met during these 3 years. Thank you for the discussion and the good time in the lab. Thank you also Karian and Sarah for help.

The people that you work with become also your family, so I need to write a special thanks to my lab-family: Florian (Doktorbrother), thank you for the talks, for the good time in the lab and conferences, for being my friend; Simon and Julia for

all evenings we spent grilling and the good time in SB; Xabi for your help and support in the lab and outside; Remi (officemate) for your positive attitude; the dancing doctor Elise for being the first officemate and friend in the lab.

Thank you Petra and Jana for teaching me how not to kill or contaminate my Hep-2 cells; I forgive you for cooking the pasta in the microwave.

Last but not least, Chiara, my Italian partner in crime in the lab. Thank you for your help, for the gossip and for being my friend. *Se i muri del laboratorio parlassero italiano*

I want to thank also the people that I met outside the lab, my Italian family in SB. Starting with Filomena and Gianluca (everybody should have a Filomena in their life) for your support and for all the dinners with ramen. Thanks to Federica, Paul (with the small Mathilde) and Gloria for all the Italian evenings and the good time together. You all made SB a special city.

I would like to thank my friends in Abbiategrosso (Libera, Siriana and Federico) for visiting me in Saarbrücken and being there every time I came back home.

I want also to mention my “new” friends, that I met when I came back to Italy and supported me during the writing of this long thesis (Filomena, Nino, Biagio, Martina, Melissa, Cristina, Elena, Linda, Enrico).

A quick thank goes to my current boss and colleagues; despite the hard work, you made my days lighter letting me finish this thesis and the article.

To my parents, Dark and relatives: I really thank you for believing in me, sharing my sorrows and happiness, teaching me how to believe in myself and all the sacrifices you did for me. Everything that I am and I have done would not have been possible without your support and nor it would have meant anything without sharing it with you.

*“Io non dimentico nessuno. Non dimentico chi ha toccato con mano, almeno per una volta la mia vita. Perché se lo hanno fatto, significa che il destino ha voluto che mi scontrassi anche con loro prima di andare avanti.”*

That’s all folks!!!!